December 2020

Considerations for the Design Optimization of Floating Offshore Wind Turbine Blades

Evan M. Gaertner
University of Massachusetts Amherst

CONSIDERATIONS FOR THE DESIGN OPTIMIZATION OF FLOATING OFFSHORE WIND TURBINE BLADES

A Dissertation Presented

by

EVAN M. GAERTNER

Submitted to the Graduate School of the
University of Massachusetts Amherst in partial fulfillment
of the requirements for the degree of

DOCTOR OF PHILOSOPHY

September 2020

Mechanical and Industrial Engineering

CONSIDERATIONS FOR THE DESIGN OPTIMIZATION OF FLOATING OFFSHORE WIND TURBINE BLADES

A Dissertation Presented

by

EVAN M. GAERTNER

Approved as to style and content by:

Matthew A. Lackner, Chair

James F. Manwell, Member

Yahya Modarres-Sadeghi, Member

Sanjay R. Arwade, Member

Sundar Krishnamurty, Department Head
Mechanical and Industrial Engineering

DEDICATION

To my best friend and wife, Bia.

Graduate school brought us together.

As one chapter ends, a new and exciting one begins.

ACKNOWLEDGMENTS

First, I would like to thank my committee members; Prof. Matthew Lackner, Prof. James Manwell, Prof. Yahya Modarres-Sadeghi, and Prof. Sanjay Arwade. I would also like to thank my honorary committee member, Dr. Katherine Dykes of the Technical University of Denmark. Additionally, I would like to thank Katherine and Dr. Garrett Barter for their guidance and mentorship at the National Renewable Energy Laboratory. To all my colleagues at NREL who have patiently waited for me to finish this dissertation and picked up the slack in the meantime, I am extremely grateful. Finally, thank you to my friends and colleagues at the UMass Amherst Wind Energy Center, as well as IGERT fellows from other departments, for your help and support over the years on our shared paths through graduate school.

I owe a huge dept of gratitude to my various funders. This work was supported in part by the Edwin V. Sisson Doctoral Fellowship and National Science Foundation's Offshore Wind Energy Engineering, Environmental Science, and Policy IGERT, number 1068864. Additionally, I recieved assistantships from the UMass Amherst Wind Energy Center for a variety of projects over the years.

ABSTRACT

CONSIDERATIONS FOR THE DESIGN OPTIMIZATION OF FLOATING OFFSHORE WIND TURBINE BLADES

SEPTEMBER 2020

EVAN M. GAERTNER

B.Sc., JAMES MADISON UNIVERSITY

M.Sc., UNIVERSITY OF MASSACHUSETTS AMHERST

Ph.D., UNIVERSITY OF MASSACHUSETTS AMHERST

Directed by: Professor Matthew A. Lackner

Floating offshore wind turbines are an immature technology with relatively high costs and risk associated with deployment. Of the few floating wind turbine prototypes and demonstration projects deployed in real metocean conditions, all have used standard turbines design for onshore or offshore fixed bottom conditions. This neglects the unique unsteady aerodynamics brought on by floating support structure motion. While the floating platform has been designed and optimized for a given rotor, the global system is suboptimal due to the rotor operating in conditions outside of which it was design for. If the potential offered by floating wind turbines is to be realized, offering access to deep water near-shore, costs need to continue to be reduced. This dissertation is the first known design study that considers the optimization of wind turbine rotors specifically for floating conditions.

Two design optimization methodologies are presented using different analysis fidelity levels. A relatively computationally efficient, state-state blade element moment

optimization of floating wind turbine blades is presented that will be useful for future systems level optimization studies. A higher fidelity methodology is then presented, using time-domain aeroelastic simulations to fully capture the unsteady aerodynamics and dynamic couplings between the rotor and platform motion throughout the optimization process. The principal finding of these studies is that low induction rotors are a promising technology pathway for future FOWT systems, reducing the severity of cyclical loading due to platform motion.

TABLE OF CONTENTS

LIST OF TABLES

Table **Page**

LIST OF FIGURES

Figure **Page**

CHAPTER 1

INTRODUCTION

1.1 Motivation

Floating offshore wind turbines (FOWTs) are a promising technology that allow access to deeper waters further from shore, avoiding view-shed and competition of use constraints nearshore. However, their non-ridged mooring systems introduce six additional translational and rotational degrees of freedom as the system moves in response to wind and waves, increasing the unsteady aerodynamic loading of the rotor [137]. Fore-aft motion of the platform in the direction of the incoming wind causes an additional effective flow velocity and causes complex interaction with the rotor wake [136]. Even low-frequency motion can cause highly unsteady responses for portions of the blades as a result rotor-wind misalignment, resulting in increased variability due to rotational sampling. Peak loads and fatigue damaged are subsequently increased compared to onshore or fixed-bottom offshore wind turbines due to more unsteady loading conditions.

Since floating support structures are a novel technology representing a significant leap in complexity, existing wind turbine designs have been employed on the small number of prototypes and demonstrations projects. This approach neglects the fundamentally different flow conditions at FOWT rotors. While floating support structures are optimized for existing turbine designs, use of turbine rotors outside of their original design space may be leading to suboptimal global systems. Optimization of turbine rotors specifically for use on floating support structures offers the potential to improve performance and reduce loads, with the goal of reducing cost of energy

and increasing reliability. A multi-disciplinary, systems engineering optimization approach is necessary due to the complex design challenges brought on by the coupled dynamics of the platform motion, mooring system, and turbine control systems. Such an approach must also account for the effects of variable metocean operating conditions throughout the design process.

This dissertation focuses on the design of horizontal axis, upwind, FOWT blades for the specific unsteady aerodynamic condition that result from platform motion. Alternatively, platform motion could be reduced through platform design, for example by using a stiffer mooring system or increasing the ballast. Advanced controls methods for the blade pitch system or additional structural, hydrodynamic, or mooring line tensioning control devices could be used to help damp platform motions. Alternate turbine configurations like light-weight, highly flexible, downwind blades might also offer weight and cost savings. These alternative design problems help illustrate the challenge and complexity of FOWT design. For the technology readiness of FOWT to continue to improve, all of the above approaches need to be explored to find the most cost-effective solutions. System level optimization of the full FOWT system and controller can explore the tradeoffs between different technology pathways and reach a more globally optimal solution. This work aims to increase the understanding of how blade technology for conventional horizontal axis, upwind turbines can be optimized and improved for FOWT applications, as a step towards the larger goal of system level optimization of the full system.

1.2 Objectives and Contributions

This work consists of comprehensive design studies considering the optimization and design of floating offshore wind turbine blades. The contributions of this dissertation are:

- A pareto-front based steady-state optimization method was developed for optimizing FOWT blades without the computational expense of dynamic simulations. This methodology allows designers to explore high level trade-offs between loading and annual energy production and will be especially useful for systems level analysis of FOWT.

- A higher fidelity time-domain optimization methodology is presented. This allows more detailed blade design and analysis of FOWT, exploring the coupled dynamics of the rotor and platform motion.

- Low induction rotors were found to be a more optimal solution for FOWT applications. Lower thrust on the rotor compensates for the increased dynamic loading, enables longer blades than can extract additional energy, and reduces average platform kinematic modes.

- Numerous contributions where made to open source design optimization tools included in NREL's WISDEM toolbox. This includes an ontology for wind turbine blade designs between analyis codes and researchers.

1.3 Document Outline

Chapter 2 provides background information and a review of the relevant literature to support the research presented in the subsequent sections. Topics include floating offshore wind turbines, low-order aerodynamic modeling, wind turbine blade design, and design optimization. Chapter 3 discusses the software tools and reference models used in this studies, highlighting contributions to those tools where applicable. In Chapter 4 methods used for optimizing floating offshore wind turbine blades in the following chapters are discussed. Chapter 5 highlights challenges in the FOWT design space and proposes a low-order, steady-state optimization methodology that accounting for those differences. This is expanded upon in Chapter 6 which uses

dynamic time-domain simulations in the optimization of FOWT blades. Finally, Chapter 7 presents conclusions and discusses opportunities for future work.

CHAPTER 2

BACKGROUND

2.1 Floating Offshore Wind Turbines

2.1.1 Overview

Europe has lead the globe in the development offshore wind. Starting with the first 5 MW offshore wind farm in Denmark in 1991, installed capacity reached 18.5 GW in 2018 [157]. The United States (U.S.) has been slower to develop its offshore potential, with the first offshore farm completed in 2016 off Block Island, Rhode Island. Building on the European experience and with a large available resource, the U.S. offshore wind industry is in a position to grow rapidly. In the scenario laid out in the Department of Energy (DOE) Wind Vision [150], U.S. offshore installed capacity could reach 22 GW by 2030 and 86 GW by 2050, supplying 2% and 7% of the total U.S. electricity demand respectively. This would require development of only 4.2% of the technically feasible resource area within 200 nautical miles (nm) from shore [117].

Offshore wind is an attractive option because generation can be located in close proximity to coastal city load centers. Relative to development onshore, there are fewer potential conflicts such as competition of use and acoustic and view shed concerns. Higher capacity factors can be achieved offshore since the wind speeds tend to be higher and with less turbulence. Additionally, without the restrictions of onshore transportation, offshore turbines can also be significantly larger; GE has announced plans to offer a 12 MW offshore wind turbine, the Haliade X [51].

Development of fixed bottom offshore wind has been limited to depths of approximately 50 m, shown in Figure 2.1. Monopile foundations are depth limited to about

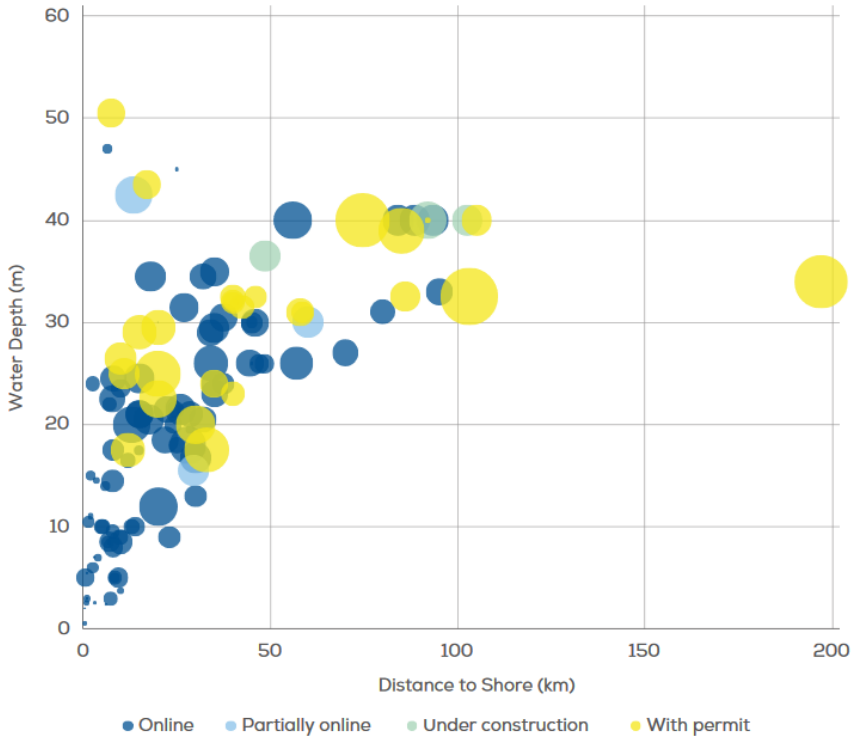

Figure 2.1: European offshore wind farms, bubble size indicates relative capacity [157]

30 m due to engineering constraints on tower skin thickness and resonance avoidance. Multi-member structures such as jackets are limited to about 60 m, largely due to manufacturing and installation costs [118]. An estimated 58% of the technically feasible U.S. wind resource is at depths greater than 60 m [117]. This is especially important for regionals with deep water close to shore such as the Gulf of Maine, the West Coast, and Hawaii in the United States and the Mediterranean Sea and off the coasts of Japan internationally.

Floating support structures are needed in order to provide access to deep water and expand the feasible regions for development. Honnef [71] is credited with first known floating offshore wind turbine (FOWT) concept in 1932, a large multirotor system on anchored pontoons. FOWTs were first analyzed in detail and popularized by William Heronemus [24, 70, 145] in the 1970s at the University of Massachusetts

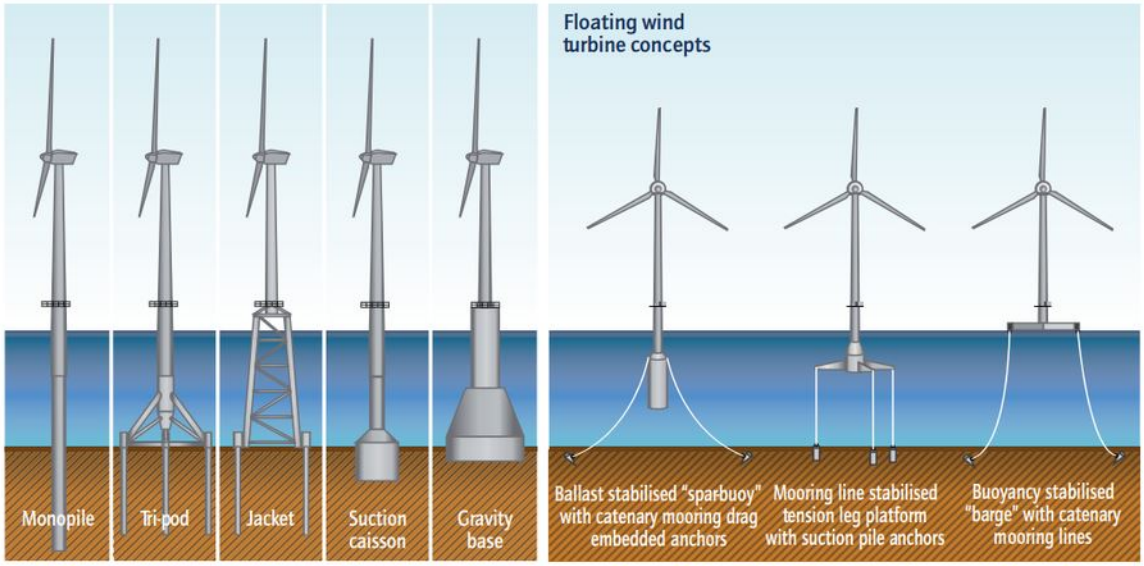

Figure 2.2: Fixed-bottom and floating foundations for offshore wind turbines [36]

Amherst, who proposed flotillas of multi-rotor wind ships using electrolysis to produce and store hydrogen and ammonia. As the wind energy industry matured in the 1990s and early 2000s, FOWT concept designs and feasibility studies were further developed by the engineering research community [3, 64, 69, 115, 148], drawling on knowledge and experience from the offshore oil and gas industry. The first floating prototype was deployed by Blue H Technologies off the coast of Brindisi, Italy in 2007, consisting of a two bladed turbine on a tension leg platform [72]. A wide variety of floating concepts have since been proposed and several prototyped, summarized in [75, 161], but all achieve stability through a combination of ballast, buoyancy, and mooring line tensions, shown in Figure 2.2. As the technology has improved, the first pilot floating offshore wind farm was commissioned in 2017, Hywind Scotland, consisting of 5 6 MW turbines installed on spar buoys.

In addition to providing access to deeper water, FOWTs offer several potential benefits including reduced installation costs, higher wind speeds over deeper water, fewer ecological impacts, and standardized manufacturing through reduced sensitivity

to site conditions [116]. Economic forecasting suggests that as FOWT technology matures, FOWTs could reach cost parity with fixed-bottom offshore wind turbines in the 2030s [4]. Such low-cost scenarios envision mass production of floating wind turbines that are erected in port and towed out for installation, minimizing the need for at-sea heavy lifting operations that require specialized vessels [34].

2.1.2 Unsteady Aerodynamics

The non-rigid mooring system of FOWTs introduces 6 translational and rotational degrees of freedom, shown in Figure 2.3. The platform kinematic response significantly increases the unsteady aerodynamic loading on the turbine rotor as the fore-aft motion creates additional cyclical velocity components [137]. Non-axial flow through the rotor results from operational pitching motions that can be as high as 8° for floating platforms with catenary mooring systems [107]. Rotational sampling of the skewed inflow causes increased instances of dynamic stall near the blade root [49]. Additionally, fore-aft motion causes complex rotor-wake interactions, resulting in time-varying changes in the induction through rotor [136].

Modeling the coupled aerodynamic, hydrodynamics, structural dynamics, and controller interactions for a floating wind turbine is quite challenging. As a result, most research to date has used low order aerodynamic models such as blade element moment theory (BEM, see Section 2.2.2) and dynamic inflow models. One of the most commonly used tools, FAST (see Section 3.1.1), has been used to show increased loads for a wide range of floating platforms configurations. A growing body of work has used higher order aerodynamic methods to analyze the unsteady aerodynamics of FOWT, however this has come with the trade-off of decoupling the platform kinematics and aerodynamics, using prescribed platform motions. Sebastian and Lackner [136, 137] developed a free vortex wake model (FVM), WInDS, to model floating wind turbines with prescribed floating platform motions. They found that platform motion induced

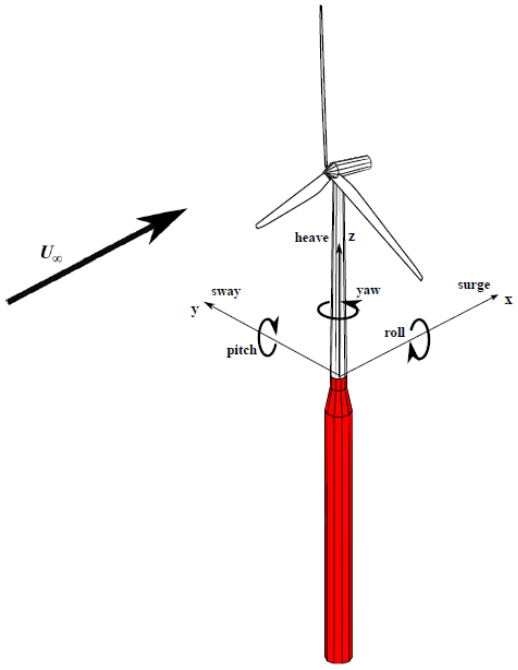

Figure 2.3: Floating offshore wind turbine platform degrees of freedom [137]

rotor-wake interactions can result in violations of the underlying assumption in blade element moment (BEM) models. This is primarily a problem at low wind speeds, where the platform induced velocity component is relatively large, and at high tip speed ratios, where shed tip vortices are more closely spaced and have a larger impact on the rotor induction. Sant et al. [41, 134] has built on this work, comparing experimental observations with WInDS FVM results. They found that under prescribed single DOF platform surge for a tension leg platform, rotor power standard deviation increases with tip speed ratio. Computational fluid dynamics (CFD) analysis of floating wind turbines under prescribed motions have reached similar conclusions, that the magnitude of unsteady aerodynamic load variations are very sensitive to the metocean conditions [97, 149].

2.1.3 Fatigue and Ultimate Loads

The overall effect of platform kinematics in response to wind and wave loading on a FOWT is increased peak loads and fatigue damage compared to onshore or fixed-bottom offshore wind turbines. In general, blade root bending moments are relatively insensitive to wave conditions, being driven almost entirely by the wind loading for flapwise bending and gravity for edgewise bending. Tower base bending moments however, are far more sensitive to the wave loading and wind-wave misalignment, being driven primarily by platform pitch and roll.

The magnitude of load changes relative to onshore turbines is specific to the platform design and stability method several authors have compared the loads for different floating concepts [85, 106, 132, 143, 154]. Tension leg platforms, with the least platform pitch and roll, are the most similar to fixed-bottom systems. Spar buoys and semi-submersibles with catenary mooring systems have increased platform pitch and roll, and consequently, larger tower base bending moments. These platforms can actually have lower blade root bending moments due to modifications to the above-rated pitch controller. This is necessitated by conditions with very large surge displacements, where the platform pitch frequency is reduced, potentially leading to controller induced instabilities. Platform pitch and roll also drive increased bending moments on nacelle components such as the drivetrain and yaw bearing. Loading on the anchors are more complex, as they are more sensitive to wind, waves, and directionality, and the response is far more specific to the platform design.

2.1.4 Design Challenges

All existing FOWT prototypes and pilot projects have used existing fixed-bottom offshore wind turbine designs [114]. Insufficient demand and uncertainty about the future market for FOWTs have made investing in floating-specific turbine technology too risky for turbine manufactures. Design of floating wind turbine components is

particularly challenging due to the dynamic couplings between subsystems. This can create non-convex design spaces, making optimization more challenging, caused by non-linearities in the system. Sources include mooring line dynamics, control actuation, and breaking waves. The coupled dynamics also mean that a change in the design of one subsystem will have potentially large impacts on others; changes to aerodynamic properties will also causes changes in the hydrodynamic response and vice versa. Increased mass above the waterline requires an increased volume of displaced water to maintain buoyancy, requiring larger, more costly floating support structures. For a spar-buoy platform, Young [160] found that removing 1 kg of tower or rotor-nacelle assembly (RNA) mass allowed 2 kg of steel and 7 kg of ballast to be removed from the floating foundation. The controls system also significantly impacts the loading and performance of a FOWT; it can potentially be used to damp platform motions, but can also cause controller induced instabilities and negative damping that exacerbate platform motions. Proposed controls strategies and devices for FOWT including structural tuned mass and liquid column dampers, dynamic mooring line tensioning, and modifications to existing generator torque and blade pitch control strategies [42, 83, 90, 92, 123, 151]. Complete systems level design optimization studies of the full rotor, tower, floating platform, moorings, and control systems are needed to continue to reduce mass and system costs, however this has proven to be an intractable problem to date. To mature the technology, the design challenges are not only limited to component design, but also include simplifying installation, reducing maintenance requirements, standardizing designs for different depths and soil conditions, better characterization of metaocean conditions, and continually improving and reducing uncertainty in design and modeling software tools [16, 107, 161].

2.2 Low-Order Aerodynamic Modeling

2.2.1 Overview

Wind turbines operate in complex unsteady flow fields. Environmental effects in the incoming wind field include turbulence, gusts, atmospheric boundary layer interactions, directional and vertical shear, and upstream turbine wakes. Additionally, the dynamics of the turbine can increase the unsteadiness of the aerodynamic loads, such as rotor yaw, wake-tower interactions, wake-rotor interactions, and displacements from blade bending and flapping. The rotor experiences three-dimensional effects like spanwise flow and vortex shedding off the blade tip which are a modelling challenge for lower order analysis methods.

The combination of these factors makes it quite difficult to predict accurate estimates of aerodynamic loads and performance [94]. Even experimental measurements from a controlled setting are difficult to reproduce. This was demonstrated by Sims et al. [140] where a blind comparison of twenty independent aerodynamic models was conducted, validated against wind tunnel data. In the simplest case of no-yaw, steady state, and no-stall, power predictions ranged from 25% to 150% of the measured value and blade bending predictions range from 85% to 150%.

A wide range of modelling methods are available, providing tradeoffs between the rigorousness in the representation of the physical phenomenon and the computational intensity. The following section will provides a brief overview of Blade Element Moment Theory (BEM) for horizontal axis wind turbines. This method is employed by the software tools used in this work and introduces many key concepts to wind turbine rotor design. Higher order methods such as Free-Vortex Wake Methods (FVM) and Computational Fluid Dynamics (CFD) are beyond the scope of this work due to their high computational costs.

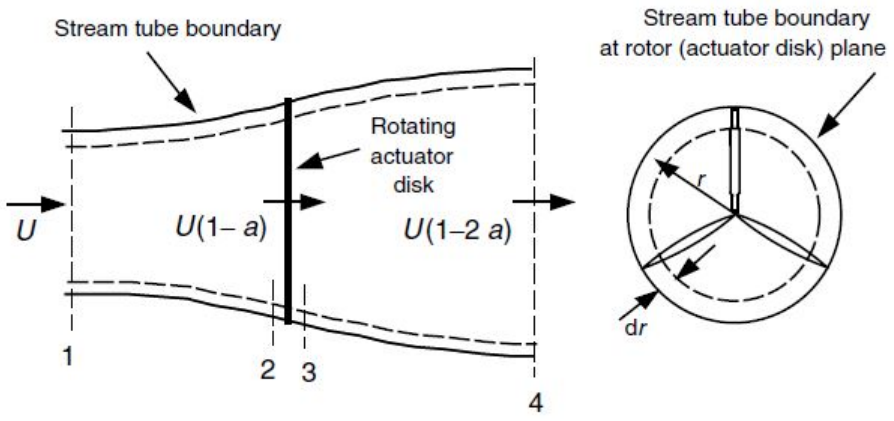

Figure 2.4: Stream-tube model for flow through an actuator disk [104]

2.2.2 Blade Element Momentum Theory

Blade element momentum theory is one of the simplest and most commonly used analysis methods for estimating the aerodynamic loads on wind turbines. Classical BEM solutions are typically attibuted to Betz [7] and Glauert [54] and further adapted for numeric simulations by [25, 155, 156].

Under classical 1-D momentum theory, the rotor is represented as an actuator disk that induces an instantaneous drop in pressure as kinetic energy is extracted from the flow. The mass flow rate is constant, causing the stream-tube control volume to expand as velocity decreases downstream, shown in Figure 2.4. The axial induction factor, a, is defined as the fractional decrease in flow velocity between the free stream and the rotor disk:

$$a = \frac{U_1 - U_2}{U_1} \quad \text{or} \quad U_2 = U_1 (1 - a) \tag{2.1}$$

Bernoulli's equation can be applied to show that the downstream wake velocity, U_4, is

$$U_4 = U_1 (1 - 2a) \tag{2.2}$$

The force acting on the rotor, thrust (T), can then be expressed as the conservation of momentum in a linear, steady, incompressible flow, where ρ is the air density and A is the cross section area of the actuator disk.

$$T = \frac{1}{2}\rho A\left(U_1^2 - U_4^2\right) = \frac{1}{2}\rho A U^2\left[4a\left(1-a\right)\right] \tag{2.3}$$

The power out of the rotor, P, is thrust times the velocity at the rotor:

$$P = \frac{1}{2}\rho A U^3\left[4a\left(1-a\right)^2\right] \tag{2.4}$$

It is often more useful to express power and thrust as non-dimensional coefficients of power and thrust to be used as performance metrics, shown in Equations 2.5 and 2.6. This represents the percentage of power available in the wind that is extracted by the rotor.

$$C_P = \frac{P}{\frac{1}{2}\rho A U^3} = 4a\left(1-a\right)^2 \tag{2.5}$$

$$C_T = \frac{P}{\frac{1}{2}\rho A U^2} = 4a\left(1-a\right) \tag{2.6}$$

Momentum theory is valid for $a < 1/2$, after which it predicts a downstream flow circulation. In reality, the flow beginnings to transition to a turbulent wake state for $a = 0.4 - 0.5$ requiring more sophisticated models or empirical corrections [67]. The theoretical maximum $C_p = 16/27 \approx 0.5926$ is achieved when $a = 1/3$, known as the Betz limit.

In 1-D momentum theory discussed thus far, the actuator disk is an unspecified device causing the drop in pressure. A rotating disk like a wind turbine rotor, however, turns with some angular velocity, Ω, and experiences an aerodynamic torque. Under 2-D angular momentum theory, an equal and opposite toque is applied to the air passing through the rotor, resulting in rotation of the downstream wake. The tangential induction factor, a', is used to express the change in tangential velocity over the rotor

disk. The velocity directly behind the rotor is defined in Equation 2.7, where r is the local radial distance. The addition of rotational kinetic energy to the wake reduces the energy available to be extracted by the rotor, reducing C_P as a function of the tip speed ratio.

$$U_\theta = 2\Omega r a' \tag{2.7}$$

BEM is based on the classical momentum theory presented thus far, extended to rotors with a finite number of blades with a given geometry. The stream tube is discretized into annular elements of size dr. The local aerodynamic forces are calculated at each element and integrated to give the total loads over the full rotor. The full set of equations can be found in [15, 67, 104, 111], however the general solution method is described in Algorithm 1 [67]. The various forces, angles, and velocites in Algorithm 1 are defined in Figure 2.5.

To improve the accuracy of the model, a number of semi-empirical corrections must be applied. Tip and hub loss models, such as Prandtl's [54] or Goldstein's [55] accounts for vortex shedding near the blade root and off the blade tips. The Glauert correction [53] accounts for turbulent wake states where $a > 0.4$; an empirical correction for the turbulent mixing for of the wake with the surrounding air where momentum theory predicts non-physical flow reversal. BEM assumes axisymmetric flow, several corrections [53, 66, 122, 127, 141] extend the model for skewed inflow, however these models are highly empirical and assume a lightly loaded rotor. A dynamic stall model [94] improves peak load predictions during transient stall events. Three-dimensional span-wise flow effects are accounted for using stall-delay models [29, 37] that modify the airfoil lift and drag properties.

Despite the many limitations and reliance on empirical corrections, BEM theory is still in heavy use in wind turbine design and research due to its computationally efficiency. For example, a recent reformulation of the model [119, 122] offers more robust and faster convergence for use in gradient-based optimization problems. This

Algorithm 1: RotorSE/OpenFAST based blade design optimization

Data: Rotor geometry, instantaneous element-wise velocity
Result: Rotor loads

```
for all time steps do
    while Δa > tolerance do
        Calculate flow angle, φ
        Calculate the angle of attack, α
        Calculate or table look-up C_l(α) and C_d(α)
        Calculate C_N(φ) and C_T(φ)
        Calculate a and a′
    Calculate local and total blade loads
```

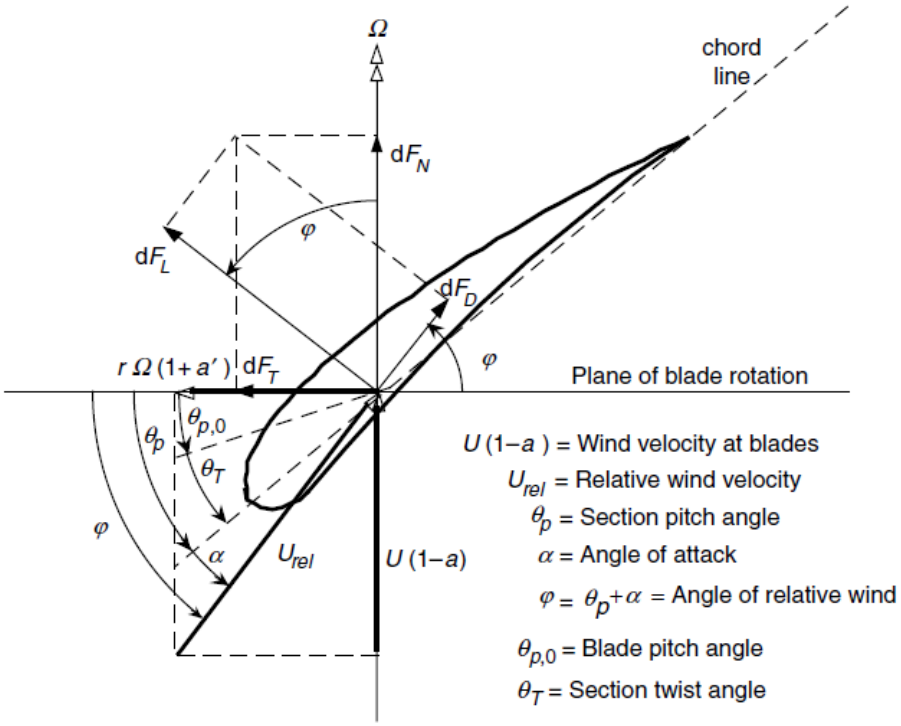

Figure 2.5: Forces, angles, and velocities for a blade element [104]

was accomplished by expressing the BEM equations in terms of the inflow angle, φ, rather than the induction factors a and a', going from a two-variable, two-equation fixed-point iteration problem to a one-variable, root-finding problem.

2.3 Wind Turbine Blade Design

Wind turbine blades are the load bearing aerodynamic structure by which wind turbines extract kinetic energy from the wind. Modern wind turbine blades consist of an aerodynamic shell that is supported by internal shear webs and spar caps, shown in Figure 2.6. The design must meet a number of conflicting goals:

- Maximize the annual energy production (AEP) through aerodynamic efficiency
- Survive extreme and fatigue loads
- Limit tip deflection to prevent striking the tower
- Avoid resonance and aeroelastic dynamic instabilities
- Limit aeroacoustic noise
- Minimize costs from materials, manufacturing, installation, operation and maintenance and impacts on other system components

This dissertation is focused on the design of blades for up-wind, variable speed, horizontal-axis wind turbines (HAWTs), which are the most common configuration in the modern wind industry. Several topics in wind turbine blade design are discussed in the following sections.

2.3.1 Aerodynamic Considerations

BEM theory can be used to determine the chord and twist distribution to produce a Betz theoretical optimal C_P. The maximum achievable C_P is a function of the tip

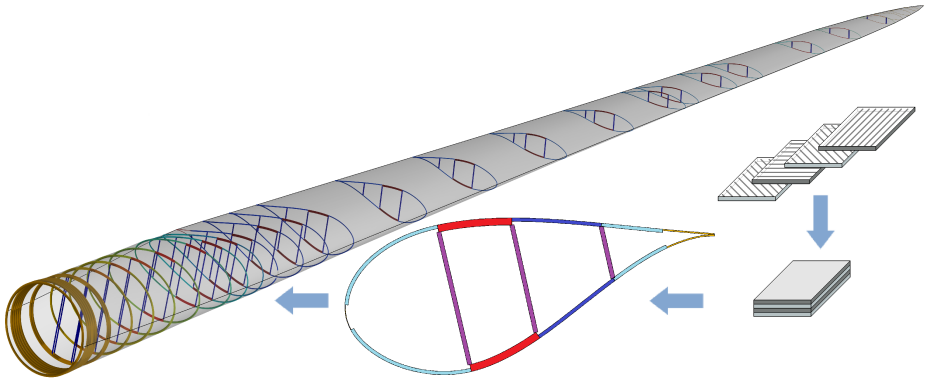

Figure 2.6: Typical layout of a utilitiy scale wind turbine blade [133]

speed ratio (λ), the number of blades, and the lift to drag ratio of the blade airfoils, as shown in Figure 2.7.

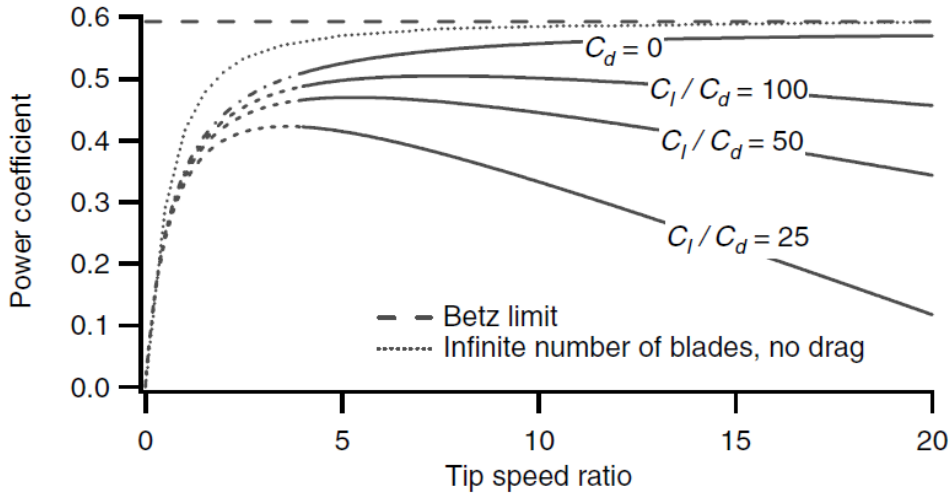

Figure 2.7: Betz optimal C_P for a three-blade wind turbine with drag and wake rotation [104]

The design tip speed ratio, the ratio between the blade tip speed and the free stream wind, is one of the most important design drivers. To a point, increasing the tip speed ratio will increase C_P, with most utility scale wind turbines operating in the $\lambda = 6$ to 10 range. Low tip speed operation, with high torque, results in larger

wake rotation losses. Additionally, lower torque from higher tip speed ratios can offer significant cost saving through smaller drive trains and gearboxes [121, 130]. The maximum allowable tip speed is limited by aeroacoustic noise considerations [112], however this may be less of a factor for offshore wind turbines.

Figure 2.7 clearly demonstrates the negative effects of aerodynamic drag, necessitating the use of airfoil families with high lift to drag ratios. Due to the blade rotation, the relative wind speed increases towards the blade tip, changing the angle of attack distributions along the blade. The blade twist orientates the airfoils at their optimal angle of attack to provide the maximum lift to drag ratio at the design tip speed ratio. Wind turbine airfoils are also designed to be less sensitive to leading edge roughness, which can result from surface erosion and fouling from insects. Opperating at higher tip speed ratios can lead to increased surface erosion. Roughness on the leading edge surface can cause premature flow separation, decreasing lift and increasing drag, if unaccounted for.

A number of practical simplifications must be made to the optimal aerodynamic design, reducing its overall efficiency. Cylindrical sections are used at the blade root so the blade can be connected to the pitch bearing and to provide additional stiffness to overcome large root bending moments. The blade smoothly transitions from cylindrical sections to thick airfoils for the first 10 to 20% of its length. This is a significant departure from large chords near the root for a Betz optimal blade, which are impractical for both structural and cost concerns. Airfoil thickness gradually decreases down the length of the blade to improve aerodynamic performance as the strucutural load carrying requirements decrease. The chord and twist distribution are typically simplified to reduce manufacturing complexity, for example by using a linear taper. Ultimately, the maximum chord or blade curvature is limited by transportations constraints, particularly onshore.

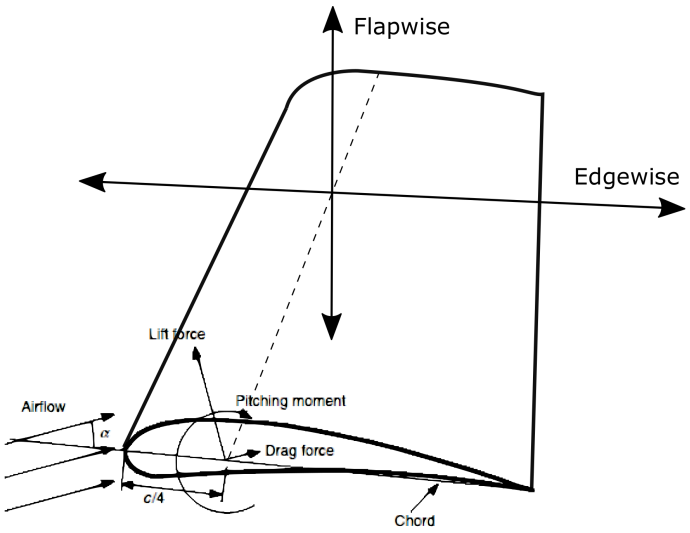

Figure 2.8: Blade flapwise and edgewise coordinate system. Adapted from [104]

A wide range of advanced aerodynamic design topics are beyond the scope of this work. Swept blades, curved in the direction of the rotor plane, can use bend-twist coupling to reduce fatigue loads and reduce noise [1, 98]. Blade tip winglets can be used to reduce vortex shedding tip losses [147], however this might come with impractical structural costs. A number of relatively low cost passive flow control devices can be added to the blade surface to improve stall characteristics or reduce noise, such as vortex generators [113], spoilers [138], and trailing edge serration [108].

2.3.2 Structural Considerations

2.3.2.1 Loads

Loads on wind turbine blades can be divided into aerodynamic, gravitational, inertial, and operational. These can act on the blade in the coordinate system shown in Figure 2.8, where flapwise and edgewise are respectively the weak and strong principle axes. Due to blade twist and pitch, they do not lie in the plane of rotation, however roughly speaking flapwise is perpendicular and edgewise is parallel.

During operation, aerodynamic thrust causes the blades to bend in the flapwise direction. The blade must be stiff enough to prevent the tip from striking the tower, which would result in catastrophic failure. This is a significant design driver in the blade stiffness requirements. Flapwise bending also places the suction side of the blade under compression. This can result in buckling, typically occurring spanwise where chord is the largest or near the blade root at the trailing edge [59, 120]. Buckling is an important consideration in the design of composite layer thicknesses and in the placement of shear webs and reinforcement panels, potentially increasing blade mass.

As wind turbine blades get larger, gravitational loads are of increasing concern. Blade mass increases roughly cubicly with blade length according to conventional scaling laws [59]. The blade experiences large cyclical gravity loads as the blade is under compression at the top of its rotation and under tension at the bottom. Large blades experience substantial edgewise bending moments, with the largest occurring at the blade root at the horizontal position. For conventional fiber glass blade designs larger than approximately 40 m, the gravity dominant edgewise fatigue equivalent load at the blade root exceeds the aerodynamic dominant flapwise fatigue equivalent loads [15, 59]. The design of the blade root is therefore governed by fatigue loads and significant fatigue analysis and testing is required in the design standards [73].

Operational loads are also an important consideration. They are typically characterized as loads resulting from controller actions such as braking, yawing, or blade-pitching, or a failure that prevents such actions. Wind turbine design certification process requires extensive simulations of candidate designs, outlined in [27, 73, 74]. The governing design load cases often include extreme turbulence during normal operation, emergency shut down breaking, and a parked turbine during an extreme storm with no power to the control systems [135].

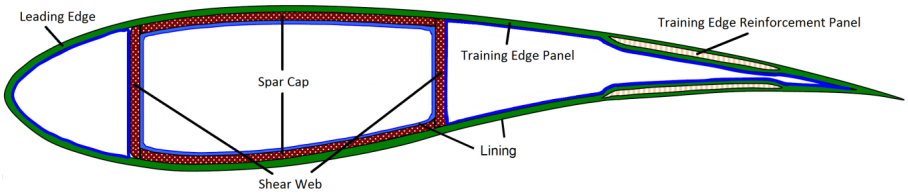

Figure 2.9: Example blade cross section using two shear webs

2.3.2.2 Structural design

The interior of a wind turbine blade provides the structural support for the aerodynamic skin. Figure 2.9 shows a typical design and nomenclature. One or more shear webs provide the main support, resisting blade bending in the flapwise direction. The spar caps transfer loads from the outer aerodynamic skin to the shear webs and provide additional stiffness in the edgewise direction. Reinforcement panels might be used in sensitive areas, like the leading and trailing edges, to prevent buckling.

Modern blades are constructed with composite materials due to their high strength, high stiffness to weight ratio, and ease of shaping to aerodynamic forms. Fiberglass in a polyester resin are the most common, however vinyl ester and wood-epoxy laminates are also in use [104]. Carbon fiber can be added to reinforce glass composites, taking advantage of its superior strength properties, but at much higher costs. "Sandwich" designs are common for shear webs and trailing edge reinforcement, where a foam or balsa wood core is placed in-between two composites layers.

Typically blades are manufactured in two parts, with separate molds for the suction and pressure sides of the blade. The spar caps and shear webs are also manufactured separately. The finally blade is constructed by bonding together these separate parts, including a hub connection piece.

2.3.3 Large Rotors

Wind turbine rotor sizes have steadily increased over time, shown in Figure 2.10 for United States onshore machines. This trend is primarily driven by economies of scale, where the installation and balance of system costs for a smaller number of larger turbines is lower. This also explains the rapid growth in the size of offshore turbines, where installation and operation and maintenance costs are much higher and blade size is not constrained by onshore transportation.

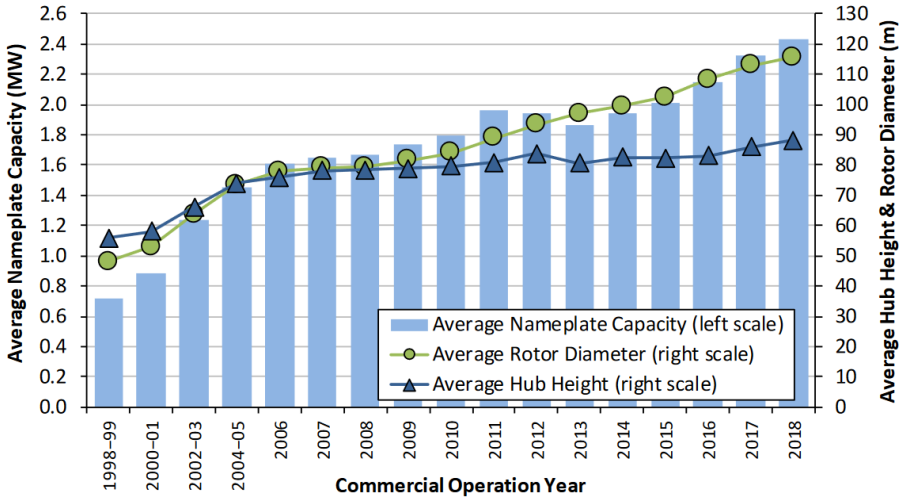

Figure 2.10: Trend in rotor size over time [158]

Embedded in the trend towards larger turbines is a trend towards lower specific power, shown in Figure 2.11. Specific power is the ratio of turbine nameplate capacity to swept area, effectively achieved by using larger blades for the same generator size. This can enable higher capacity factors, and thus higher energy production, by operating at rated power a higher percentage of the time. Lower specific power turbines are a key technology to enabling cost effective development of lower wind speed sites.

Similarly, low induction rotors, characterized as having an axial induction $a < 1/3$, are an active area of research. As induction decreases, the thrust coefficient (C_T)

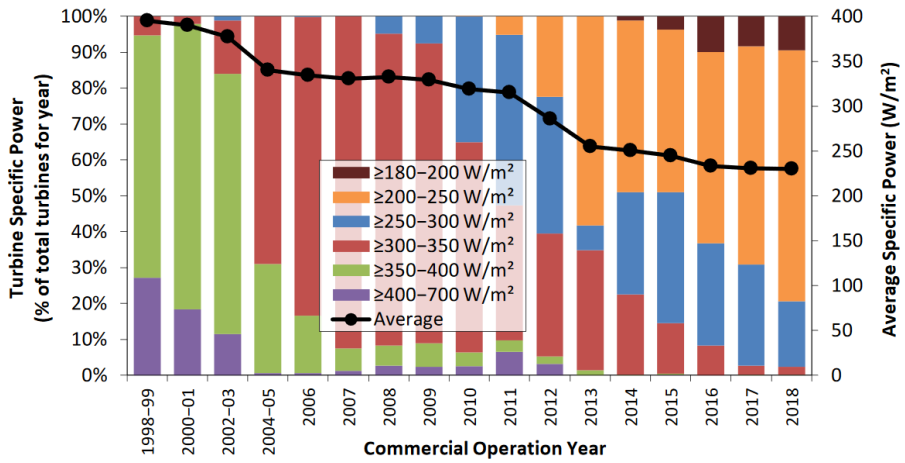

Figure 2.11: Trend in rotor specific power over time [158]

decreases faster than the power coefficient (C_P). Maintaining constant loading on the blades and decreasing induction, it is possible to increase energy captured with longer blades operating at lower C_P. This can have positive impacts on the rest of the system design, where the loading on the drivetrain and tower are potentially reduced at increased power production. Chaviaropoulos et al. [18, 19] showed the for constrained root bending moment, AEP was optimized at $a = 0.2$. Kelley [88] similarly showed a parametric blade optimization study, applying different relative weights to the objectives of maximum C_P and AEP, with constrained blade root bending moments. A 11% increase in rotor diameter allowed a 5% increase in AEP; larger increases in AEP are possible, but with diminishing returns as blade length begins to grow much faster. All low induction rotors have a low specific power, but low specific power rotors are not inherently low induction.

2.4 Design Optimization

A wide range of previous research has addressed many aspects of wind turbine design optimization [13, 28, 46, 47, 48, 89, 102]. Projects have ranged from aerodynamic optimization of airfoils, shape optimization of rotor blades, and systems engineering

approaches to optimize full wind turbine systems. An exhaustive summary of the literature can be found in [20]. The following sections will provide an overview of objective functions, constraints, algorithms, and design under uncertainty, as they relate to HAWT rotor optimization.

2.4.1 Objective Functions

BEM theory can be used to maximize the power coefficient of a wind turbine rotor to the theoretical limit. However, the resulting C_P is only maximized at the chosen design point. A more effective measure of aerodynamic performance is the annual energy production (AEP) for a probability density function (PDF) of expected operating conditions. This is still an over simplified design objective though; in reality a wide range of structural, manufacturing, transportation, installation, and operation and maintenance factors require significant design tradeoffs. Using AEP as an objective function is also not a well formulated optimization problem because it can yield non-unique solutions, where multiple blade designs with different masses yield very similar AEPs. Aerodynamic only optimization can lead to unrealistic designs. For example, in the absence of a structural model, cylindrical root diameters are reduced to decrease drag. This neglects structural requirements for blade stiffness and providing adequate space for bolt connections to the pitch mechanism.

Thus, aerodynamic performance alone is not a sufficient design objective, nor any other single engineering performance metric. There is growing consensus that cost of energy (COE) is the most appropriate objective function because it improves the competitiveness of wind energy compared to other generation technologies [20, 31]. Equation 2.8 defines COE, where FCR is the fixed charge rate, TCC is the turbine capital costs, BOS is the balance of station costs, and OM is the operation and maintenance costs.

$$COE = \frac{FCR \cdot (TCC + BOS) + OM}{AEP} \tag{2.8}$$

Minimizing COE is inherently multi-disciplinary, requiring the inclusion of a structural models and a wide range of other cost models for manufacturing, installation, balance of station, and financing. While this may require a large number of assumptions, a detailed cost model allows for wide ranges of design tradeoffs and their implications to be accounted for. Furthermore, the solution tends to activate the physical constraints on the problem, rather than somewhat arbitrary design variable bounds. For example, an improvement in AEP is not practical if it increases the capital costs at a faster rate in order to maintain stiffness requirements. Using cost of energy as an objective for offshore design optimization studies may be problematic, however, since there is considerably less data available, particularly in new markets like the United States or for new technologies like FOWTs [118].

When a cost model is not available, minimization of mass per unit of AEP, m/AEP, is often used as a surrogate to capital costs. This is based on the assumptions that $m \propto TCC$ and TCC is the most sensitive portion of total costs to changes in turbine design. This metric has been shown to produce similar results as minimizing COE, successfully activating structural constraints. However, m/AEP can be sensitive to how design variables are selected and which components are included in the mass calculation. Including the tower design can yield the unintentional consequence of minimizing thrust, reducing tower loads to reduce tower mass, at the expense of AEP. A COE model, by comparison, would make the distinction that while the tower makes up a large percentage of the overall mass, it is a much smaller percentage of the overall TCC. Similarly, including blade length as a design variable can be problematic as mass scaling effects for some components may not accurately reflect cost scaling.

2.4.2 Constraints

Constraints on candidate blade designs are essential to ensure a realistic solution. At a minimum, blades need to be assessed to make sure they will not fail, satisfying tip clearance, buckling, fatigue, and resonance constraints. However, detailed analysis in an iterative design process comes at significant computational cost which may be prohibitive. A number of simplifying assumptions need to be made and as a result, the solution should be considered the preliminary design and may need additional post-processing using higher fidelity models and analysis techniques.

2.4.2.1 Tip Deflection

Design standards specify that under an extreme load condition, the blade tip to tower clearance must be greater than a fraction of the unbent distance, determined using partial safety factors [27]. If the tower design is unknown, tip deflection can be constrained relative to a reference turbine or initial design [120].

2.4.2.2 Fatigue

Fatigue analysis in wind turbines is conducted according to Miner's Rule [109]. Total lifetime damage is determined by rainflow counting the cumulative number of cycles at all operating states and stress levels that are expected over a lifetime of operation. When total damage is greater than 1, failure occurs. A subset of shorter times series can be used to extrapolate the lifetime damage, discussed in more detail in [68, 146].

Estimates of lifetime fatigue damage are very computationally expensive in an iterative design loop. In [32, 130], lifetime fatigue damage for each candidate design was determined from 66 10-minute simulations, representing 6 random seeds for 11 different mean wind speeds. For offshore designs, the required number of samples is significantly larger, where IEC design standards [74] stipulate a sampling grid of wind speed, wave height, wave period, and wind-wave misalignment, resulting in over

200,000 sample conditions. Graf et al. [56] determined that an integrated Monte Carlo sampling of these conditions can reliably reduce the required number of samples to about 1,000, however this is still impractical for most iterative design studies.

Clearly, simpler approaches are needed. Chehouri et al [21] made a number of simplifying assumptions about the stress states of the blade composites in order to derive a fatigue failure criteria from the Tsai-Wu criteria. Ning et al. [120] simplified the fatigue damage estimate to only include edgewise root-bending gravity loads. Bottasso et al. [13] assumed that structural loads change slowly relative to changes in the structural design variables, therefore the structural loads were assumed to be constant for small changes in the design variables. Fuglsang et al. [48] used a semi-emperical approach, creating an approximation of fatigue damage as a function of wind speed and turbulence intensity. This was calibrated based on a full fatigue analysis which was updated periodically throughout the optimization.

2.4.2.3 Buckling

Buckling is an important consideration for the composite aerodynamic shell of wind turbine blades, especially for large chord lengths near the blade root [50]. High-fidelity nonlinear buckling loads can be computed with a finite-element solver like ANSYS, a procedure which can be simplified by using NuMAD [6] to generate the 3D finite element model of the blade.

Lower fidelity models are more common for preliminary iterative design work. Ning et al [120] used the method proposed by Bir [9] to find a linear critical buckling strain for simply supported flat composite panels under compression. Sale [133] followed a similar procedure, but for curved panels under both shear and compression.

2.4.2.4 Resonance

Resonance can potentially lead to failures and increasing system natural frequencies helps reduce vibration and fatigue damage. The most common resonance avoidance

technique in HAWT optimization is a constraint on the first flapwise natural frequency such that it is greater than the 3P blade passing frequency, at all rotor speeds [13, 120]. Similarly, natural frequencies can be constrained to have minimum separation distances, set with safety factors [87, 95, 162]. Maalawi et al. [100, 101] went further, defining an optimization problem to maximize the blade natural frequencies in order to reduce vibrations.

2.4.3 Algorithms

Optimization algorithms used in wind turbine design can be divided into two main categories, gradient-based and gradient-free. The following sections provide a brief overview of their strengths and weaknesses, as applied to HAWT optimization problems. More detail on the formulation of individual algorithms can be found in found in [128] or a similar text.

2.4.3.1 Gradient-based Methods

Gradient-based methods are used in traditional optimization problems, with convex, differentiable design spaces. They are the preferred method whenever possible due to their fast convergence.

A number of conditions can prevent the use of gradient-based methods. Complex systems may be non-convex with multiple local minimums, preventing the global solution to be found or requiring multiple executions with different initial conditions. Discrete or integer variables cannot be used as they are non-differentiable. Discrete variables could include different system configurations, such as the number rotor blades or layers in a composite, or the selection of options in a list, such as airfoil or material selection. The use of numeric simulations to perform objective function evaluations can also lead to problems [103]. Numeric solver instabilities, discrete time steps, and internal convergency tollerances can lead to discontinues in gradient-based search methods.

Despite these limitations, gradient-based methods can be quite useful for wind turbine optimization problems given that the problem is well formulated. Fuglsang et al. [48] used Sequential Linear Programming (SLP) [43] in the aeroelastic optimization of rotors for site specific conditions. Sequential quadratic programming (SQP) [124] was used for similar studies [89, 120].

2.4.3.2 Gradient-Free Methods

Gradient-free methods, often refered to as meta-heuristics, are a broad field of optimization algorithms used for complex problems, often taking inspiration from nature. They provide a pseudo-global search that is less sensitive to local minima than gradient-based methods. Algorithms can be inherently multi-objective, where the optimum is the Pareto front solution set of non-dominant trade-off designs. Their main drawback is they require orders of magnitude larger computational costs, since most methods rely on probabilistic sampling of the design space. This can be improved through parallelization of objective function evaluations and by using hybrid gradient-based and gradient-free techniques.

Genetic Algorithms (GA) are by far the most common approach. They are based on natural selection concepts, where more fit designs are combined and pass on their traits to the next generation, with the potential for random mutations. These methods are well represented in the literature for HAWT optimization, examples include [5, 28, 38, 87, 139, 153]. Particle Swarm Optimization (PSO) is based on the behavior of animal colonies or swarms, where distributed individuals move through the design space, sharing information about the best positions with the population, which is used to inform their future positions. Examples of HAWT optimization using PSO include [39, 95].

2.4.4 Design under uncertainty

Several studies have focused on the influence of uncertainty in design optimization of wind turbine rotors using robust design techniques that seeks to minimize the variability of the system response to variable or uncertain inputs. The effects of geometric uncertainty derived from manufacturing tolerances has been minimized for turbine rotors [17, 110] and for offshore fixed bottom support structures [159]. Petrone et al. [126] optimized rotor blades while minimizing variability of aerodynamic performance and noise generation as a result of uncertainty from insect fouling on the blades. Finally, Ning et al. [120] addressed the importance of considering multiple wind speed probability density functions to account for meteorological variability in the location of an operating wind turbine.

CHAPTER 3

SOFTWARE DEVELOPMENT

A number of software tools have been created or modified to support this work. This chapter provides an overview of software tools used in this work and discusses contribution to those tools where applicable.

3.1 Software Tools and Reference Models

3.1.1 OpenFAST

OpenFAST (Fatigue, Aerodynamics, Structures, and Turbulence) [76, 80, 82] is a comprehensive open source computer-aided engineering tool, developed by NREL, for time marching simulations of operational horizontal axis wind turbines. OpenFAST is a multi-physics analysis tool that includes computational modules for aerodynamics, hydrodynamics of offshore support structures (floating or fixed bottom), controls and electrical systems, and structural dynamics, to give the coupled non-linear response of the system. FAST is widely used by the wind energy research community.

3.1.2 WISDEM

WISDEM is the Wind-Plant Integrated System Design and Engineering Model developed at NREL [35]. WISDEM is an open source multidisciplinary design, analysis, and optimization (MDAO) tool consisting of a suite of discipline specific Python submodules, from the component level to the plant level, that modelers can interconnect to answer multidisciplinary research question. Data exchange, workflow management, and optimization algorithms are provide through OpenMDAO, an open

sourced MDAO framework written in Python, developed at the NASA Glenn Research Center [57]. Key WISDEM modules relevant to this work include AeroelasticSE and RotorSE.

3.1.2.1 AeroelasticSE

AeroelasticSE is a Python-based FAST driver, supporting FAST7, FAST8, and OpenFAST. Key features include FAST text input file reading, writing, and modification, turbulent and IEC load case wind input file generation, parametric load case drivers, FAST execution with tools for HPC parallelization, and FAST output file parsing. Significant modifications to AeroelasticSE were made to support this work. Contributions include:

- Support for OpenFAST
- Inclusion of input file reading and writing for FAST hydrodynamics and offshore support structure modules, HydroDyn and SubDyn
- Wind file creation for IEC design load cases
- Creation of design load case drivers for generating FAST input file for arbitrary parametric studies or IEC DLC analysis
- MPI parallelization of FAST executions for HPC

3.1.2.2 RotorSE

RotorSE is the rotor aerodynamics and structural dynamics module in WISDEM. The complexity of modeling rotor dynamics is reflected in the large number of submodules used by RotorSE, described below.

CCBlade is the low fidelity rotor aerodynamics solver in WISDEM, using steady-state blade element momentum theory. The theoretical implementation is described

by Ning [119], providing guaranteed super-linear convergence with continuously differentiable solutions.

PreComp is a preprocessing tool for calculating the span-variant stiffness and inertial properties of wind turbine blades [10]. PreComp requires the detailed composite design as inputs. Structural properties are calculated using the analytic solution to a combination of classic laminate theory and a shear-flow approach. The resulting distributed properties can then be used as inputs to aeroelastic analysis codes such as FAST. PreComp was originally built as a stand-alone tool written in Fortran. It is now included in the RotorSE installation as a Python wrapped extension module that can be imported and executed from within Python scripts.

pBEAM (Polynomial Beam Element Analysis Module) is WISDEM's Euler-Bernoulli beam finite element code used for modeling wind turbine blade and tower deflections and strains. Its primary distinguishing feature is the ability to model sectional properties with higher order polynomials, allowing higher accuracy with fewer elements and the calculation of derivatives and integrals analytically. pBEAM was written in C++ for higher computation speeds and is called as a Python wrapped extension module.

CurveFEM is an alternate finite element method included in the pBEAM installation. Originally developed by Larwood [93], CurveFEM is a finite element module specifically intended for calculating mode shapes for rotating, tapered, twisted, and curved wind turbine blades. It is typically not used in the RotorSE workflow due to redundancies with pBEAM, which is more computationally efficient and provides analytical gradients. Its primary use is to calculate blade mode shapes and natural frequencies as a preprocessor to FAST, as a Python wrapped alternative to BModes [8].

BladeCostSE is a detailed blade cost model for modern multi-megawatt composite wind turbine blades [11]. It includes models to estimate the costs associated with the bill of materials, labor hours, and manufacturing processes. This work contributed to the model by collaborating in the development of the WISDEM Python port of the original standalone Excel model.

RotorSE has undergone significant updates to support this work. Formerly, the analysis was exclusively steady state. In order to more accurately calculate operational and extreme loads brought on by dynamic events, AeroelasticSE has been implemented in RotorSE to allow OpenFAST DLC analysis. A multi-fidelity switch seamlessly allows the user to select the traditional steady state analysis or the OpenFAST enabled dynamic loads. This dramatically reduces the barriers to using FAST in optimization design studies. Additionally, the rotor geometry representation in RotorSE was completely refactored to use the IEA Wind Task 37 Wind Turbine Ontology as its primary input and output method, allowing improved flexibility and accuracy in specifying blade geometries, discussed in detail in Section 3.2.5. Figure 3.1 shows a representation of the multi-fidelity RotorSE workflow options.

3.1.3 Reference Models

Several existing reference wind turbine models have been developed for use by the international research community. The NREL 5MW [84] is the most commonly used. Since the model was developed in 2009, it is no longer representative of modern wind turbine designs, however, there is a wealth of knowledge and experience for this design making it an attractive option. Several floating support platform concepts have been developed, including the OC3/Hywind spar buoy [81], the MIT/NREL tension leg platform [105], and the OC4/DeepCwind semi-submersible [131], shown in Figure 3.2.

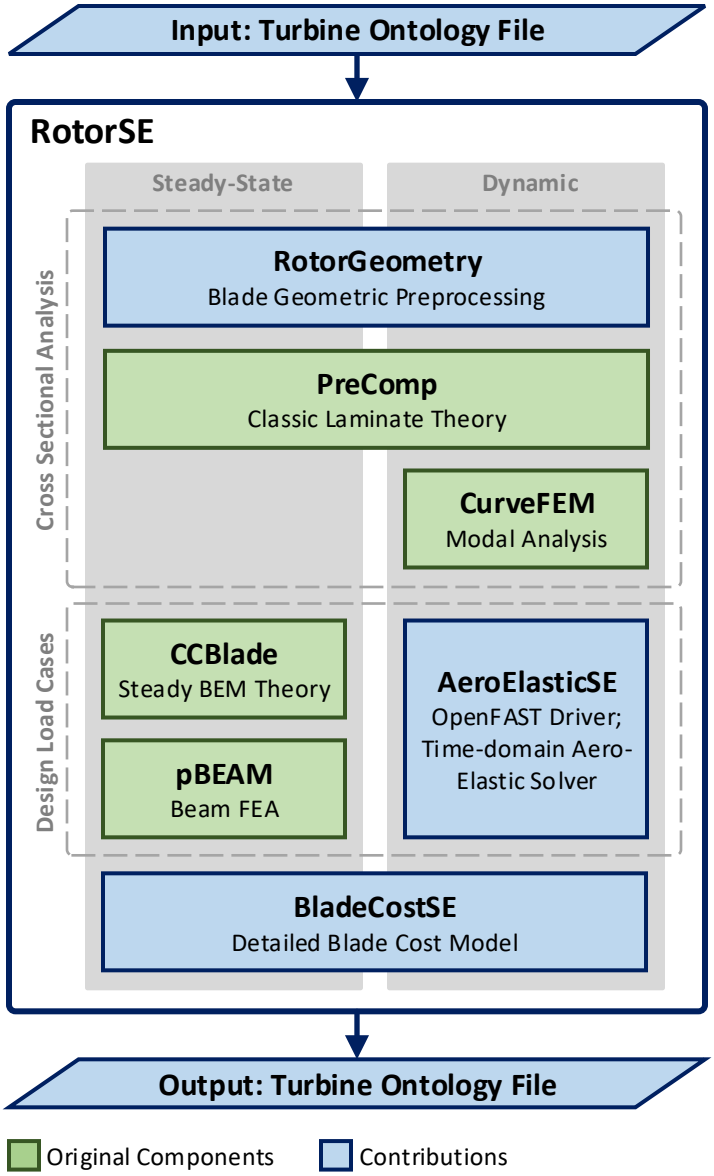

Figure 3.1: Multi-fidelity workflow options in WISDEM's RotorSE

The DTU 10MW [2] is the successor to the NREL 5MW and is more representative of modern offshore wind turbine designs. The DTU 10MW was recently refreshed and redesigned with the IEA 10MW Offshore Reference Turbine [12]. The most significant design change is a larger rotor diameter and reduction in the specific power from 400 W/m^2 to 350 W/m^2. As part of the same design undertaking, the IEA 3.4MW Onshore Reference Turbine was also released, representing the state of the art in

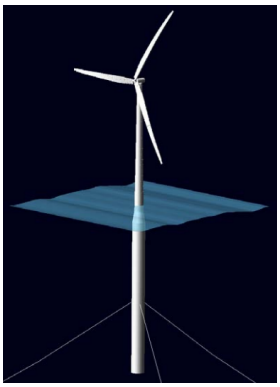

(a) OC3/Hywind spar buoy [81]

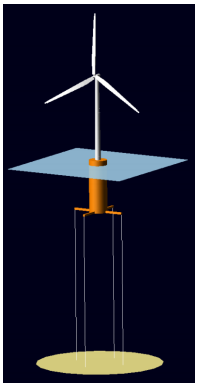

(b) MIT/NREL tension leg platform [105]

(c) OC4/DeepCwind semi-submersible [131]

Figure 3.2: Floating platform designs for the NREL 5MW

onshore horizontal axis wind turbines. Sandia National Labs also developed a series of 100m blades for a 13.2 MW wind turbine, the SNL100 [58, 60, 61]. These blades have a sophisticated focus on the structural and composite design.

Table 3.1 summarizes key attributes of the five reference wind turbines. Of these options, the NREL 5MW was selected for design studies for this work, since it is the only model with existing open-source floating support structures for FAST.

Table 3.1: Reference Wind Turbine Designs

	IEA 3.4MW	NREL 5MW	DTU 10MW	IEA 10MW	SNL 100-2
Rated Power, MW	3.4	5	10	10	13.2
Rated Wind Speed, m/s	9.8	11.4	11.4	11.	11.4
Rated Rotor Speed, RPM	11.75	12.1	9.6	8.68	7.4
Hub Height, m	110	90	119	119	146.4
Rotor Diameter, m	130	126	178.3	198	205
Blade Mass, kg	16,441	17,740	41,716	47,700	59,047

3.2 Development of a Wind Turbine Definition Ontology

3.2.1 Introduction

A common barrier in MDAO research for wind energy systems is the challenges associated with the transfer of data and information between one discipline to another, between fidelity levels, and between collaborators using different toolsets or workflows. The International Energy Agency (IEA) Wind Task 37: Wind Energy Systems Engineering: Integrated Research, Design, and Development [33] has begun an effort to address this problem by developing a standardized wind turbine ontology, or hierarchical framework of characteristics, described in full detail by Dykes et al. [30]. My contributions to this effort include:

- Development of the data formats for wind turbine blade composite geometric definitions
- Implementation of wind turbine ontology in the RotorSE workflow
- Modifications to the NREL 5MW Reference Turbine, enabled by the ontology, to have a more realistic composite design

3.2.2 Wind Turbine Ontology Overview

Within the field of computer science, an ontology is defined as a specification of a conceptualization [62, 63]. Here, a conceptualization is an abstraction of all the knowledge, concepts, and objects, as well as the relationships between them, that exist within a domain [52]. Building an ontology requires expert knowledge of the system or domain, so that the formalized characteristics defined in the ontology are truly representative of the breadth of distinctions in the system. A common ontology can provide specifications for diverse applications, without requiring that each application use the vocabulary and structure of the ontology within its internal processes. In this case, a translation step must occur from the ontological description to the specific vocabulary used for each application.

It is this translation capability that makes an ontological definition so appealing for wind energy applications, especially within the context of MDAO. There exists a diverse set of model frameworks and approaches to wind energy applications, with many similarities across these different research and commercial efforts. A common, agreed-upon data structure provides a more efficient basis for translation between different applications, as shown in Figure 3.3. With communication between n components, a point-to-point scheme requires $n(n-1)$ translators, where as a centralized scheme converting between a common standard only requires $2n$ translators.

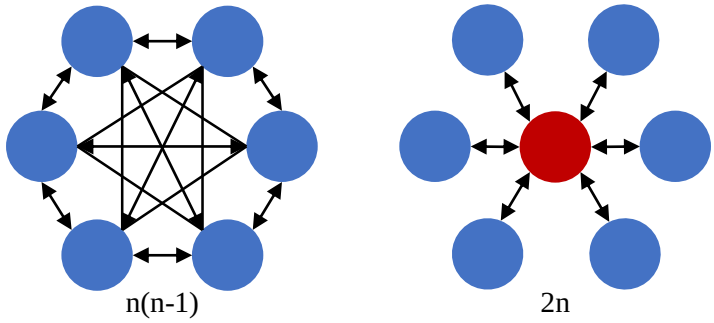

Figure 3.3: Data transfer efficiency improvements moving to common format (adapted from CPACS [22])

When creating the ontology, the following criteria were used as guiding principles, defined by Gruber [63]:

- *Clarity*: The ontology should be unambiguous in the definition and documentation of terms. The data structures in the ontology should be able to accurately represent realistic physical structures and properties.
- *Coherence*: Consistency against the ontology schema to be tested using automated tools.
- *Extendibility*: Allow the definition of non-standard and unanticipated future designs and features.

- *Minimal encoding bias*: The ontology should not overemphasize a particular discipline or existing modelling toolset. While the focus of the initial ontology is on the most common, low fidelity models, sufficient detail should be provided or allowed for higher fidelity models, without having to change the ontology.

- *Minimal ontological commitment*: This requirement can be summarized as a guarantee of consistency but not completeness. The ontology is a tool for sharing data but does not require users to have complete data for the entire system. For example, an aerodynamic modeler may not need or possess data on the blade composite schedule and is not required to provide that information.

Using the wind turbine rotor ontology within a workflow requires the adoption of a standard input and output format that is consistent with the ontology vocabulary. YAML [40] text files were selected for the sharing of data. The YAML format is a human- and machine-readable data-serialization language that was designed to be user friendly and portable between different programming languages, many of which natively support the reading and parsing of YAML files. YAML supports hierarchical data structures, as shown in Figure 3.4, depicting the top-level data organization, where filled in nodes have further sub-variable objects that could be expanded out. The ontology is described in a JSON Schema [86] which is used for automated data validation of turbine files and provides annotation of the ontology vocabulary.

3.2.3 Survey of Existing Composite Formats

Several existing wind turbine CAE tools require composite schedules as inputs, each with unique coordinate systems and formatting requirements. Take for example, PreComp, which uses laminate theory to calculate stiffness and inertia properties at blade cross sections as a preprocessor to finite element beam models. The primary inputs to PreComp are the airfoil cross section profile and the composite definition projected onto that shape. The composite definition is defined separately for the

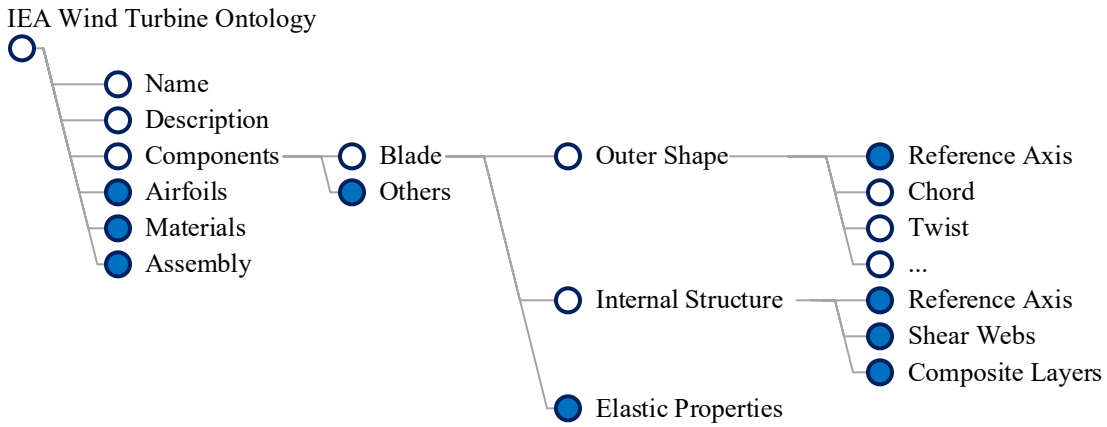

Figure 3.4: Visualization of top-level data objects in the IEA Wind Turbine Ontology

suction side, pressure side, and shear webs. The suction and pressure sides are divided into normalized chordwise sectors, each with different laminas, shown in Figure 3.5. The division points between sectors are defined from 0 to 1, the leading edge and trailing edge respectively.

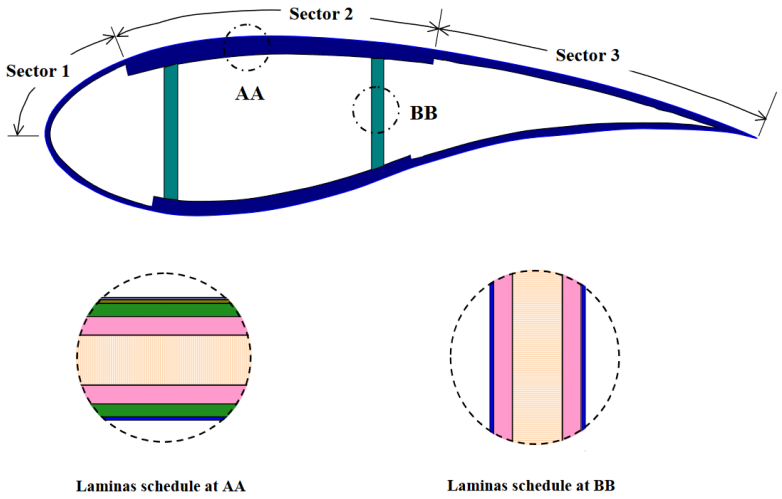

Figure 3.5: Sector-based composite definition scheme in PreComp [10]

In an optimization context, this format is very difficult to work with. Each spanwise cross section is independent of each other, making it problematic to determine which

layer in a laminate, in which sector, corresponds to the same spanwise element. Furthermore, the normalized chord-wise coordinate system makes it difficult to ensure geometric consistency. For example, a modern blade design will likely have uniform or linearly tapered spar cap widths due to standard composite roll dimensions and manufacturing costs associated with cutting laminate layers. If an existing PreComp model is used while optimizing blade chord, maintaining a constant spanwise spar cap arc-width along the curved surface requires recalculating the sector bounds for each spanwise cross section.

To determine what input method would be most useful to users and existing software tools, a non-exhaustive survey of input methods was conducted to determine their respective strengths and weaknesses. Table 3.2 shows the different cross sectional coordinate systems used by the tools for defining the start and end of composite sections. The methods vary from using normalized chordwise positions (PreComp, Numad), to normalized arc-length positions around the surface of the airfoil profile (Sonata, FusedWind), to dimensional distances from reference points (CpMax). CpMax, FusedWind, and NuMAD define the spanwise properties of layup elements, where as PreComp and Sonata treat each cross section independently. CpMax and FusedWind make assumptions about the blade topology and are less flexible to non-standard geometries than the other methods. When chordwise positions are used, especially with dimensional coordinate systems like CpMax, defining new blades is relatively user friendly compared to arc lengths definitions. Arc length coordinates are highly precise; however, they are sensitive to different spanwise interpolation schemes where small variations in spanwise airfoil cross-sections results in inaccurate component placement.

Based on this survey, the following goals for the composite schedule ontology were identified:

- *User Friendly*: Easy for users to create new blade design input files

Table 3.2: Survey of composite definition cross sectional coordinate systems

Software Tool	Variable	Grid	Split SS/PS
PreComp	Chordwise %	$LE = 0$, $TE = 1$	Yes
CpMax	Chordwise Dist.	Dist. to Pitch Axis, LE or TE	Yes
Sonata	Arc Length	$TE_{SS} = 0$, $TE_{PS} = 1$	No
FusedWind	Arc Length	$TE_{PS} = -1$, $TE_{SS} = 1$	No
NuMAD	Chordwise %	$TE_{PS} = -1$, $LE = 0$, $TE_{SS} = 1$	Yes

- *Geometric Accuracy*: The ability to specify realistic design features, such as the arc width and position of composite plies laid along a curved profile or straight shear webs in a curved and twisted blade
- *Unambiguous*: Provide sufficient detail that a variety of software converters arrive at the same result
- *Flexibility*: Allow the definition of non-standard and unanticipated future designs
- *Optimization Ready*: Enable parameterization of spanwise elements

3.2.4 Composite Section Ontology

The arrived upon coordinate system is a compromise solution that aims to combine the best features of the surveyed methods. Composite layers are defined as spanwise elements relative to the pitch axis, which is superimposed on the curved reference axis. The spanwise grid for each variable, of each element, is defined independently for ease of input. Layers are not required to extend the full length of the blade, nor start and end at the root and tip. Layers can either be projected onto the airfoil surface or onto a shear web. If a layer is part of a shear web, the layer position is not explicitly defined, but inherited from the assigned shear web. Shear web positions are assigned in the same manner as composite layers; however, it is assumed that the web forms a straight line between their start and end points, rather than following the airfoil

surface. Layers are listed in stacking sequence with the outermost layer listed first for surface layers and the closest to the leading edge listed first for web layers.

The required variables for every composite layer include a unique name, a material name that links to the ontology material property list, and a spanwise thickness. For defining layer positions, there are a variety of input options that a user can chose from to fit the needs of a given layer, explained in detail the following bulleted list. The full list of potential variables are listed in Table 3.4. Table 3.3 gives the possible combinations of variables that need to be defined to provide the layer position. The list in Table 3.3 is hierarchical, where if multiple variables defining the position are provided, the top most combination will be used.

- Dimensional: The location of an element is perpendicular to a rotated offset about the pitch axis as shown in Figure 3.6. For a surface layer, this represents the layer midpoint, requiring the arc width and side of the airfoil (suction or pressure) to be specified. For shear webs, the start and end points are determined by the intersection of the perpendicular axis with the airfoil surface. Rotation can be explicitly specified or fixed to existing variable elsewhere in the ontology, such as planform twist. This notion is most useful for shear webs and spar caps.

- Arc-length midpoint: Surface layers are specified according to their midpoint in normalized arc-length coordinates (s), where the suction side trailing edge equals zero and the pressure side trailing edge equals one. For flatback airfoils, the trail edge is defined as the midpoint of the flatback surface. Midpoints can optionally be fixed to either the trailing edge or leading edge positions. This notation is most useful for trailing edge and leading edge reinforcement panels.

- Arc-length start and end: Similar to the midpoint notation, the start and end of an element are given as normalized arc-length positions. Start or end positions can be optionally be explicitly fixed to other layer elements. Start points are

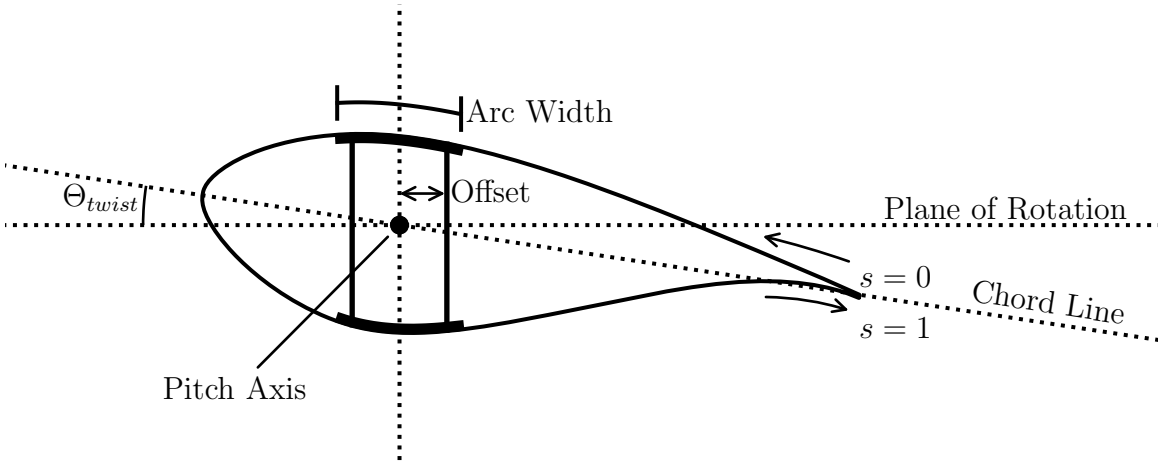

Figure 3.6: Placement of composite elements using a rotation and offset about the pitch axis

Table 3.3: Hierarchy of input coordinate systems

Acceptable Variable Combinations
1. web
2. width, rotation, offset_x_pa, side
3. width, midpoint_nd_arc
4. start_nd_arc, end_nd_arc
5. *none*, (full circumference)

fixed to the end point of the specified element, and conversely, end points are fixed to the start point of the specified element. Since layer width is not specified, this input method is most useful for filler sections between fixed elements.

- Full Circumference: If no positioning variables are specified, it is assumed that the element is a surface layer that wraps around the full circumference of the airfoil. This is most common for shell skin elements and root build up.

Table 3.4: List of composite layer variables

Variable	Sub-Vars.	Description
name	-	Unique naming identier for the layer.
material	-	Material name, links to the ontology list of materials.
thickness	grid, values	Layer thickness (m), spanwise list.
n_plys	grid, values	(*Optional*) Number of plies, multiplier for width, spanwise list; if not include, 1 assumed.
width	grid, values	Layer arc width (m), spanwise list.
rotation	grid, values	Rotation of reference axis (°), spanwise list.
	fixed	Variable name, link to an existing ontology variable.
offset_x_pa	grid, values	Offset along the rotated reference axis (m), spanwise list.
start_nd_arc	grid, values	Non-dimentional arc-length start position from $TE_{SS} = 0$ to $TE_{PS} = 0$.
	fixed	Variable name, link to an existing ontology variable.
end_nd_arc	grid, values	Non-dimentional arc-length end position from $TE_{SS} = 0$ to $TE_{PS} = 0$.
	fixed	Variable name, link to an existing ontology variable.
midpoint_nd_arc	grid, values	Non-dimentional arc-length end position from $TE_{SS} = 0$ to $TE_{PS} = 0$.
	fixed	Variable name, link to an existing ontology variable.
web	-	(*Optional*) Shear web name, if layer is projected on a shear web rather than the airfoil profile.
side	-	(*Optional*) If using dimentional coordinate system, 'pressure'or 'suction' side must be specified.

3.2.5 Implementation in RotorSE

The existing RotorSE input module, RotorGeometry, was not well suited to arbitrary inputs. Turbine models were hard coded into RotorGeometry as classes, with the analysis initialized by loading turbine class and inheriting its attributes. Creating new turbine models was quite onerous and error prone for the user. Furthermore, at the end of an optimization, there was no built-in method for output of the final blade design in a format that could then be reused by the analysis.

PreComp input files were also required as inputs to RotorSE. All spanwise inputs, include PreComp models of the composite cross sections, used the same spanwise grid spacing. Requiring PreComp input files created significant barriers for researchers not already using PreComp in their workflows. The geometric parameterization of composites was severely limited, offering oversimplified methods for modifying the input PreComp definitions. Spanwise design variables existed to modify the spar cap and trailing edge reinforcement sections, but these variables scaled the entire composite layer stack thickness rather than the specific composite layer. For example, if the goal was to increase the carbon fiber spar cap thickness by 15%, the glass fiber skin thickness for the spar cap sector would also be increased by 15%.

RotorSE was overhauled to use the IEA turbine ontology as its primary input file. All interpolation of the blade geometry is handled by the converter, rather than requiring the user to define all variables on a common spanwise grid. This includes remapping all spanwise planform and composite variables and interpolation between airfoil profiles to create the lofted blade shape and blending airfoil polars. PreComp inputs are generated automatically by converting the ontology data format to the PreComp format. Additionally, turbine ontology files can now be written out, providing an output mechanism for RotorSE. By removing hard-coded turbine inputs, RotorSE is now far more flexible to the turbine models that can be provided as inputs and can handle a wider range of composite design variables. Combined with RotorSE's

AeroelasticSE-based FAST driver, it is now very easy to generate new or modified FAST blade input files for near-arbitrary blade designs.

3.2.6 Modifications to the NREL 5MW Reference Turbine

When originally released, the NREL 5 MW Offshore Reference Turbine [84] did not include a structural design. Rather, the spanwise elastic properties where provided, estimated based on the 62.6 m LM Glasfiber design used in the DOWEC study [96]. To fill this gap, Sandia National Labs conducted a study to reverse engineer a composite schedule for the NREL 5 MW, extending the reference design's usefulness in structural and blade design optimization studies [129]. There are several geometric assumptions in the Sandia 61.5 m blade that are impractical from a manufacturing perspective, but easily corrected using the IEA Turbine Ontology.

The primary oversimplification of the Sandia 61.5 m composite schedule is the assumption that shear webs are perpendicular to the chord line. The spar caps are defined at +/- 0.3 m from the blade pitch axis, with the shear webs extending from the spar cap end points. This leads to two unrealistic design features:

- The arc-length of the spar cap composite layers are non-uniform due to varying curvature of the blade surface as the airfoil thickness decreases spanwise. This would result in unnecessary composite fabric cutting during the manufacturing process.

- Blade rotation is not accounted for in the spar cap and shear web positioning, resulting in twisted load-bearing components and increased manufacturing complexity.

Figure 3.7 shows the lofted blade shape, with shear webs and spar caps positions included, for the original Sandia 61.5 m composite schedule, faithfully rendered. The twisted spar cap and shear web positioning can be clearly seen. Figure 3.7 shows the modified design when straight structural components are defined using the width,

rotation, and offset_x_pa ontology input methodology outlined in Section 3.2.4. This modified composite schedule was used in all optimization studies in the remainder of this document, wherever the NREL 5 MW is referred to.

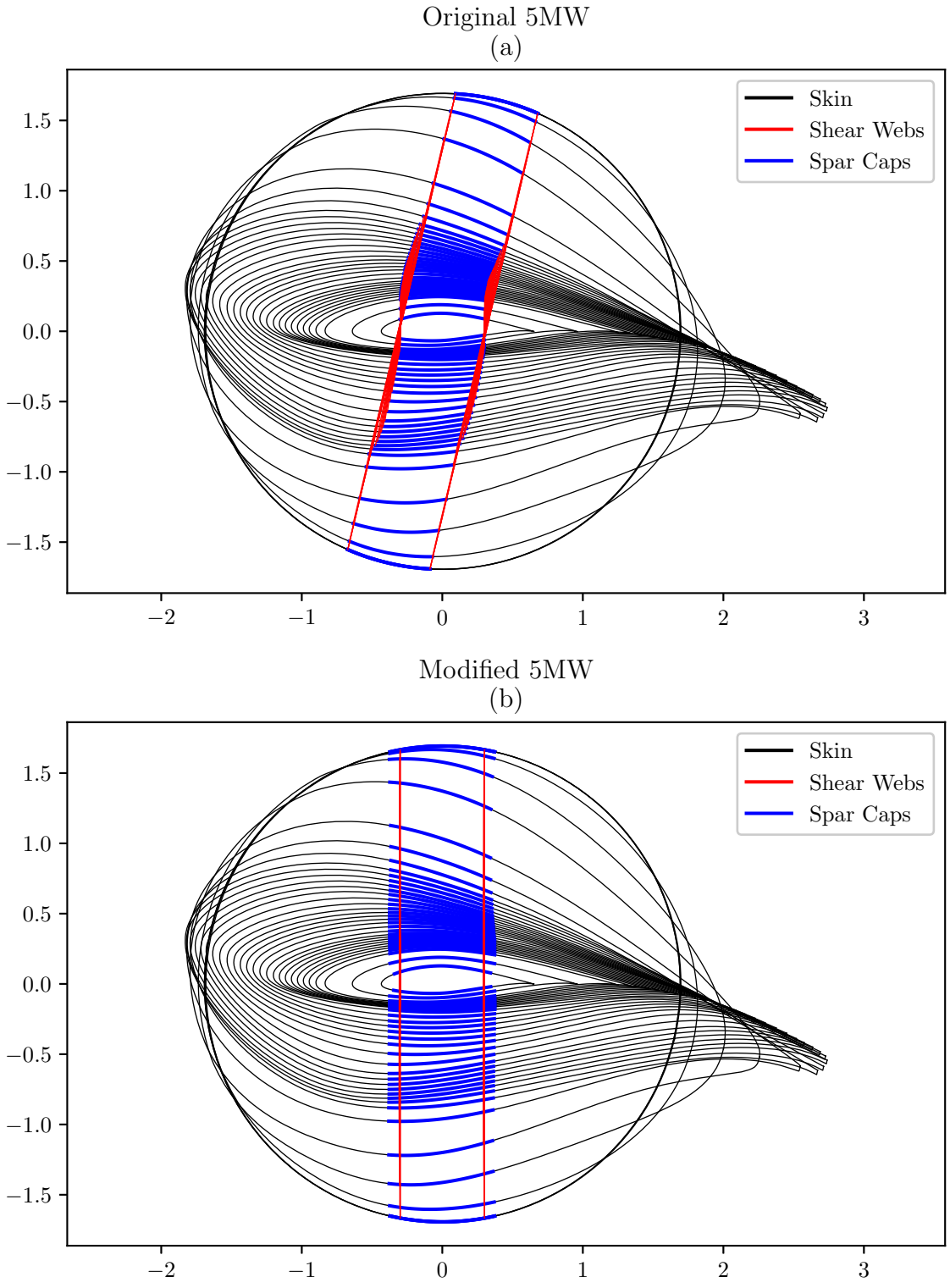

Figure 3.7: Lofted blade shape for the NREL 5MW / Sandia 61.5m (a) Unmodified, (b) Modified

CHAPTER 4

GENERAL OPTIMIZATION METHODOLOGY

Optimization problem formulations and workflows vary for specific design studies, but generally, how they are evaluated using the tools outlined in Section 3.1 is discussed here.

4.1 Design Variable Parameterization

Spanwise properties such chord, twist, airfoil thickness, precurve, sweep, and composite thicknesses are parameterized with a series of spanwise control points, shown in Figure 4.1. Key control points are set at the root, the furthest outboard position of cylindrical airfoil cross sections ($r_{cylinder}$), the position of maximum chord ($r_{c_{max}}$), and the blade tip. Additional linearly spaced control points can be added between $r_{cylinder}$ to $r_{c_{max}}$ and $r_{c_{max}}$ to r_{tip}. The continuous spanwise distributions between control points are calculated with PChip splines [45]. PChip splines are useful for such geometric interpolations because extrema in the supplied data are preserved, at the expense of second derivative continuity, preventing overshoot in the interpolated distributions. During an optimization study, new blade designs are generated by assigning design variables to some subset of these control points, often leaving the blade root unchanged since it requires higher fidelity structural analysis tools to evaluate. Additional topology and controller design variables can also be assigned, setting quantities such as blade length or tip speed ratio.

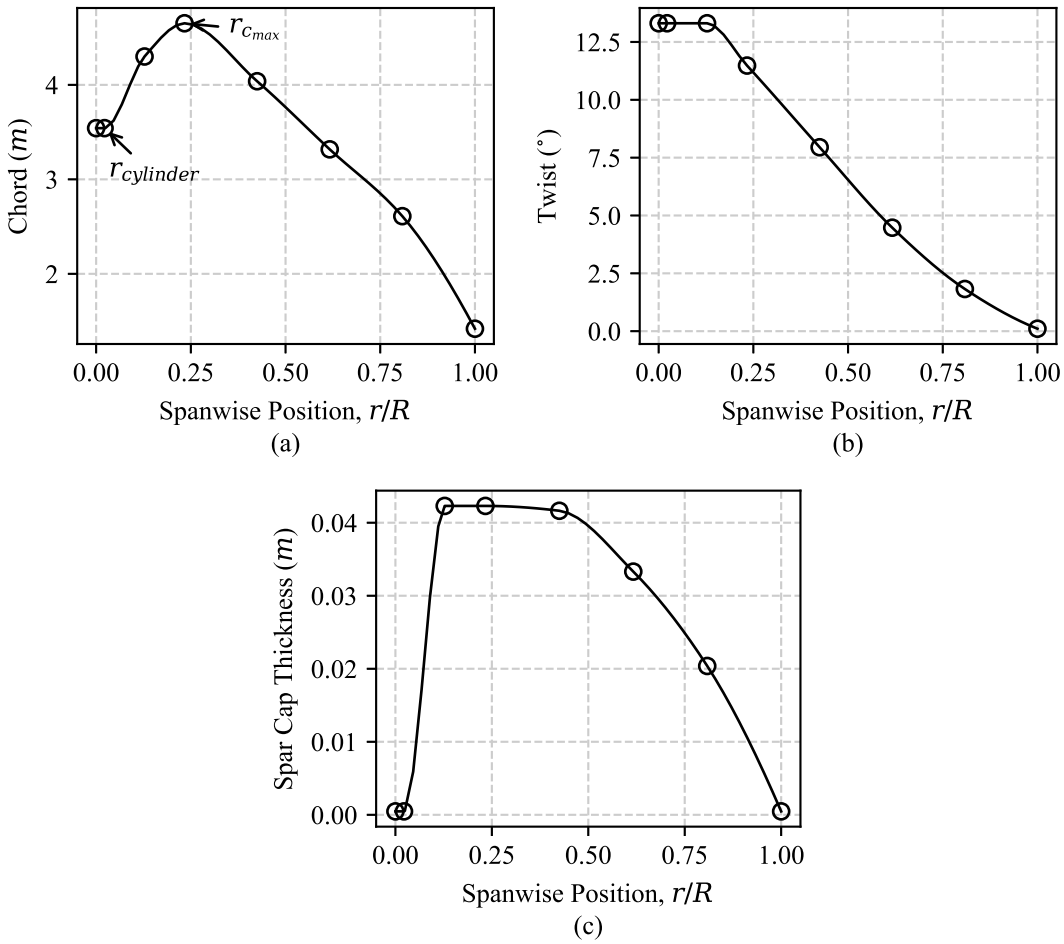

Figure 4.1: Example control point parameterizations of spanwise variables

4.2 Objectives

4.2.1 Annual Energy Production

For a variable speed wind turbine, control of the turbine is broken down into a series of regions employing different strategies [78, 91]. Region I consists of wind speeds below the cut-in speed of the turbine, where the rotor is in a freewheel state with no torque supplied from the generator. Region II includes operational wind speeds below the rated speed. The turbine operates at its designed tip speed ratio and blade pitch angle to operate at an optimal C_P for the blade design. The generator

provides optimal torque matching. Region III includes above rated wind speeds, where the generator provides constant rated torque and the blades are pitched to regulate the rotation speed. Region II.5 additionally provides a linear transition from Region II and III generator torques, if the rotor reaches its maximum rotation speed before reaching rated power.

Determining the power curve using steady state models is relatively simple. The rotor speed as a function of wind speed is determined by the design tip speed ratio and maximum allowable tip speed. The rated wind speed can be iteratively solved for using a simple 1D search algorithm. Above rated, the pitch schedule can be iteratively solved for such that the rated rotor speed is maintained and power is at its maximum. Through this process, a simple steady-state regulation trajectory for the torque and pitch controllers is determined, with the associated loads and power production as a function of wind speed.

When using OpenFAST or another dynamic model, the torque and pitch controller must be modified for new blade designs, so the controller can dynamically employ these strategies in response to varying wind speeds. The primary value that needs to be changed is the Region II torque control gain, K. The generator torque τ_c is the proportional to the square of rotor speed, given in Equation 4.1. Here, K is given by Equation 4.2, where λ is the tip speed ratio corresponding to $C_{P_{max}}$. Additional values that need to be modified include the rated torque and the pitch controller reference rotation speed, determined by the blade length and maximum tip speed. The above rated pitch controller uses a proportional-integral control scheme to minimize overspeed error from the rated rotor speed. Assuming the above rated controller accomplishes its goal of maintaining maximum torque and constant rotation speed, the above rated pitch controller has negligible impacts on AEP and the design optimization of the blades. It was assumed that the baseline pitch controller gains did not need to be modified for the purposes of this study.

$$\tau_c = K\omega^2 \tag{4.1}$$

$$K = \frac{1}{2}\rho A R^3 \frac{C_{P_{max}}}{\lambda_*^3} \tag{4.2}$$

OpenFAST can then be executed over a range of wind speeds to determine the power production as a function of wind speed. During iterative design optimization, it is desirable to run as few simulations as possible to keep computational expense low. Therefore a relatively coarse sample grid is used for expected below and above rated wind speeds, with a finer sampling grid near rated to capture the transition between control regions. The product of the resulting power curve and the wind probability density function is integrated to give the AEP.

To determine the AEP for a floating wind turbine, the sea state as well as the wind speed must be considered. Ideally, the power production for the full joint probability density function for all wind speeds, significant wave heights, and peak spectral periods would be considered, according to Equation 4.3. This, or even a surrogate model sampling multiple sea states for a given wind speed, is too computationally expensive for iterative design optimization, quickly requiring 100s or 1000s of simulations depending on the sampling grid. Rather, the expected wave height and period for each wind speed bin was used, according to the offshore reference sites defined by Stewart et. al [144].

$$AEP = T \int\int\int P\left(U, H_s, T_p\right) p\left(U, H_s, T_p\right) \mathrm{d}U \mathrm{d}H_s \mathrm{d}T_p \tag{4.3}$$

4.2.2 Cost of Energy

Using BladeCostSE [11], WISDEM's detailed blade cost model, it is possible to get a sophisticated estimate of blade capital costs for new blade designs generated during an optimization. However, this is only a small part of the overall cost of energy.

Figure 4.2 show that the turbine costs for a typical United States land based wind farm only account for about 67.3% of total capital expenditures, with the rotor only accounting for 19.1%. For offshore fixed bottom and floating plants, the rotor costs are an even smaller portion, 9.4% and 6.7% respectively, as the support structure, installation, and balance of system costs all increase. Estimating such costs for the offshore United States market are particularly difficult because there is very little industry experience.

A simplifying assumption was made, due the challenges and uncertainties surrounding FOWT cost of energy estimates. An initial COE of \$60/MWh was assumed for the NREL 5MW reference turbine, using the calculated blade cost and AEP, the rest of system COE (δ_{COE}) was calculated. During design optimization, δ_{COE} is fixed to this initial value, updating COE with updated blade costs and AEP, Equation 4.4. While this method neglects system level impacts to the turbine design and cost structure as a result of changes to rotor design, it attempts to weigh blade capital costs appropriately so that increases in blade cost in order to increase AEP can be achieved.

$$COE \approx \frac{CapEx_{blades} + \delta_{COE}}{AEP} \tag{4.4}$$

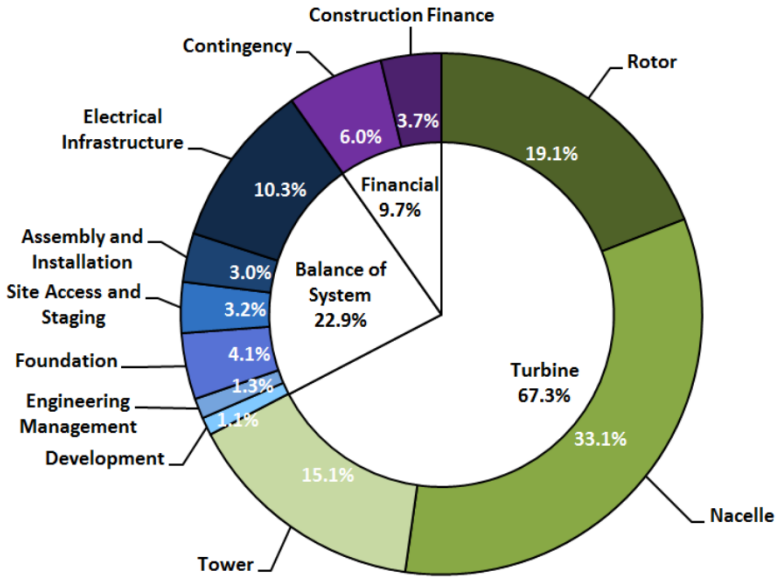

(a) Onshore

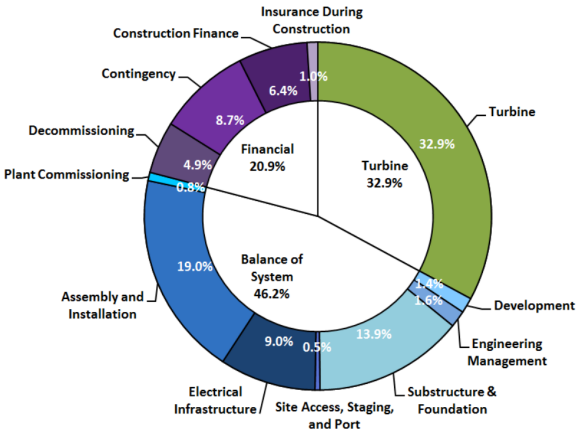

(b) Fixed Bottom Offshore

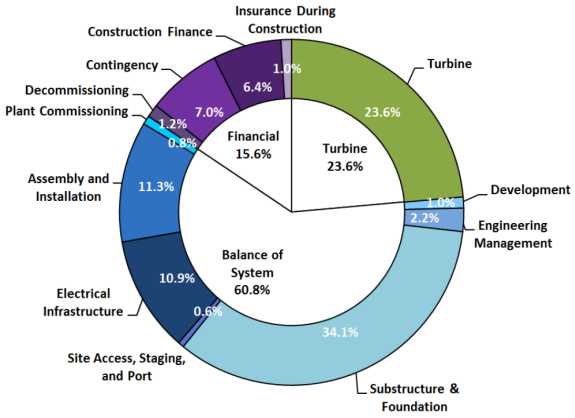

(c) Floating Offshore

Figure 4.2: Turbine capital expenditures [142]

4.3 Constraints

4.3.1 Tip Deflection

Maximum tip deflections occur during dynamic events such as extreme operating turbulence, shutdowns, or gusts, where are the wind speeds change quickly on an already heavily loaded rotor, faster than the turbine pitch controller can respond. Modeling such unsteady conditions with a steady state BEM model, such as CCBlade

used in RotorSE, is problematic. In RotorSE, this is handled by taking a conservative approach. The IEC extreme operating gust wind speed, V_{gust}, is used, at rated rotation speed and blade pitch, with a partial safety factor γ_m applied to the deflection. Equation 4.5 gives the constraint on tip deflection, which is the ratio of the deflection in the x direction towards the tower, δ, and the unbent distance to the tower. The blade is allowed to deflect approximately 70% of unbent distance towards the tower, x_{unbent}.

$$\frac{\gamma_m \delta}{x_{unbent}} \leq 0 \tag{4.5}$$

When FAST is used in the analysis workflow, a gust can be more accurately modeled using IEC DLC 1.4, an operational extreme coherent gust with a direction change. For a floating wind turbine, the rotor thrust can be higher under gust conditions due to the additional fore-aft velocity component. This can result in higher blade tip deflections and root bending moments, as shown in in Figure 4.3. The NREL 5 MW was modeled under the same conditions, onshore and on the OC3 spar buoy, resulting in the FOWT case having 17% higher maximum blade tip deflection. During an optimization, this would further constrain the design space for the floating case, requiring either a stiffer, and likely heavier blade, or a lower induction rotor operating with lower thrust.

4.3.2 Spar Cap Panel Buckling

Candidate blade designs are evaluated for panel buckling, where the compressive strain on the suction side of the blade during out-of-plane bending exceeds the critical panel buckling strain. Given the stiffness and inertial properties from PreComp, panel buckling is determined using classical laminate theory, as follows. Equation 4.6 gives the constitutive equations for a laminate sequence, where N and M are the applied

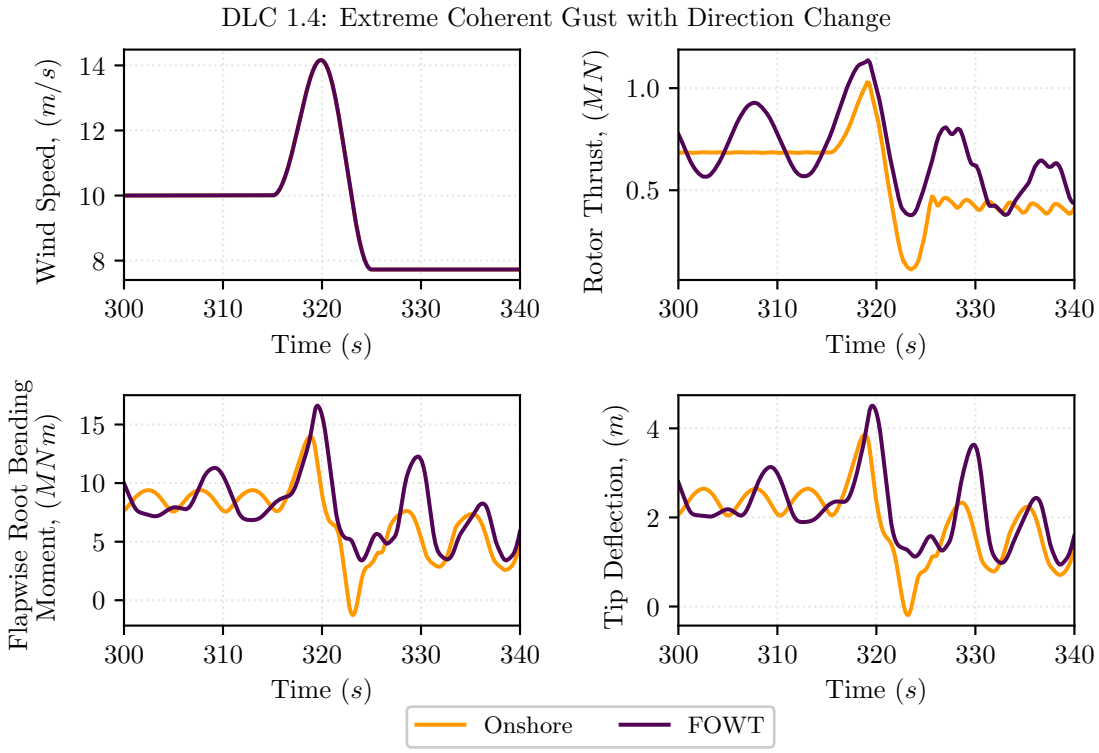

Figure 4.3: Comparison of onshore and offshore loads during an extreme gust

tractions and moments matrices, A, B, and D, are the extensional, coupling, and bending stiffness matrices, and ϵ^0 and k are the midplane strains and curvature [65].

$$\begin{bmatrix} N \\ M \end{bmatrix} = \begin{bmatrix} A & B \\ B & D \end{bmatrix} \begin{bmatrix} \epsilon^0 \\ k \end{bmatrix} \tag{4.6}$$

Assuming the composite panels are orthotropic, the bending stiffness matrix is of the form

$$D = \begin{bmatrix} D_{11} & D_{12} & 0 \\ D_{12} & D_{22} & 0 \\ 0 & 0 & D_{66} \end{bmatrix} \tag{4.7}$$

The blade cross sections can be treated as a series of long, simply supported panels. The critical buckling load, N_{cr}, is then given by Equation 4.8, where w is the panel width [77].

$$N_{cr} = 2\left(\frac{\pi}{w}\right)^2 \left[\sqrt{D_{11}D_{12}} + D_{12} + 2D_{66}\right] \tag{4.8}$$

A reasonable approximation for long, slender wind turbine blades is the assumption that laminate shear and bending moments are negligible. In the case of symmetrical panels, bending moment effects are in fact zero. By taking the inverse of the laminate stiffness matrix in Equation 4.6 and integrating the laminate stresses to approximate the effective smeared modulus of elasticity, E_{zz}, the critical buckling strain under compression, ϵ_{cr}, is given by Equation 4.9, where h is the thickness of the full laminate stack.

$$\epsilon_{cr} = -\frac{N_{cr}}{hE_{zz}} \tag{4.9}$$

The spanwise strain on the blade spar caps are evaluated using the pBEAM FEM model, loaded according to IEC DLC 6.1, a parked turbine with a 50-year return period wind speed. The optimization is constrained such that the magnitude of the calculated strains cannot exceed the spanwise critical panel buckling strain, Equation 4.10. A partial safety factor for loading, γ_f, is applied to the spanwise strain. Satisfaction of this constraint from an infeasible point can be achieved by increasing blade stiffness or by decreasing loading on the rotor.

$$\epsilon_{cr}(r_i) - \gamma_f \epsilon(r_i) \leq 0 \tag{4.10}$$

4.3.3 Resonance Avoidance

Blades are constrained to avoid potential resonant excitation. The blade natural frequencies are provided as an output of pBEAM. The first 5 blade natural frequencies

(F_{N_i}) are required to be outside a safety factor margin (γ_{freq}) about the rated blade rotation passing frequencies, f_{1P} and f_{3P}, shown in Equations 4.11 and 4.12.

$$\min \begin{bmatrix} f_{N_i} - \dfrac{f_{1P}}{\gamma_{freq}}, \\ \gamma_{freq} f_{1P} - f_{N_i} \end{bmatrix} \leq 0 \tag{4.11}$$

$$\min \begin{bmatrix} f_{N_i} - \dfrac{f_{3P}}{\gamma_{freq}}, \\ \gamma_{freq} f_{3P} - f_{N_i} \end{bmatrix} \leq 0 \tag{4.12}$$

4.3.4 Blade Mass

When blade costs or cost of energy are not used as objectives, blade mass must be constrained to a reasonable value to prevent unrealistically cost prohibitive designs. This is especially true if blade length is used as a design variable. Assuming identical materials, geometry, and technology, blade mass scales cubically with blade length according to Equation 4.13. Historically however, new blade designs with increasing blade lengths have outperformed this trend through technological improvements. Analysis of blades offerings from wind turbine manufactures has shown actual scaling ratios of about 2.1 to 2.3 [23, 99]. Equation 4.14 constrains the blade mass to the initial value, allowing it to scale with blade length with a ratio of 2.2.

$$m = m_0 \left(\frac{L}{L_0} \right)^3 \tag{4.13}$$

$$m - m_0 \left(\frac{L}{L_0} \right)^{2.2} \leq 0 \tag{4.14}$$

4.3.5 Blade Root Bending Moments

Root bending moments are a major design driver for the blade root skin thickness, blade-to-hub bolt connections, and fatigue of the composite laminates. For this work, the root design is unchanged, as it requires higher fidelity finite-element analysis

modeling to accurately capture the physics and failure modes. Since the baseline NREL 5MW blade root design is used, root bending moments are constrained to the initial values for the baseline NREL 5MW operating in a given configuration (i.e. onshore or FOWT).

CHAPTER 5

STEADY FLOATING OFFSHORE WIND TURBINE BLADE OPTIMIZATION

The goal of this chapter is to optimize wind turbine blades for the conditions expected on floating platform, without the computational expense of dynamic time marching simulations. The effects of metocean conditions and floating platform motion on the turbine loads and performance are examined in order to inform the optimization study. Blades are then optimized in steady state conditions that aim to emulate floating operation and the performance of the resulting blades assessed using dynamic simulations.

5.1 Effects of platform motion on design driving loads

For floating platforms with catenary mooring lines, like the OC3/Hywind spar buoy and the OC4/DeepCwind semi-submersible, pitch is the primary driver of unsteady structural and aerodynamic loads from platform motion. Surge occurs at a much lower frequencies, reducing its overall contribution to unsteady loading. To demonstrate the relationship between platform pitch and metocean conditions, the NREL 5MW on the OC3/Hywind spar buoy was modeled in OptenFAST over a range of wave height, wave period, and wind speed combinations and Figure 5.1 shows the mean and standard deviation of platform pitch. The average pitch is a function of the wind speed and is insensitive to wave conditions; as thrust on the rotor increases, the platform is pitched backwards. The pitch frequency and amplitude are dictated by the wave conditions, shown by the pitch standard deviation, which is most sensitive to wave period. The

turbine has more time to accelerate forward and backwards between wave peaks as period increases.

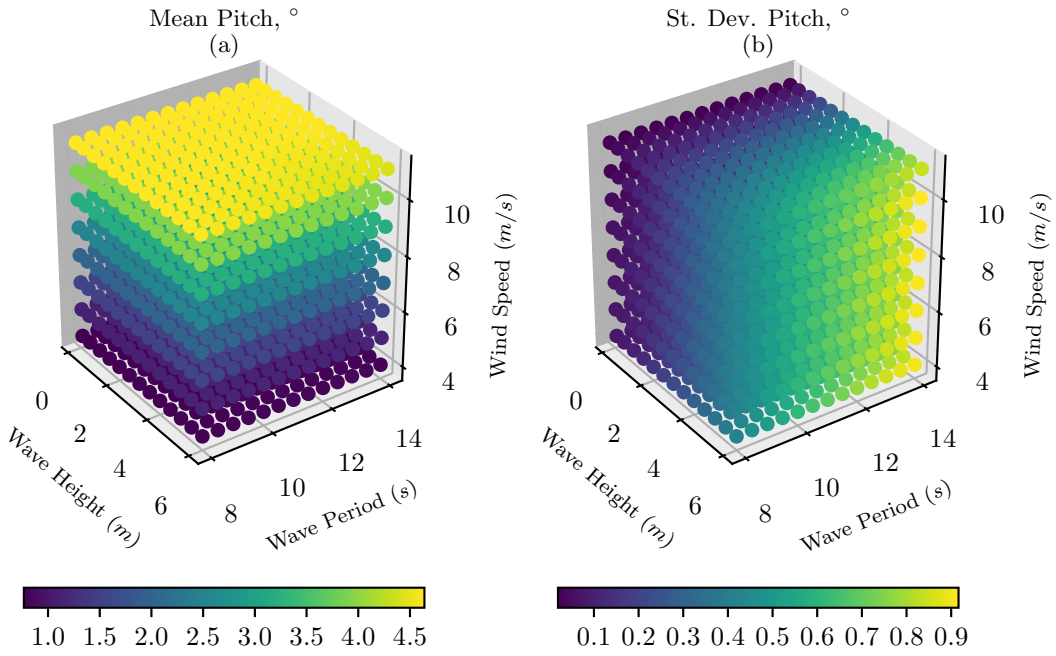

Figure 5.1: Platform motion as a function of metocean conditions

Both mean pitch offset and pitch amplitude contribute to unsteady loading, but through different forcing mechanisms. A pitch offset results in skewed inflow through the rotor, similar to yaw misalignment, decreasing power production and increasing the unsteady loads. Rotational sampling results in larger angle of attack variations, especially near the root with low relativity velocities, making dynamic stall more likely. To demonstrate the effects of an average pitch offset, isolated from the time-varying velocity component, the NREL 5MW was modeled in OpenFAST with fixed platform pitch angles and all other platform degrees of freedom locked in place. Fig 5.2 shows the power, thrust, flap-wise blade root bending moment, and flap-wise blade tip deflection, normalized by the baseline with 0° of platform pitch. Considering an

expected mean platform pitch of about 4.5° at rated conditions from Figure 5.1, the power losses will be roughly 3% compared to the nominal, with the thrust coefficient (C_T) increased by about 0.4%. The increase in flap-wise root bending moments and tip deflections standard deviations, approximately double the baseline, can be attributed to both the rotational sampling and gravity loads.

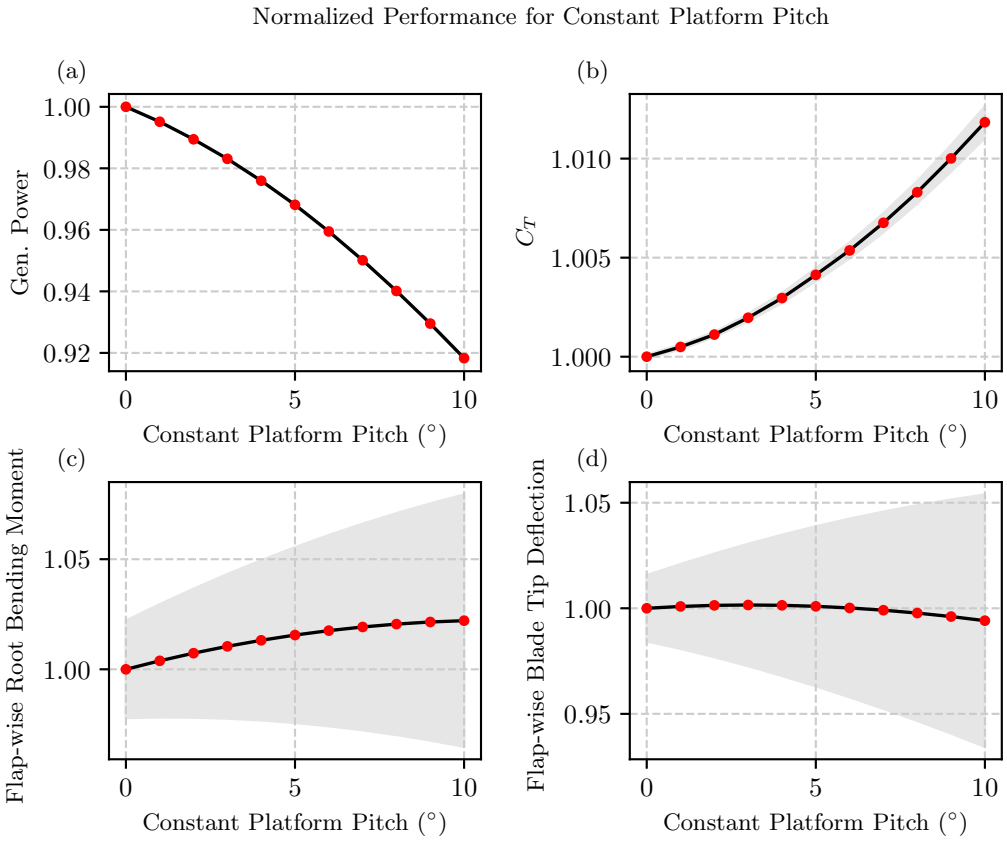

Figure 5.2: Effects of constant platform pitch offsets. The shaded regions represent the normalized standard deviation about the mean.

Cyclical pitch variation about the mean results in an additional unsteady fore-aft velocity component seen by the rotor. The average power production may actually increase due to the cubic relationship between power and wind. Expressed in Equation 5.1, more power is gained on the forward stoke as effective rotor velocity increases than is lost on the backwards stroke. Peak and fatigue loads are increased due to

these cyclical variations. Fore-aft motion from both pitch and surge can also result in rotor-wake interactions, causing dynamic changes in the induction through the rotor unaccounted for by BEM; this is beyond the scope of this work since higher fidelity aerodynamic models such as FVM and CFD are required to model these effects.

$$P(U + \Delta U) - P(U) > P(U) - P(U - \Delta U) \tag{5.1}$$

Figure 5.3 shows the changes in power production and key design driving loads, normalized by the onshore case at each wind speed. All floating platform, tower and blade bending, and generator degrees of freedom were used in OpenFAST. In subplot (a), power production is increased at low wind speeds and large wave heights and periods. Driven by low mean pitch angles and large pitch amplitudes, the increased power from the forward pitching stroke outweighs losses from rotor misalignment and the velocity reduction on the aft pitching stroke. As wind speed and mean platform pitch increases, these power increases diminish. At near rated wind speeds, the large mean pitch angles and low pitch amplitudes result in power losses of up to 3%, especially for smaller wave periods and heights. For above rated conditions, the blades are pitch towards feather in order to maintain the rated rotor speed and changes in power production are negligible compared to the onshore case.

Thrust, flap-wise bending moments and tip deflections are increased for all below rated metocean conditions. The thrust coefficient increases by about 2-3% over the expected range of metocean conditions. Maximum flap-wise root bending moments and tip deflections at 11 m/s are increased by 5% for short wave periods and up to 20% for large wave periods. As mean thrust increases with wind speed, aerodynamic damping also increases, with platform pitch standard deviation slightly decreasing with increased wind speed, but it is a much weaker dependance than wave height or period.

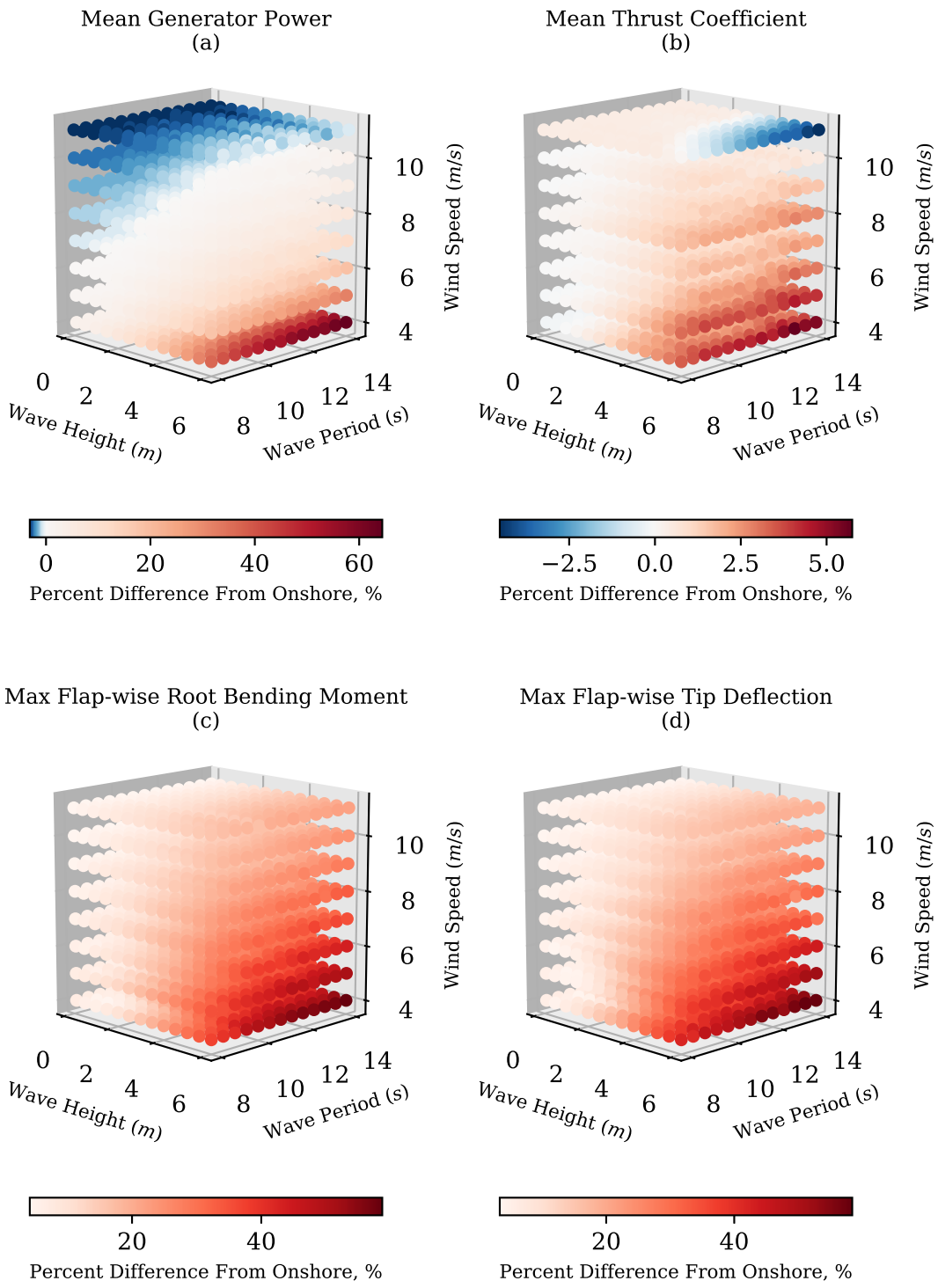

Figure 5.3: Percent change in performace for the NREL 5MW on the OC3/Hywind relative to onshore

Table 5.1: Expected metocean conditions at offshore refence sites with resulting FOWT loads and percent difference relative to onshore

	Metocean Conditions				Performance					
	U	H_s	T_p	CDF	P_{mean}		T_{max}		$M_{y,max}$	
	m/s	m	s	%	kW	(%)	kN	(%)	$kN \cdot m$	(%)
West										
	4	1.91	12.24	11.6	167	(9.0)	279	(34.7)	2811	(16.3)
	5	1.93	12.19	17.9	381	(4.3)	338	(31.9)	3537	(15.3)
	6	1.96	12.14	25.2	691	(1.7)	405	(29.0)	4395	(14.6)
	7	2.01	12.02	33.2	1118	(1.9)	480	(26.7)	5304	(13.0)
	8	2.06	11.90	41.5	1661	(0.0)	565	(24.7)	6361	(12.3)
	9	2.14	11.71	49.8	2344	(-0.8)	673	(23.1)	7732	(11.1)
	10	2.22	11.52	57.8	3183	(-1.5)	791	(21.5)	9211	(10.2)
	11	2.36	11.29	65.2	4199	(-2.2)	905	(20.7)	10647	(10.8)
	12	2.49	11.05	71.9	4995	(-0.1)	927	(30.8)	10640	(18.1)
	13	2.80	10.65	77.8	5000	(0.0)	732	(19.5)	8075	(4.0)
	15	3.18	10.28	87.0	5004	(0.1)	660	(28.1)	7002	(8.5)
	20	4.18	10.28	97.7	5006	(0.1)	616	(50.6)	5875	(23.4)
	24	5.42	10.96	99.6	5007	(0.2)	611	(63.1)	5173	(25.0)
East										
	4	1.10	8.52	11.0	160	(4.3)	260	(25.2)	2546	(5.3)
	5	1.14	8.41	17.1	372	(1.8)	317	(23.5)	3416	(11.3)
	6	1.18	8.31	24.1	685	(0.8)	383	(22.0)	4194	(9.4)
	7	1.25	8.16	31.7	1107	(0.0)	457	(20.6)	5066	(7.9)
	8	1.32	8.01	39.7	1651	(-0.6)	540	(19.3)	6141	(8.4)
	9	1.43	7.83	47.8	2333	(-1.3)	646	(18.2)	7472	(7.4)
	10	1.54	7.65	55.6	3168	(-2.0)	759	(16.7)	8949	(7.0)
	11	1.69	7.55	63.0	4170	(-2.8)	876	(16.7)	10346	(7.6)
	12	1.84	7.44	69.8	5004	(0.1)	894	(26.1)	10406	(15.5)
	13	2.19	7.46	75.8	5001	(0.0)	696	(13.7)	7705	(-0.7)
	15	2.60	7.64	85.3	5002	(0.1)	626	(21.5)	6691	(3.7)
	20	3.62	8.52	97.1	5002	(0.1)	589	(44.0)	5647	(18.6)
	24	4.52	9.45	99.4	5003	(0.1)	582	(55.4)	4949	(19.6)

While looking at such a broad range of metaocean condition is instructive to understand the unsteady response of the system and changes in loads, it should be noted that many of these events are highly improbable. Large wave heights are generally correlated with higher wind speeds, so many of the worst case increases in loads and losses in power in Figure 5.3 are relatively unlikely. Table 5.1 gives the expected wave heights, periods, and cumulative density functions (CDF) for two representative sites on the east and west coasts of the United States [144] and the corresponding loads, both in the absolute values and percent difference from baseline onshore case. The west coast site has larger wave periods, making the low speed power gains and increased loading more pronounced. At near rated wind speeds, maximum thrust and root bending moment are increased by 26-30% and 15-18% respectively.

Using the combined probability density function for the full range of metocean conditions, the annual energy production was calculated in Table 5.2. The AEP for the floating cases is relatively unchanged compared to onshore. There is a small increase in AEP, but gains at low wind speeds and losses at near rated wind speeds are largely average out.

Table 5.2: FOWT performance at expected metocean conditions for two reference sites

East			West		
$AEP_{Onshore}$ GWh	$AEP_{Floating}$ GWh	Difference %	$AEP_{Onshore}$ GWh	$AEP_{Floating}$ GWh	Difference %
23.43	23.56	0.55	22.76	22.83	0.32

5.2 Steady optimization with load amplification

The previous section showed the changes to power production and loads for a FOWT when the rotor was designed for onshore or fixed bottom conditions. In

this study, new blades are optimized for the same FOWT configuration using low-fidelity, steady-state models that decouple the power production and loading from the hydrodynamic response and platform kinematics. Percent increases in the steady-state design constraining loads are used to approximate the dynamics effects of the floating platform, assuming that AEP is unchanged. A pareto front is then created to examine design trade-offs between reducing unsteady loading and increasing AEP. While this simplified method neglects the numerous dynamic couplings, it is informative in identifying design trends and potential technology pathways for FOWT rotors prior to conducting costly time-domain optimization, discussed in the following chapter.

5.2.1 Problem Formulation

For this study, WISDEM's blade structural analysis tool, RotorSE, and steady Blade Element Momentum solver, CCBlade, were used as the primary analysis tools. These tools were wrapped in Python OpenMDAO optimization assemblies according to Figure 5.4. The primary optimization loop is driven by the Python library Py-OptSparse's [125] implementation of the CONMIN [152] gradient-based algorithm. Objective function evaluations during finite differencing are parallelized to leverage HPC resources. The inner structural design loop is limited to a single design variable such that a single constraint is satisfied. This allows the inner design loop to be treated as a root-finding problem to significantly reduce computational costs, in this case the Brent [14] method implemented in Python's SciPy [79] package.

The nested optimization framework in Figure 5.4, where the spar cap thickness is sized for a given planform design, is necessary due to the finite-differencing schemes employed by gradient-based optimization methods. During finite differencing, the gradient is approximated by assessing the objective function and constraints at small step changes in each design variable independently. Optimizing the aerodynamic and structural design variables in a monolithic approach can lead to suboptimal designs.

For example, consider a scenario where a blade is being optimized for maximum AEP subject to a maximum tip deflection constraint and the tip deflection constraint is active for the current candidate design. A step change in planform variables towards a higher C_P will increase AEP but will increase thrust and violate the tip deflection constraint, yielding an infeasible search direction. A step increase in spar cap thickness will increase stiffness and reduce tip deflection, but this does not result in a change in the objective, AEP. Intuitively, the designer knows that a higher AEP solution is feasible by changing the planform variable towards higher C_P and the structural variable towards higher stiffness simultaneously. In a gradient-based domain, this is accomplished by nesting the structural design optimization within the aerodynamic design optimization, optimizing the structural design for each candidate planform. Alternatively, a gradient free approach, such as a Genetic Algorithms, could be used, but with much higher computational costs. A nested approach can even accelerate Genetic Algorithm convergence, as more of the randomly generated initial population would start with feasible solutions, translating into lower penalties applied to the fitness function.

5.2.1.1 Objective and Constraints

Annual energy production was selected as the objective function for the steady optimization of FOWT blades. Equation 5.2 gives the formal problem definition, where X_P and X_S are the planform and structural design variables, F and f are the outer and inner design loop objective functions, and G and g are the outer and inner constraints respectively. A blade cost model [11] was implemented and COE estimated by assuming a constant value for the remaining turbine capital costs and operation and maintenance costs. COE was not used for the objective function since the effects of the load mitigations under consideration in this study will primarily

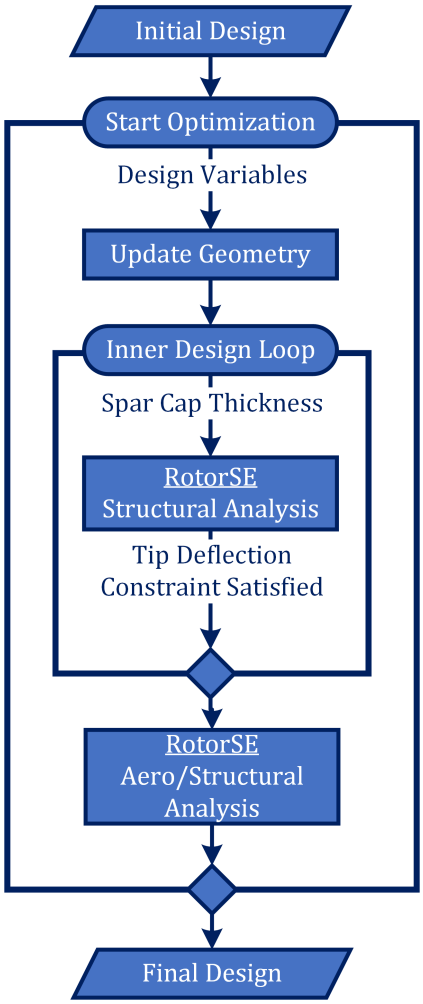

Figure 5.4: Workflow for steady optimization

benefit mass savings elsewhere in the system and reduced operation and maintenance, which are not captured by the COE estimated from blade costs alone.

$$\begin{aligned} \min_{X_P, X_S} \quad & F(X_P, X_S) = \frac{-AEP(X_P, X_S)}{AEP_0} \\ \text{s.t.} \quad & G(X_P, X_S) \leq 0 \\ & X_S \in \arg\min_{X_S} \{ f(X_P, X_S) : g(X_P, X_S) \leq 0 \} \end{aligned} \tag{5.2}$$

The steady-state BEM solutions from CCBlade were used to generate a power curve for a candidate design and the AEP calculated for IEC Class I-B conditions.

The steady-state model is for an onshore turbine, with no hydrodynamic loading. The power curve solver for regulated variable-speed rotors implemented within RotorSE assumes the design tip speed ratio for Region II, maintains either maximum rotor speed or maximum tip speed in Region II.5, and rated power in Region III until the cut-out wind speed.

The primary constraints on the optimization were tip deflection and the magnitude of the blade root bending moment vector under both gust conditions and the thrust at rated wind speeds. The maximum values are limited to the baseline loads for the NREL 5MW. The gust design load cases specified in the IEC 61400-1 is inherently dynamic, with the gust velocity ramping up over time. The steady implementation within RotorSE is quite conservative, using a constant gust velocity, V_{gust}, defined for an extreme operating gust (EOG), at rated rotor speed and blade pitch angles. The resulting loads are higher than would be predicted by a time domain simulation, where the variable speed pitch controller would feather the blades to alleviate loads and attempt to maintain rated rotational speed as the gust velocity ramped up.

Modeling the quasi-FOWT dynamic load increases in a steady domain is accomplished by applying a dynamic amplification safety factor, γ_{LA}, to the steady design constraining loads predicted by the BEM solver. The safety factor is applied to the spanwise force along the blade calculated by BEM, and the resulting rotor thrust and root bending moment are constrained such that they do not exceed the values for the baseline NREL 5 MW without load amplification. Clearly, as the load amplification factor increases, the blades design will have to be adjusted to lower forces and satisfy these constraints. When evaluating AEP, the load amplification factor is not utilized.

Blade mass is constrained relative to the baseline NREL 5MW, but allowed to scale with blade length, L, as shown in Table 5.3. A scaling-law-based mass constraint aims to maintain reasonable blade masses while allowing tradeoffs between AEP and loads (which both vary with blade length) to be considered. Table 5.3 summarizes

all constraints. The thrust and root bending moments are constrained to the initial baseline NREL 5MW values.

Table 5.3: Constraints

Constraint	Value
Blade tip tower clearance ratio	> 0.5
Rotor thrust	$\leq$ baseline value
Blade root bending moment	$\leq$ baseline value
Blade mass	$\leq m_0 \left(\frac{L}{L_0}\right)^{2.2}$

5.2.1.2 Design Variables

The blade planform was parameterized by assigning control points for the chord and twist distributions. PChip splines [45] were used to fit spanwise distributions between the control point knots. The chord control point at the blade root (C_{r_0}) is fixed to the baseline value, as root design is driven by hub-bolt connections and fatigue, outside the scope of this work. An additional design variable defined the spanwise position of the first control point, $r_{c_{max}}$, which is typically the spanwise position of maximum chord. The twist distribution was also held at a constant value inboard of $r_{c_{max}}$. The airfoil distribution and relative thickness were held to the baseline values. Table 5.4 summarizes the design variables.

Table 5.4: Design Variables

Design Variable	# of D.V.	Bounds	
		Lower	Upper
Chord	4	0.9375 m	6.2 m
Twist	4	-5°	25°
Spanwise Position of 1st Control Point	1	0.15	0.35
Blade Length	1	55 m	80 m
Spar Cap Thickness	1	10 mm	200 mm

Blade length was also a design variable but had to be treated carefully. Since the loads were constrained to the initial baseline values and were artificially increased, the initial design was always outside of the feasible domain. The simplest way to alleviate loads was a large reduction in blade length in the first design iteration. In many cases, the gradient search did not recover, leading to a suboptimal local minimum.

The solution to this problem was a multi-stage optimization approach. First, the blade was optimized without the blade length as a design variable, returning to the feasible domain by altering the planform to reduce loads and C_P. The optimization was then repeated, using the final design from the first stage as the initial design and activating blade length as a variable. This results in a feasible starting point and dramatic improvements in convergence.

5.2.2 Optimized blade designs

A sensitivity study was conducted using a range of load amplification values, from 0 to 16%, to optimize blades using the framework outlined in Section 5.2.1. Figure 5.6 summarizes the steady outputs for the resulting blades, normalized by the baseline NREL 5MW design. The gray line represents the first optimization stage, where the blade length was held constant at 61.5 m. The black line represents the second optimization stage where blade length was included as a design variable.

The $\gamma_{LA} = 1.$ case is instructive, because it represents a direct re-optimization of the NREL 5MW, constrained by its initial load envelop and blade mass. In Figure 5.6.a, the constant blade length design, denoted here as Blade(61.5, $\gamma_{LA} = 1.$) for convenience, sees only a slight increase in AEP. This is to be expected due to the highly constrained nature of the problem, where only the chord and twist distributions can be modified. This design is then used as the initial position for re-optimization, including blade length as a design variable, Blade(L, $\gamma_{LA} = 1.$).

Longer, lower C_P blade designs can produce more power, or the same power with reduced loads, because rotor aerodynamic power increases linearly with C_P and quadratically will blade length. This is summarized in Figure 5.5 which shows the normalized power production relative to normalized changes in blade length and C_P. The tradeoff for these lower induction, lower specific power designs are increased costs associated with larger, heavier blades. These trends are reflected in the re-optimized blades in Figure 5.6, where Blade(L, $\gamma_{LA} = 1.$) has increased AEP by over 4%, achieved with a longer blade length and lower C_P while still satisfying the baseline load envelope constraints.

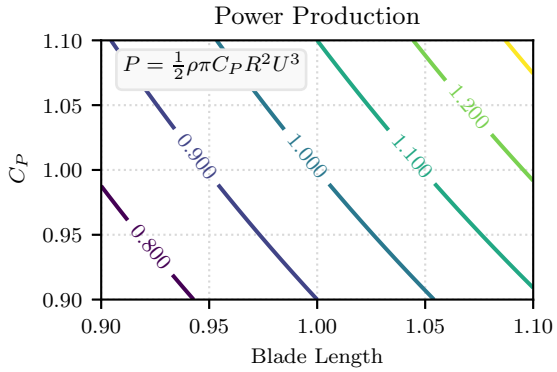

Figure 5.5: Normalized changes in aerodynamic power as a function of normalized changes in blade length and power coefficient

As γ_{LA} increases, the blade length optimized designs continue to have higher AEP than the corresponding fixed blade length designs, but with diminishing returns. Counter intuitively, as γ_{LA} increases, blade length decreases, where lower specific power blades could potentially satisfy the amplified load constraints and further increase AEP. This outcome is a direct result of the mass constraint, since higher γ_{LA} requires stiffer blades to satisfy the tip deflection constraint, increasing the proportion of spar cap mass relative to the total blade mass.

While COE was not an optimization objective, it was calculated for each solution. For Blade($L,\ \gamma_{LA} = 1.$) to Blade($L,\ \gamma_{LA} = 1.05$), the COE was lower or equivalent to the baseline NREL 5MW. The increase in AEP outweighs the increased costs associated with larger blades, while additionally providing modest load alleviation. As γ_{LA} increases further, beyond 1.05, COE rapidly increases for both optimization scenarios. This is a result of decreasing AEP and higher proportions of carbon fiber in the spar caps to provide sufficient blade stiffness.

The chord and twist design variable values are shown in Figure 5.10. The predominate trends are increased twist and reduced chord as the load amplification increases. Increased twist reduces the operational angles of attack, reducing lift and drag, and the overall thrust on the rotor. Variations in the design variables about the trend lines are caused by the relative flatness of the AEP design space; there are many non-unique solutions that can produce the same AEP.

It should also be noted how the assumed wind characteristics affected the optimization process. The NREL 5MW is an IEC class IB machine, a common design point for offshore turbines, where wind speeds are high and turbulence intensities are low. The mean wind speed is assumed to be 10 m/s and the 50-year return period gust, V_{e50}, is 70m/s. A higher wind class, with lower mean and extreme wind speeds, would decrease the annual energy production at a given C_P, but also decrease the design constraining extreme loading on the turbine. The overall trends presented would hold, but relaxation of the wind speeds for the design constraining load cases would drive the solution to longer, more flexible blades.

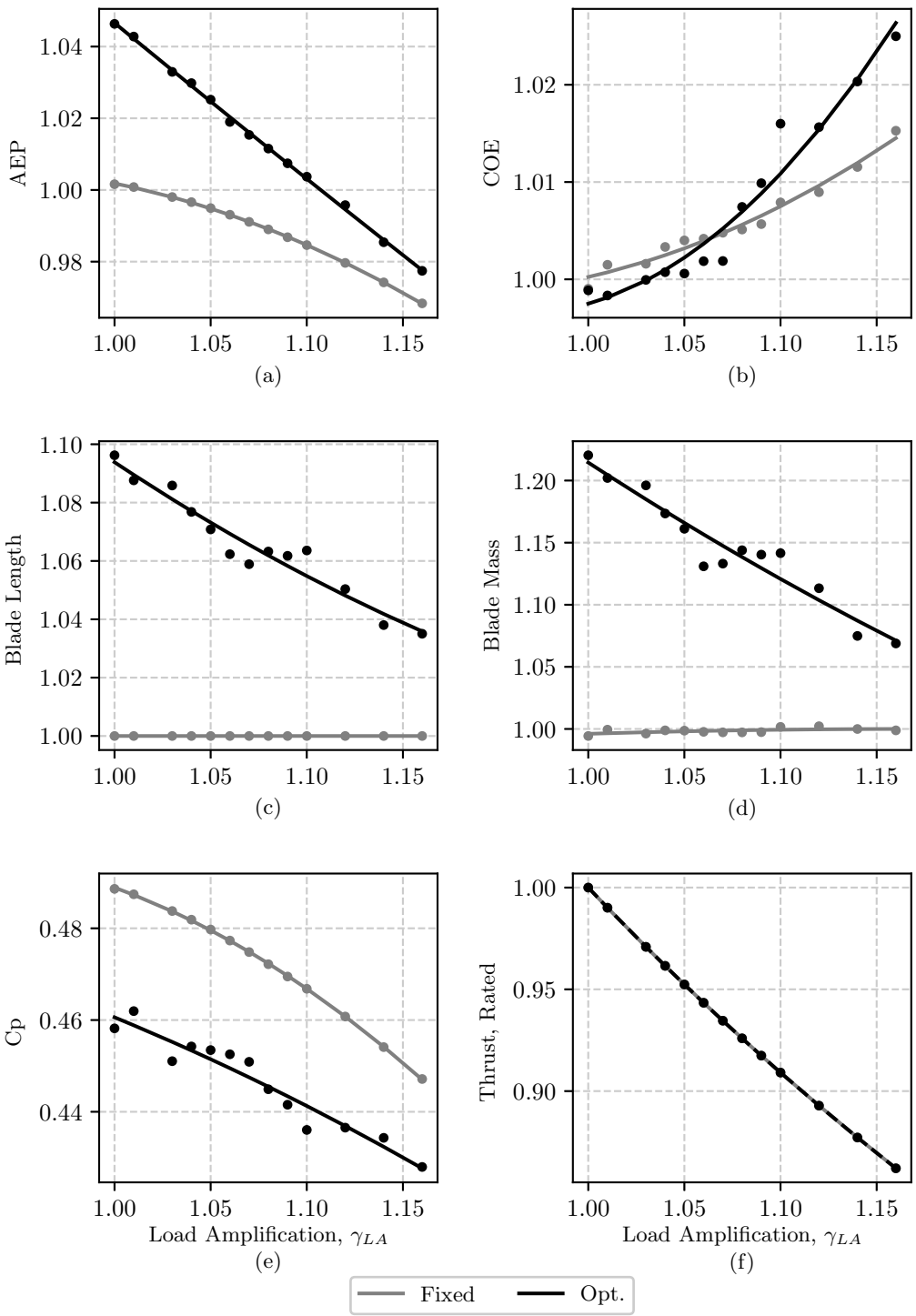

Figure 5.6: Optimized blade performance as function of load amplification

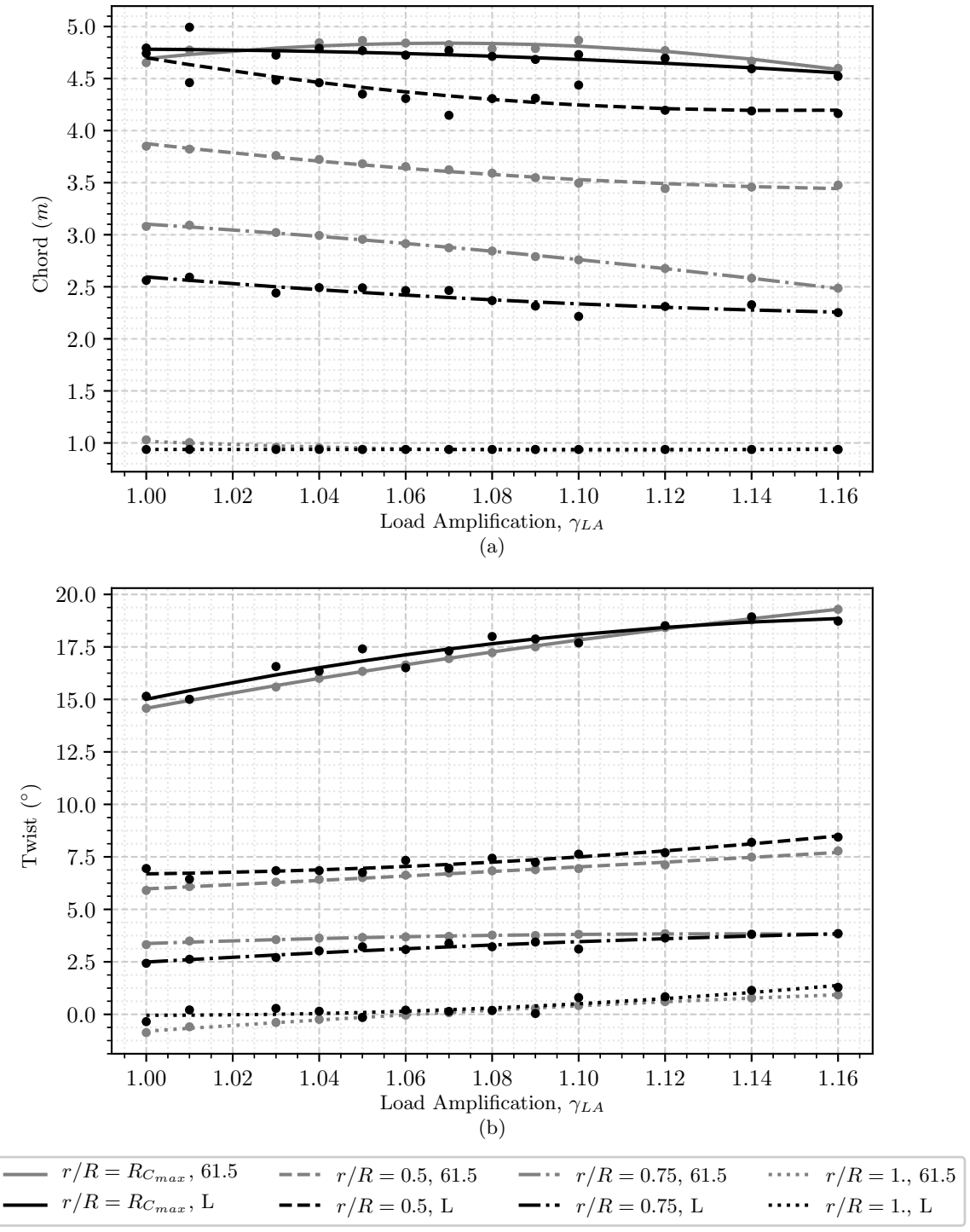

Figure 5.7: Optimized blade planform design variables as a function of load amplification

5.3 Dynamic Performance of Steady Optimized Blades

5.3.1 Design Trade-Offs

To test the effectiveness of the steady-optimized blades, the designs were simulated on the OC3/Hywind Spar buoy. NREL 5MW controller torque gains and generator speeds were updated for each blade to reflect to changes in C_P and rotor speed. The designs were simulated over a ranged of metocean conditions and the AEP calculated based on the combined cumulative density functions, in Table 5.5, for both the U.S. East and West coast offshore reference conditions normalized by the baseline NREL 5MW on the spar buoy. Table 5.6 gives the associated peak thrust for each blade.

The floating performance of the blades differs substantially from the steady-state analysis shown in Figure 5.6. Relative to the baseline NREL $5MW$ on the OC3/Hywind spar buoy, AEP changes by 0% to 6%. Recall that when using the steady-state models, AEP changes -2% to 5% relative to the steady-state baseline onshore NREL $5MW$ (Figure 5.6). The improvement in AEP relative to the baseline when modeling in OpenFAST on a FOWT can be attributed to two mechanism. First, the blades with lower thrust than the baseline have lower mean pitch angles, improving rotor alignment and increasing power production. Additionally, all the optimized blades are longer in length, allowing them to capture more of the power from the fore-aft velocity component. This table also highlights the impact of different metocean conditions. Interestingly, the East Coast reference site has a higher mean wind speed of $U = 9.77m/s$, compared to the West Coast $U = 9.5m/s$, but the West Coast site has higher percent increases in AEP. The West Coast site has more frequently long wave periods and greater wave heights, resulting in larger fore-aft strokes in which additional energy can be extracted.

Thrust is also higher than predicted by the steady-state analysis, with several low γ_{LA} designs having higher thrust than the $\gamma_{LA} = 1.0$ case. This is a direct result of dynamic effects, namely the transition from control Region II.5 to III. The linear

Table 5.5: Floating AEP Comparion for Optimized Blades

Load Multiplier γ_{LA}	East		West	
	$AEP_{Floating}$ GWh	Difference %	$AEP_{Floating}$ GWh	Difference %
Baseline	23.87	-	23.96	-
1.00	25.36	6.23	25.41	6.06
1.01	25.35	6.20	25.40	6.03
1.03	24.98	4.62	25.07	4.65
1.05	24.82	3.98	24.92	4.03
1.07	24.54	2.79	24.65	2.90
1.09	24.39	2.16	24.51	2.30
1.10	24.24	1.53	24.37	1.71
1.12	24.09	0.89	24.22	1.09
1.14	23.82	-0.24	23.96	0.01

transition between these two control states causes discontinuities in the torque control curves, which can lead to significant transient load increases, made worse as it occurs when the turbine is already under its heaviest loading. This is a known controls challenge for horizontal axis wind turbines that more sophisticated controls strategies can smooth out, for example by pitching the blades to alleviate loads, but is outside the scope of this work. Floating platform motion can exacerbate this problem at near rated wind speeds, where the cyclical fore-aft velocity component causes periodic transitions between control regions. If the FAST simulations are part of the optimization process, it can drive the solution to have a smaller Region II.5s by reaching rated rotor speed closer to rated power or by driving the design towards lower thrust, reducing the load on the rotor when the transition occurs to reduce its impact. A more globally optimal solution could potentially be reached by simultaneously designing the turbine and the controller, known as co-design.

Table 5.6: Floating Peak Thrust Comparion for Optimized Blades

Load Multiplier γ_{LA}	East		West	
	T_{max} kN	Difference %	T_{max} kN	Difference %
Baseline	864	-	867	-
1.00	889	2.83	877	1.24
1.01	891	3.16	882	1.74
1.03	900	4.12	896	3.38
1.05	877	1.48	872	0.67
1.07	842	-2.55	837	-3.45
1.09	824	-4.69	818	-5.59
1.10	806	-6.70	801	-7.58
1.12	789	-8.73	783	-9.61
1.14	772	-10.6	760	-12.3

The maximum floating thrust and AEP data is summarized in the Pareto front in Figure 5.8 and maximum floating root bending moment and AEP in Figure 5.9, normalized by the baseline NREL 5MW on the OC3/Hywind spar buoy at the same metocean conditions. The vertical dashed line demarks where thrust loads are less than or greater than the baseline and the horizontal dashed line demarks AEP. For all but the highest γ_{LA}, AEP is improved on the baseline.

The Pareto front highlights the benefits of this approach. Knowing that FOWT operation increases dynamic loading relative to onshore or fixed bottom, the rotor was optimized by artificially increasing its steady-state design constraining loads. Since the difference between the steady and dynamic loading for arbitrary new blade designs was unknown, the process was repeated for a series of load amplification factors. Blades optimized with γ_{LA} greater than 1.09, the lower induction designs, have improved AEP and decreased loading.

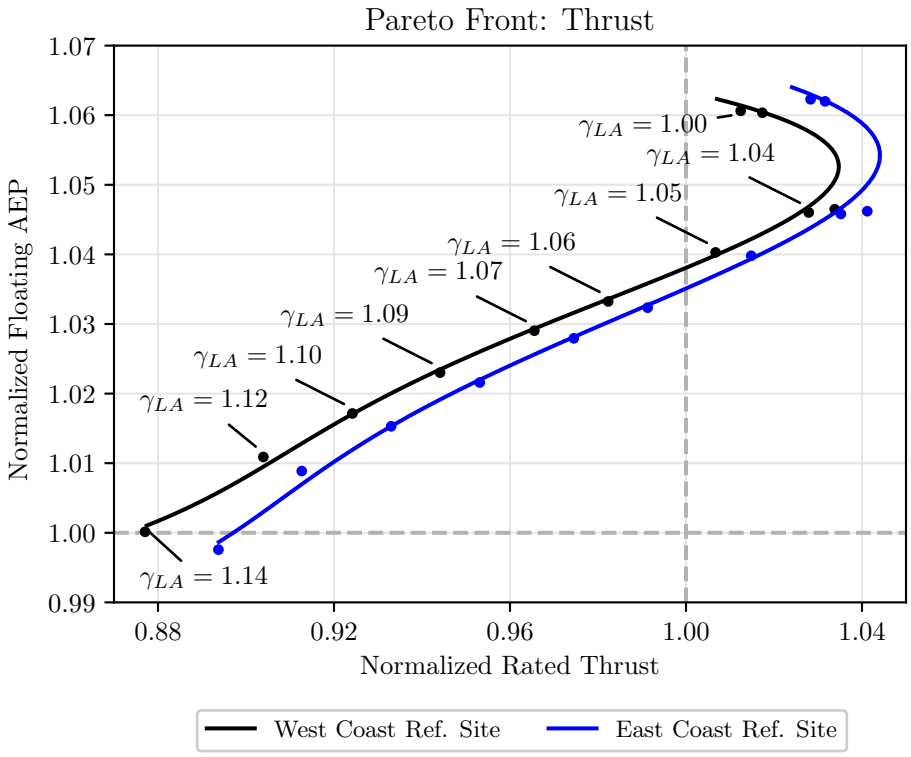

Figure 5.8: Pareto front for normalized floating AEP and peak thrust for steady-state optimized blades

A notable feature in these plots is the kink in the upper right quadrant where thrust and root bending moments initially increase with γ_{LA}. The steady state optimization has failed to fully capture the coupled dynamics between the platform and rotor, resulting in higher loads when the dynamics are considered. Furthermore, it shows that the design space using dynamic simulations is non-convex; multi-start approaches or global search methods should be used to avoid local minimums.

If an actual blade were being designed, determining the "true optimal" would require more system level analysis and detailed cost of energy modeling. A heavier, more highly loaded design may in indeed be worthwhile due to the additional energy captured, or a lighter low induction design with more carbon fiber may enable cost savings in the tower and floating support structure. This approach gives the designer

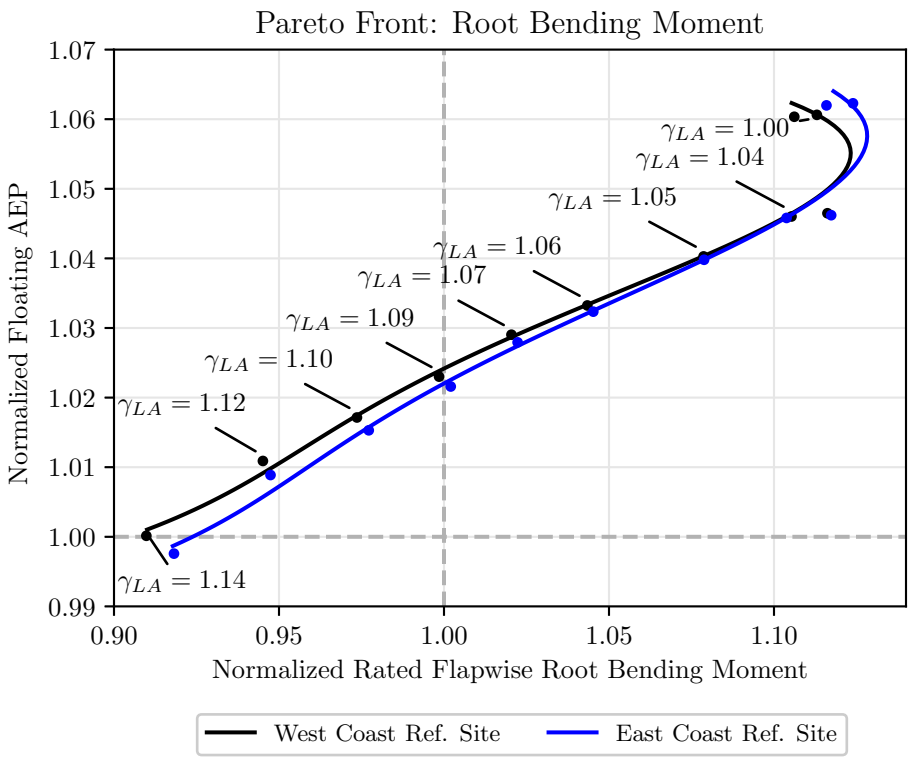

Figure 5.9: Pareto front for normalized floating AEP and peak flapwise root bending moment for steady-state optimized blades

the knowelege needed to pursue those design trade-offs further at relatively low computational cost.

5.3.2 Performance of Low Induction Rotors on FOWTs

The low induction rotors appear to be a promising technological pathway for FOWT applications. Here, two lower induction rotors, with γ_{LA} of 1.06 and 1.12 and C_P of 0.440 and 0.427 respectively, are compared against the optimized control design, $\gamma_{LA} = 1.0$ and $C_P = 0.443$. The planforms of the selected blades are shown in Figure 5.10.

Figure 5.11 shows the dynamic power curves (average power produced during a 10-minute dynamic simulation) at the expected metocean conditions for the West Coast reference site. Relative to the baseline NREL 5MW, the optimized blades

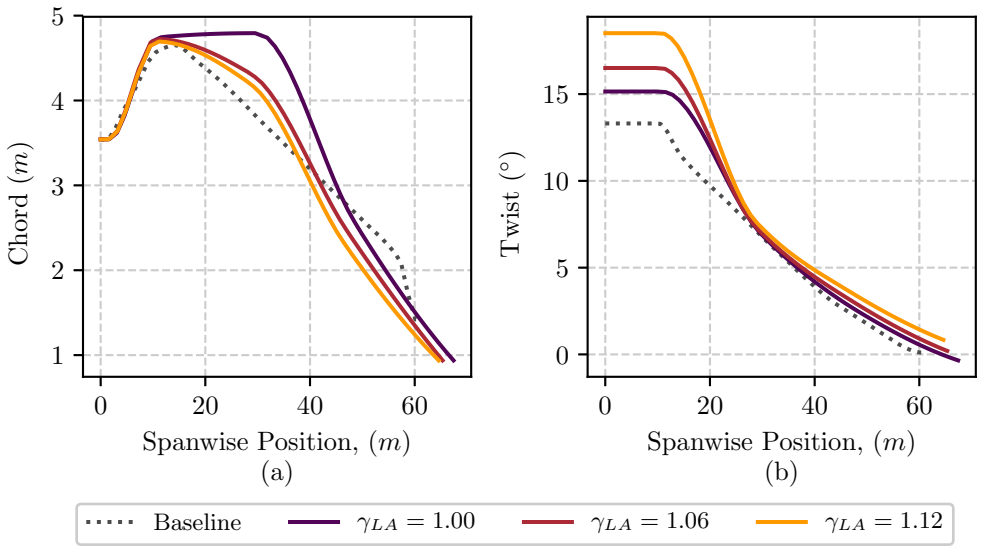

Figure 5.10: Planforms of steady optimized blades

increased power production by reducing the rated wind speed, reaching rated power at lower wind speeds due to their larger rotors. As expected, dynamic loading increases the thrust and root bending moments, with $\gamma_L A = 1.0$ exceeding the baseline loads in Figure 5.11.b and 5.11.c, which were used for its steady-state design constraints. In Figures 5.11.d, the flap-wise blade tip deflection is lower for all the optimized blade designs relative to the baseline. This can be attributed to the steady-state "gust" design load case over constraining tip deflections. A more accurate extreme load case is expected to allow longer blades, but the predominate trends to hold. This is explored limitation in the current design approach is addressed in Chapter 6 using time domain design load cases.

The results in Figure 5.11 are shown in more detail in Figures 5.12 to 5.14 over a range of metocean conditions. The figures are normalized by the $\gamma_{LA} = 1.0$ optimized blade at the corresponding metocean condition. The color scales for each output, i.e. power or thrust, are the same for $\gamma_{LA} = 1.06$ and $\gamma_{LA} = 1.12$, with blues indicating a percent decrease from $\gamma_{LA} = 1.0$ and reds a percent increase.

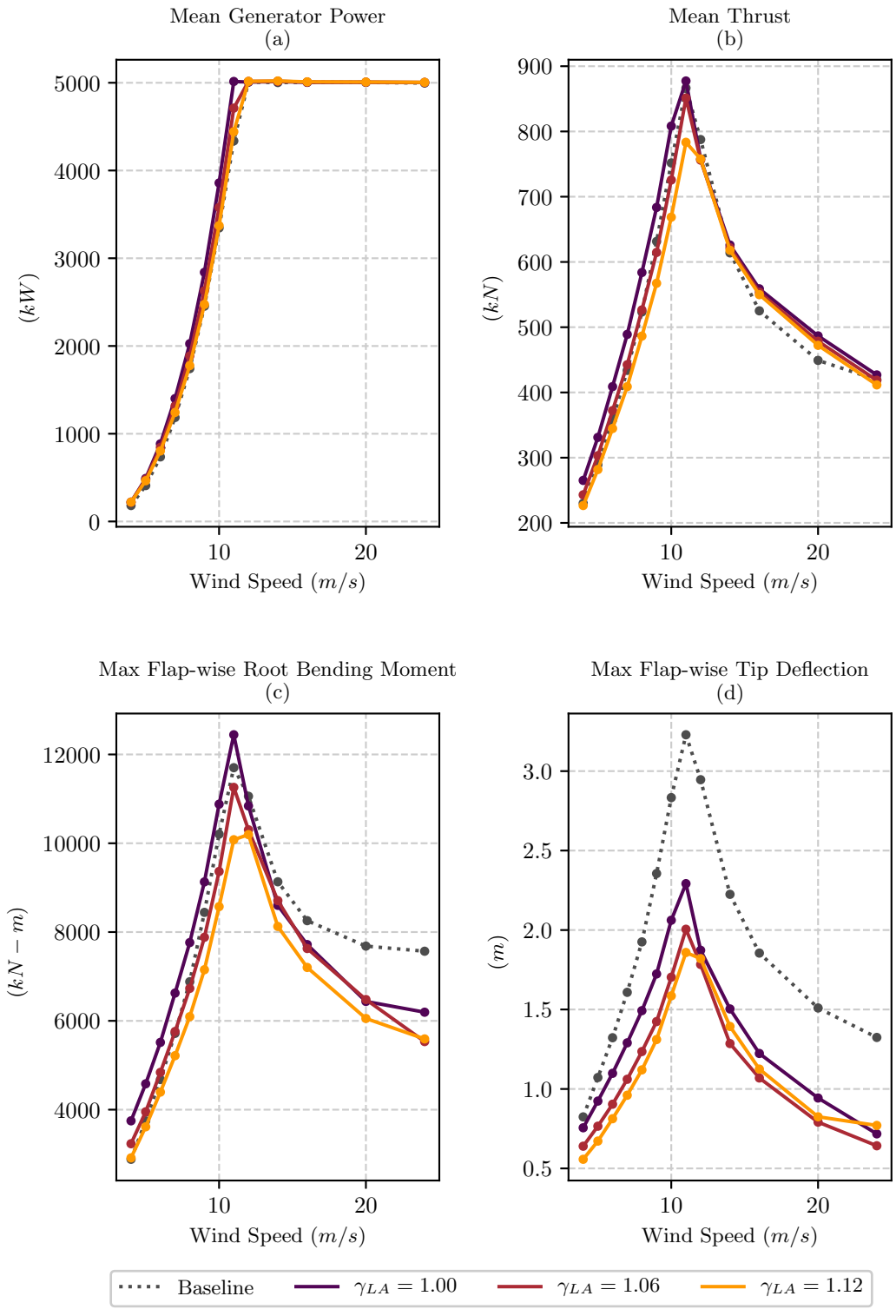

Figure 5.11: Mean floating performace as function of wind speed

In Figure 5.12, the low induction designs generally have lower generator power, as already shown in Figure 5.11.a. At very low wind speeds and relatively calm sea states, more power is generated due to better rotor alignment. For below rated conditions, both low induction designs produce significantly lower thrust. The thrust plots demonstrate some noise at wind speeds of about 10 to 11 m/s. This is a result of higher rated wind speeds, relative to the $\gamma_{LA} = 1.0$ design, resulting in Region II.5 transitions occurring at different wind speeds. In Figure 5.13, the low induction rotors show significant improvements in flap-wise tip deflections and root bending moments. Root moments are transferred into the drivetrain, so system level cost savings are likely due to these reduced loads. Finally, in Figure 5.14, below rated platform pitches are reduced by about 10 to 20% for the two low induction designs. This improves platform stability and can transfer cost savings to the tower and floating platform. Again, there is noise at near-rated conditions, based on when the various blade designs change control regions.

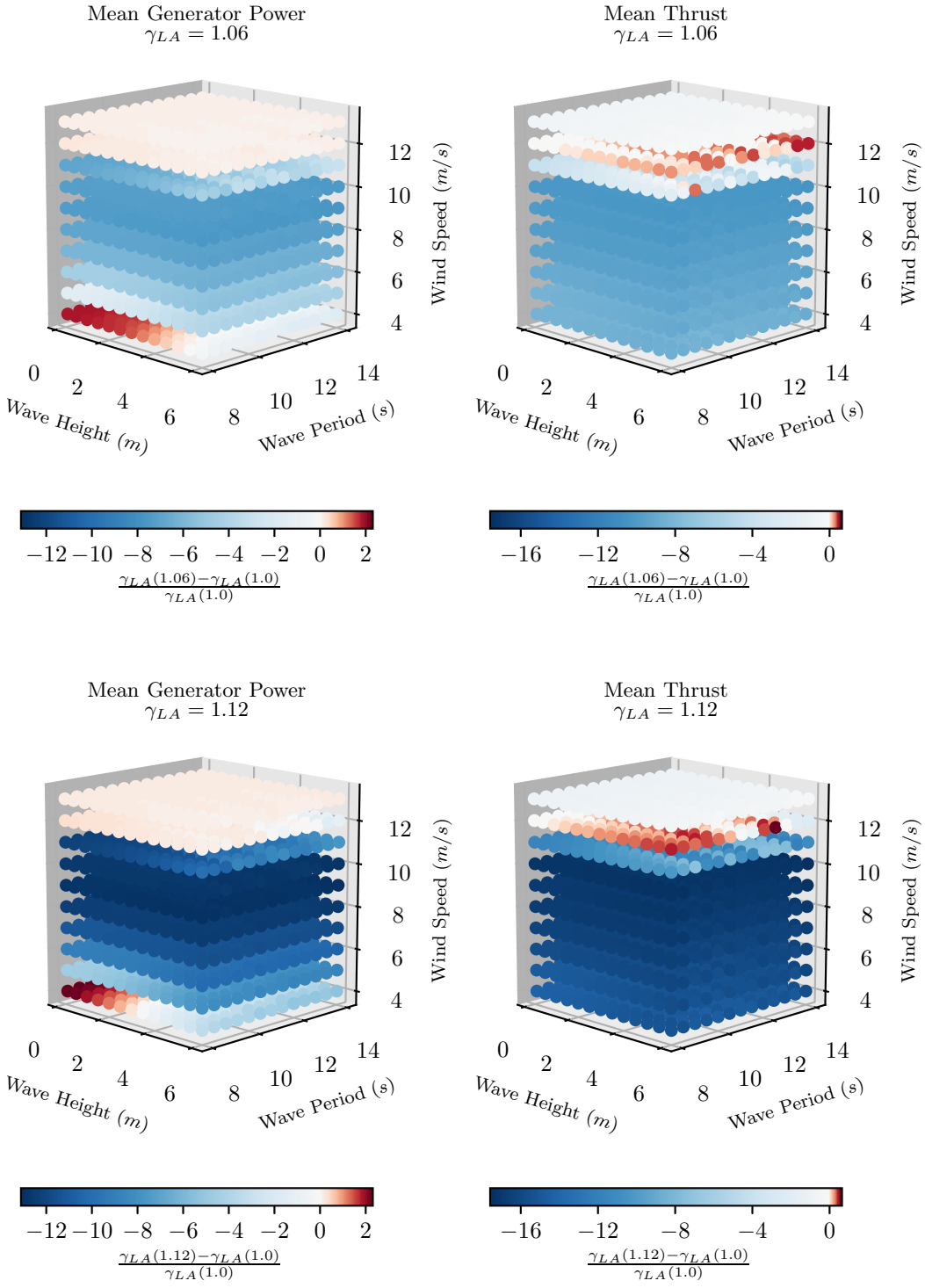

Figure 5.12: Percent change in lower induction rotor power and thrust relative to γ_{LA} = 1.

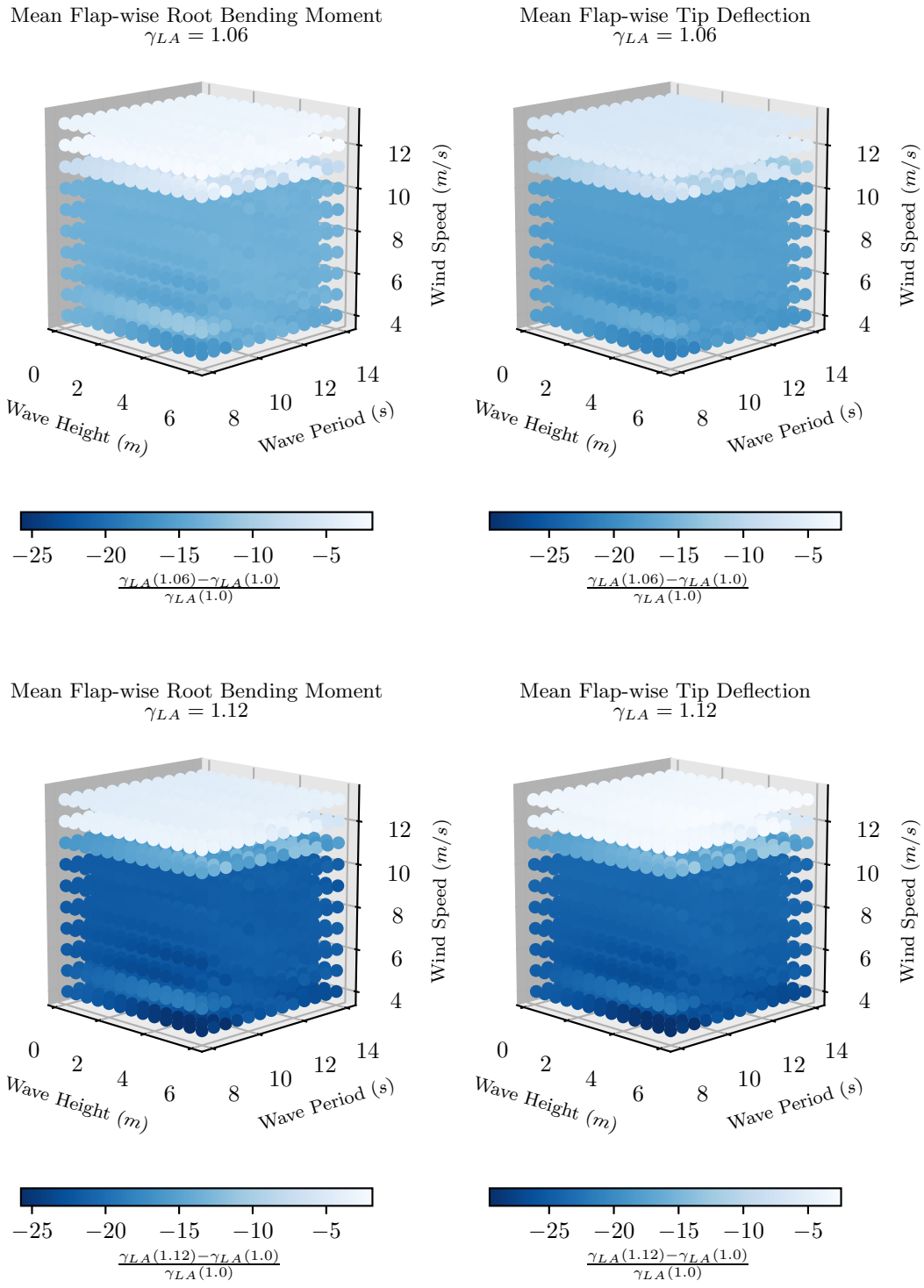

Figure 5.13: Percent change in lower induction rotor flapwise root bending moments and tip deflections relative to $\gamma_{LA} = 1$.

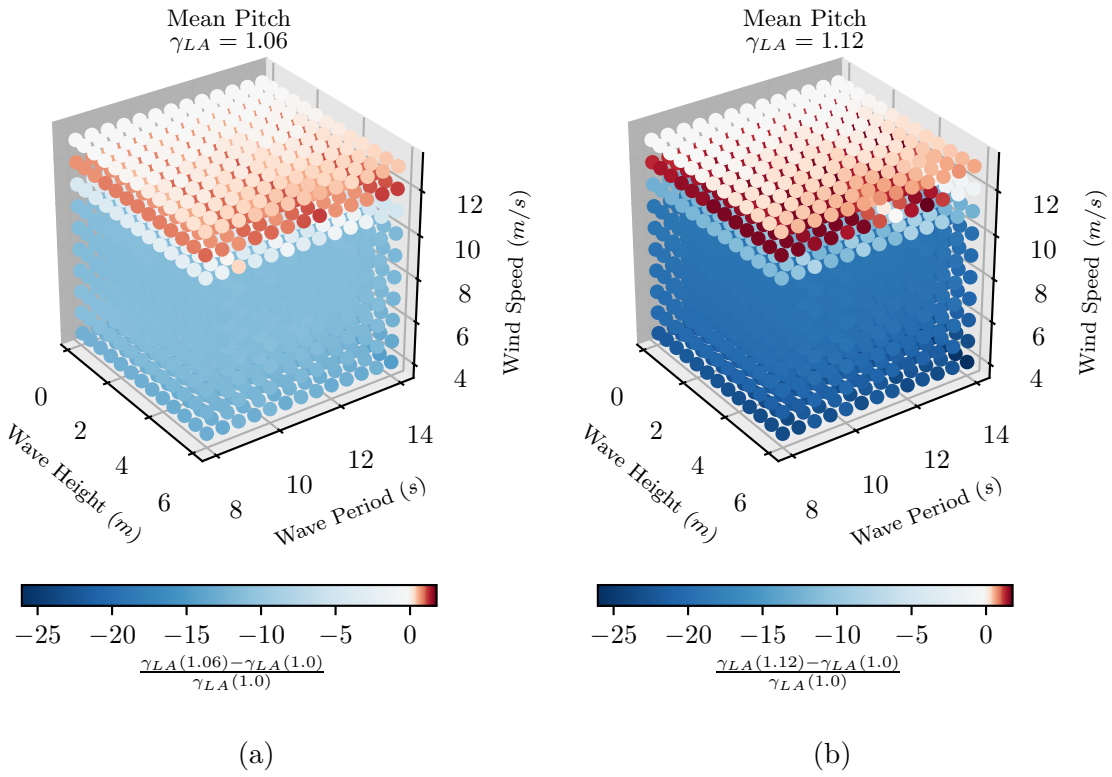

(a) (b)

Figure 5.14: Percent change in lower induction rotor platform pitch relative to $\gamma_{LA} = 1$.

5.4 Conclusions

This chapter presented a lower-order method for optimizing floating offshore wind turbine blades without the computational cost of time domain simulations. Rather, a range of steady-state load increases were assumed while optimize annual energy production. The final optimized designs were simulation with dynamic simulations to generate a Pareto front showing the trade-offs between increased AEP and loads.

The key outcome was the potential benefits of low induction rotors for FOWTs. Less thrust on the rotor reduces mean platform pitch angles, better aligning the rotor to capture more power. While cyclically pitching fore-aft, a larger rotor can capture additional power from the platform velocity component. These benefits were achieved while reducing loads on the optimized blade designs.

While this optimization framework was successful in highlighting the overall design tradeoffs in FOWT blade design, the use of steady-state aerodynamic model of extreme conditions over estimated loads and over constrained tip deflections. Furthermore, it is impossible to say whether the changes in AEP, blade mass, and loads represent 'better' designs without analyzing the system level impacts on the complete FOWT. Lower mean pitch angles and decreased cyclical loading will have benefits for the support structure, potentially allowing for cost savings. However, it is very possible that the increases in blade mass from this study are undesirable, for example by requiring additional ballast in the floating platform. A systems level optimization could find more radically different designs, such as lightweight blades using a more expensive material like carbon fiber, in order to achieve down-tower savings.

CHAPTER 6

DYNAMIC FLOATING OFFSHORE WIND TURBINE BLADE OPTIMIZATION

In the previous chapter, the use of steady-state models did not fully capture the system dynamics. Tip deflections were over predicted due to the steady-state gust case, resulting in overly conservative designs. Controller interactions near rated under-predicted thrust for some of the optimized blades. Annual energy productions were lower than when modeled using dynamic simulations that captured fore-aft motion. This chapter addresses these concerns, including dynamic OpenFAST simulations in the optimization loop.

6.1 Problem Formulation

6.1.1 Solution Workflow

RotorSE driving OpenFAST simulations are used to evaluate blade designs in this study. RotorSE was used to update the OpenFAST model for new blade designs, handled all geometric manipulations based on the design variables, calculated the spanwise stiffness and inertial properties using PreComp, and determined the blade natural frequencies and mode shapes using pBEAM and CurveFEM. The steady-state RotorSE analysis also provides the initial rotor speed and blade pitch angle conditions for OpenFAST, making the simulations much more stable.

For this study, a nested optimization approach was used, solving for the spanwise spar cap thickness, such that the structural constraints were satisfied and mass minimized in the inner design loop. The CONMIN [152] gradient-based algorithm

was used for the inner loop. Unlike the previous study, which used a 1D root-finding algorithm to scale the existing spar caps for computational speed, four spanwise design variables were used. This required $O(2)$ increase in the number of design evaluations for the inner loop, but allows for a less constrained design space.

An OpenFAST simulation of IEC DLC 1.4, an extreme coherent gust with a direction change, was used to assess the extreme loads. However, if this load case was evaluated at every iteration in the inner design loop, the computational expense would be prohibitive. Rather, a multi-fidelity approach was taken, where the steady-state estimate was corrected using an OpenFAST simulation to reduce the uncertainty. The tip deflection was evaluated with both steady-state RotorSE and OpenFAST. This was used to tune the dynamic amplification factor, Equation 6.1, and then run the inner optimization using the steady-state model. This improves the extreme loads estimate, but without excessive computational costs. Algorithm 2 summarizes the workflow.

$$\gamma_{LA} = \frac{\delta_{tip,OpenFAST}}{\delta_{tip,RotorSE}} \tag{6.1}$$

Using time domain simulations significantly increases the complexity of the design space, creating local minimum and adding noise. This was shown in Pareto Front Figures 5.8 and 5.9 in the previous chapter, where the resulting dynamic loads increased contrary to the overall trend due to the non-convex design space. Non-linear controller actions cause local extrema in the design space based on when the event occurred in the sampled time series. Such controller actuations are more common for floating platforms due to the increase in unsteady aerodynamic loading. Numeric artifacts can also increase the noise in the design space when working with time series data. For example, sampling a time series with a discrete window can result in averaging errors as the phase of signals shifts. Conservative simulation settings had to be used, such as periodic waves and steady wind speeds as opposed to random waves and turbulent

Algorithm 2: RotorSE/OpenFAST based blade design optimization

```
Data: Initial OpenFAST model, initial blade design
Result: Optimized Blade Design
for all Generations do
    for all Individuals in Population do
        Update blade geometry base based on outer design variables
        Calculate blade elastic properties
        Compile updated OpenFAST controller
        Extreme Load Analysis: Steady-State RotorSE
        Extreme Load Analysis: Dynamic OpenFAST
        Calculate γ_LA
        Inner Structural Optimization while ΔObjective > tolerance do
            Update blade geometry base based on inner design variables
            Calculate blade elastic properties
            Extreme Load Analysis: Steady-State RotorSE
        Determine power curve with OpenFAST
        Calculate AEP
```

wind, to reduce the noise in the resulting signals. Robust error handling was needed to detect and throw out erroneous numerically unstable simulations.

A gradient free algorithm was therefore used, to provide a global search. The DEAP python package [44] implementation of the NSGA-II [26] genetic algorithm (GA) was selected due to its relatively fast convergence amongst global searches. Table 6.1 gives the GA settings used. Using a GA required a massive increase in computational expense. The steady-state optimizations from the previous chapter required approximately 100 CPU hours. The GA-driven OpenFAST-based optimization required approximately 100,000 CPU hours. The problem was highly parallelized using MPI on a super computing cluster. A total of 792 cores were used, a parallel process for each fitness evaluation per generation, each of which would run multiple OpenFAST simulations and the inner optimization problem.

Table 6.1: NSGA2 Genetic Algorithm Settings

Fitness Evaluations	
Population Size	792
Generations	35
Evolutionary Properties	%
Mating Probability	90
Simulated Binary Crossover Crowding Distance	20
Polynomial Mutation Crowding Distance	20

6.1.2 Design Variables

Spanwise design variables for chord, twist, and spar cap thickness were set with spline control point knots, as discussed in Section 4.1. Additionally blade length and tip speed ratio were included as design variables. Allowing the tip speed ratio to change affects the rate at which the turbine reaches rated power and can change the size of Region II.5, potentially improving the transient loads during control region switching. Additionally, increasing tip speed ratio allows blades with smaller chords, allowing a less constrained design space for the optimizer to explore power, thrust, and mass design trade-offs. The outer design loop controls all design variables except spar cap thicknesses, controlled by the inner design loop. Table 6.2 summarizes the design variables and their bounds.

Table 6.2: Design Variables

Design Variable	# of D.V.	Bounds	
		Lower	Upper
Chord	4	0.861 m	5.5 m
Twist	4	-5°	20°
Spar Cap Thickness	4	1 mm	300 mm
Blade Length	1	55 m	80 m
Tip Speed Ratio	1	4	10

6.1.3 Objectives and Constraints

Design constraints are summarized in Table 6.3, detailed in Section 4.3. For the inner gradient-based design loop, the constraints can be directly enforced as listed in the table. For the GA however, the constraints are converted into a penalty function and applied to the fitness value. The constraints are re-expressed as ratios, for example, the thrust constraint is converted from Equation 6.2 to Equation 6.3. The product of the maximum value between each penalty and 1 gives the total penalty function, Equation 6.4. A design that satisfies all constraints will have $P_{total} = 1.$. Penalized floating annual energy production is maximized as the fitness function for the outer design loop, according to Equation 6.5. The inner design loop minimizes blade mass such that the constraints are satisfied.

$$T - T_0 \leq 0. \tag{6.2}$$

$$P_T = \frac{T}{T_0} \tag{6.3}$$

$$P_{total} = \prod_{i=1}^{n} \max\left[P_i, 1.\right] \tag{6.4}$$

$$\begin{aligned} \min_{X_P, X_S} \quad & F(X_P, X_S) = \frac{-AEP(X_P, X_S)}{P_{total}} \\ & X_S \in \arg\min_{X_S} \{ f(X_P, X_S) = \frac{m_{blade}}{m_{blade,0}} : g(X_P, X_S) \leq 0 \} \end{aligned} \tag{6.5}$$

Table 6.3: Constraints

Constraint	Value
Rotor thrust	$T - T_0 \leq 0$
Blade root bending moment	$M - M_0 \leq 0$
Blade tip tower clearance	$\frac{\gamma_m \delta}{x_{unbent}} - 1. \leq 0$
Pannel Buckling	$\epsilon_{cr}(r_i) - \gamma_f \epsilon(r_i) \leq 0$
Blade mass	$m - m_0 \left(\frac{L}{L_0}\right)^{2.2} \leq 0$
1P Resonance Avoidance	$\min \begin{bmatrix} f_{N_i} - \frac{f_{1P}}{\gamma_{freq}}, \\ \gamma_{freq} f_{1P} - f_{N_i} \end{bmatrix} \leq 0$
3P Resonance Avoidance	$\min \begin{bmatrix} f_{N_i} - \frac{f_{3P}}{\gamma_{freq}}, \\ \gamma_{freq} f_{3P} - f_{N_i} \end{bmatrix} \leq 0$

6.2 Optimized Blades Designs

Two blades were optimized using the above procedure, on the NREL 5MW OC3/Hywind spar buoy and onshore, for comparison. The expected metocean conditions from the U.S. West Coast reference site were used for AEP calculations. Table 6.4 summarizes key parameters of the optimized blades and the planforms are plotted in Figure 6.1. The immediately apparent key difference from these blades and those optimized in the last chapter is the significantly longer blade length, with 78.5 and 79.1 m for the onshore and offshore optimized blades respectively. This was enabled by the more realistic extreme design load case analysis.

The AEP for both blades is quite similar, with the onshore-optimized blade 1% higher when also operating on an FOWT. However, the blades have significantly different structures and loading profiles that will be discussed in the subsequent sections. For example, the kink in the offshore optimized blade twist distribution

results in a higher lift-to-drag ratio, reducing thrust on the blade, discussed in Section 6.2.3. The analysis emphasizes why the optimization was driven to these solutions.

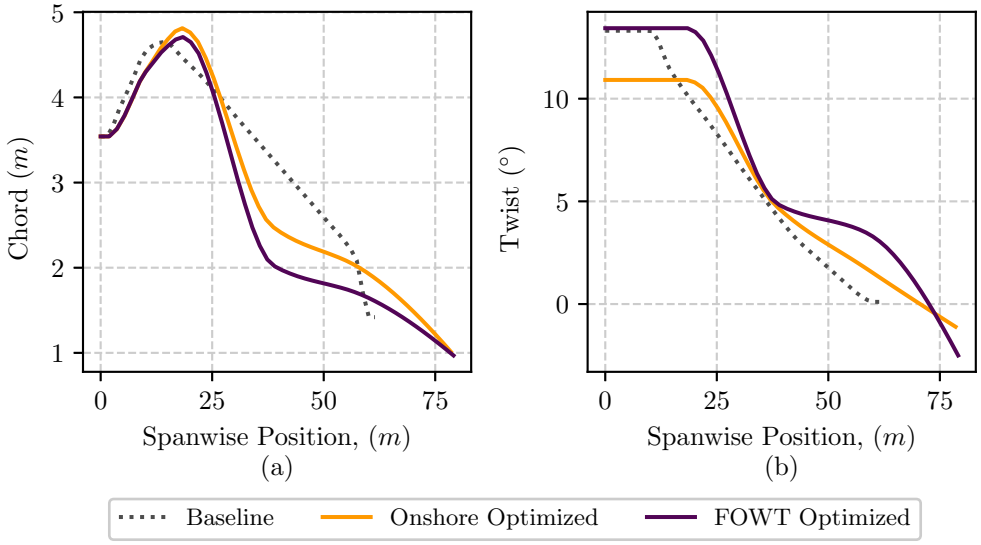

Figure 6.1: Planforms of dynamicly optimized blades

Table 6.4: Dynamically Optimized Blade Parameters

Parameter	Units	Onshore	FOWT
Blade length, L	m	78.5	79.1
Tip speed ratio, λ	-	9.37	10.0
Power coefficient, C_P	-	0.477	0.433
Thurst coefficient, C_T	-	0.686	0.597
Annual energy production, AEP	GWh	27.74	27.42
Blade mass, m_{blade}	kg	21,300	30,400

6.2.1 Power and Thrust Coefficient Characteristics

Higher tip speed ratio for the FOWT optimized blade enables a smaller spanwise chord distributions. Figured 6.2 shows the C_P and C_T surface as functions of blade pitch angle (Θ_P) and tip speed ratio (λ). The Θ_P and λ design point for both blades is below their respective $C_{P_{max}}$. This is tunable by the optimization algorithm, as

changing the blade twist shifts the C_P and C_T surfaces along the Θ_P axis and the chord distribution shifts along the λ axis. These sub-$C_{P_{max}}$ designs are lower induction solutions that allow longer blades, capturing higher AEP with lower loads in order to satisfy the design constraints. The floating optimized blade is an even lower induction design than the onshore optimized, with significantly lower C_P and C_T. Interestingly, the floating optimzied blade has a C_P similar to the steady optimized blades where $\gamma_{LA} > 1.09$ in Chapter 5, the demarcation line on the Pareto front of where loads were reduced from the baseline. The lower C_T of the floating optimized blade reduces its mean platform pitch angle and helps satisfy its design constrains when operating under more dynamic loads.

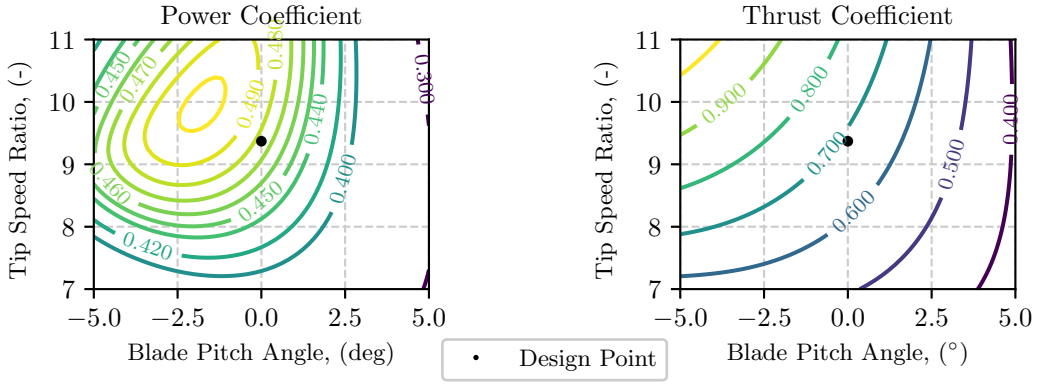

(a) Onshore Optimized

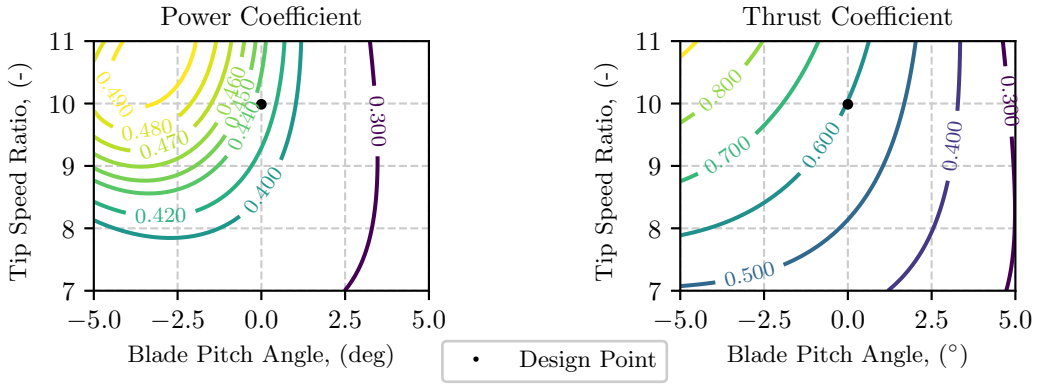

(b) FOWT Optimized

Figure 6.2: Dynamic optimized blade C_P and C_T surfaces

An additional feature that should be noted is the derivative of C_P and C_T at λ_{design} with respect to Θ_P. The floating optimized blade has steeper negative slopes, observable in the derivatives plotted in Figure 6.3. As a result, the floating optimized blade is more sensitive to pitch controller actions. Effectively, the floating optimized blade is marginally more controllable in Region II.5 and III, an appealing feature considering it was designed under more unsteady loading conditions.

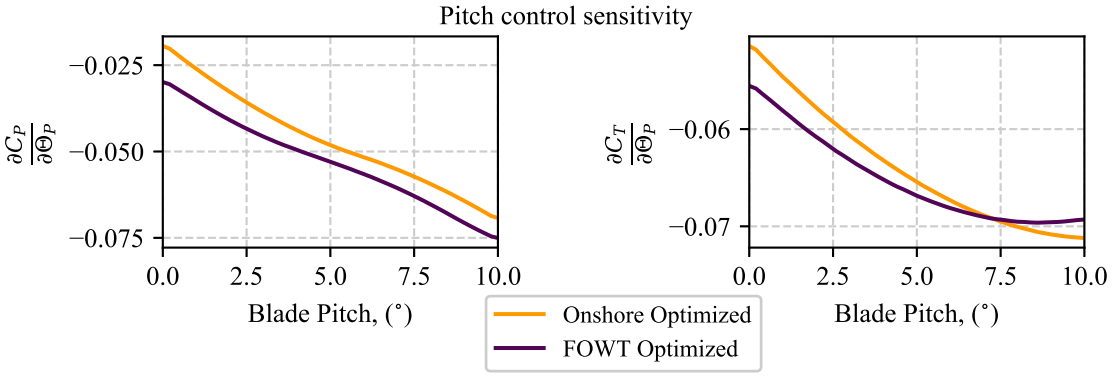

Figure 6.3: Derivatives of C_P and C_T with respect to blade pitch angle, showing sensitivity to pitch control actions

6.2.2 Effects of Design Constraints

For both designs, the dominate active constraints were operational root bending moments and extreme blade tip deflections. The mass constraint was also active for the FOWT-optimized design, with a blade mass 43% higher than the onshore blade. The interplay between these constraints can explain the key differences between the two optimized blades.

Figure 6.4 shows the response of both blades to the design constraining gust case. The onshore-optimized blade was modeled both at its design point onshore and on the spar buoy in a FOWT configuration. When operating onshore, the onshore-optimized blade has the lowest thrust and root bending moment, with tip deflection at the clearance limit. When this blade operates on a FOWT, it no longer satisfies the tip

clearance constraint and maximum thrust and flap-wise root bending moments increase by 19.9% and 20% respectively. The FOWT-optimized blade was designed with the more restrictive constraints brought on by this more dynamic loading environment. It too has higher loads than the onshore-optimized blade operating onshore, but some of these effects have been mitigated with maximum thrust and root bending moments only increasing by 10.4% and 10.5% and the tip deflection constraint satisfied.

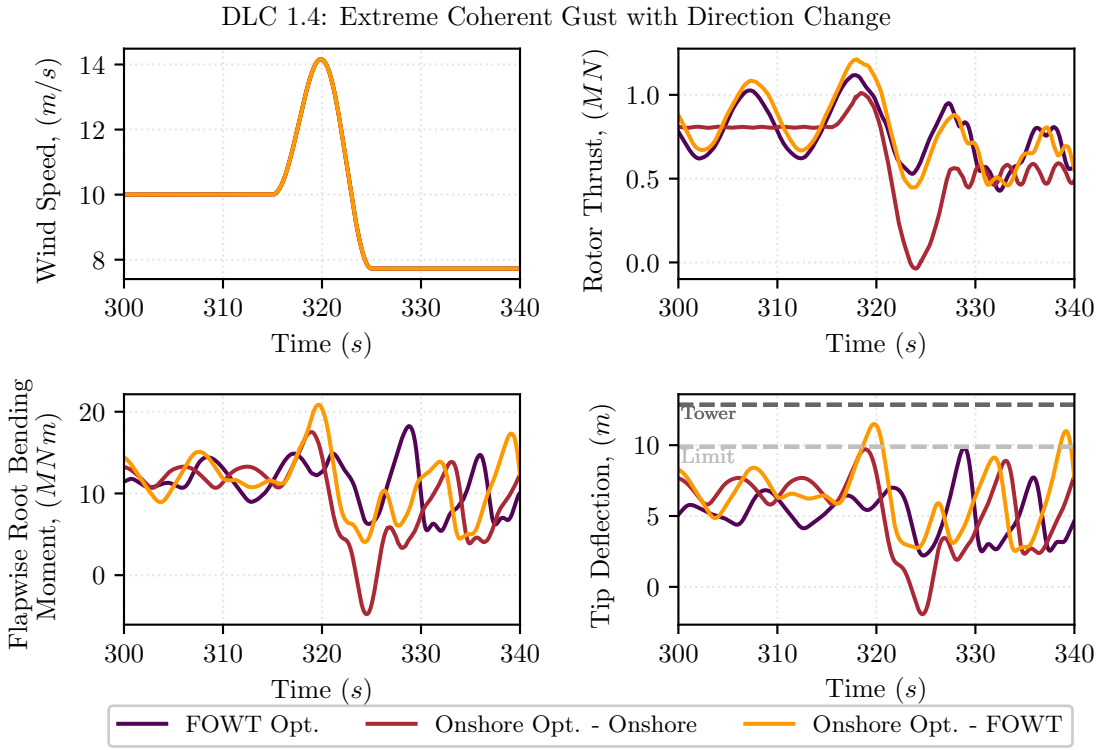

Figure 6.4: Response of optimized blades during a gust DLC

The FOWT-optimized design satisfies its more restrictive loading constraints through a combination of a lower induction factor, reducing loading, and significantly thicker spar caps, reducing deflection. The spanwise spar cap thicknesses for both blades are shown in Figure 6.5. The floating optimized blade also requires additional spar cap thickness due to its smaller spanwise chord distribution. Stiffness provided by thicker airfoils and larger chord lengths are typically more structurally efficient

than through increased spar cap thickness from a mass perspective. The very thick spar caps of the FOWT activate the mass constraint, providing the maximum possible internal stiffness without compromising the aerodynamic shape. If the mass constraint was set lower, the blades would require a combination of even lower induction to reduce stiffness requirements, increased chord to increase stiffness, or shorter blades, reducing loading and AEP.

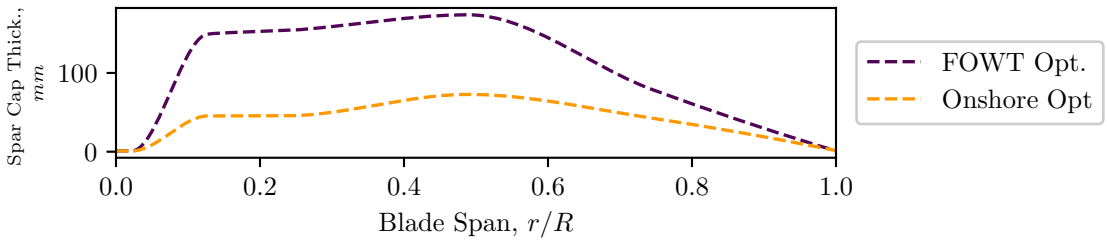

Figure 6.5: Spar cap thickness for optimized blades

6.2.3 Operational Angles of Attack

To analyze the angle of attack (α) distributions, and associated lift and drag, both blades were simulated on the OC3/Hywind spar buoy. A stochastic wave time series was generated using the JONSWAP spectrum, with the expected West Coast reference site significant wave height and peak spectral periods. A very long transient period was discarded from the beginning of the simulation, 300 s, with the subsequent 600 s used for analysis. A very small timestep of 0.001 s was used to improve frequency analysis of the time series.

The frequency content of the spanwise angle of attack distributions relative to the waves, platform degree degrees of freedom, and blade pitch are shown in Figure 6.6. The power spectral density (PSD) of α was determined, normalized by the maximum P_{xx} value across wind speeds and blade designs. The normalized power densities are logarithmic, with a maximum value of 0 indicating the highest power density.

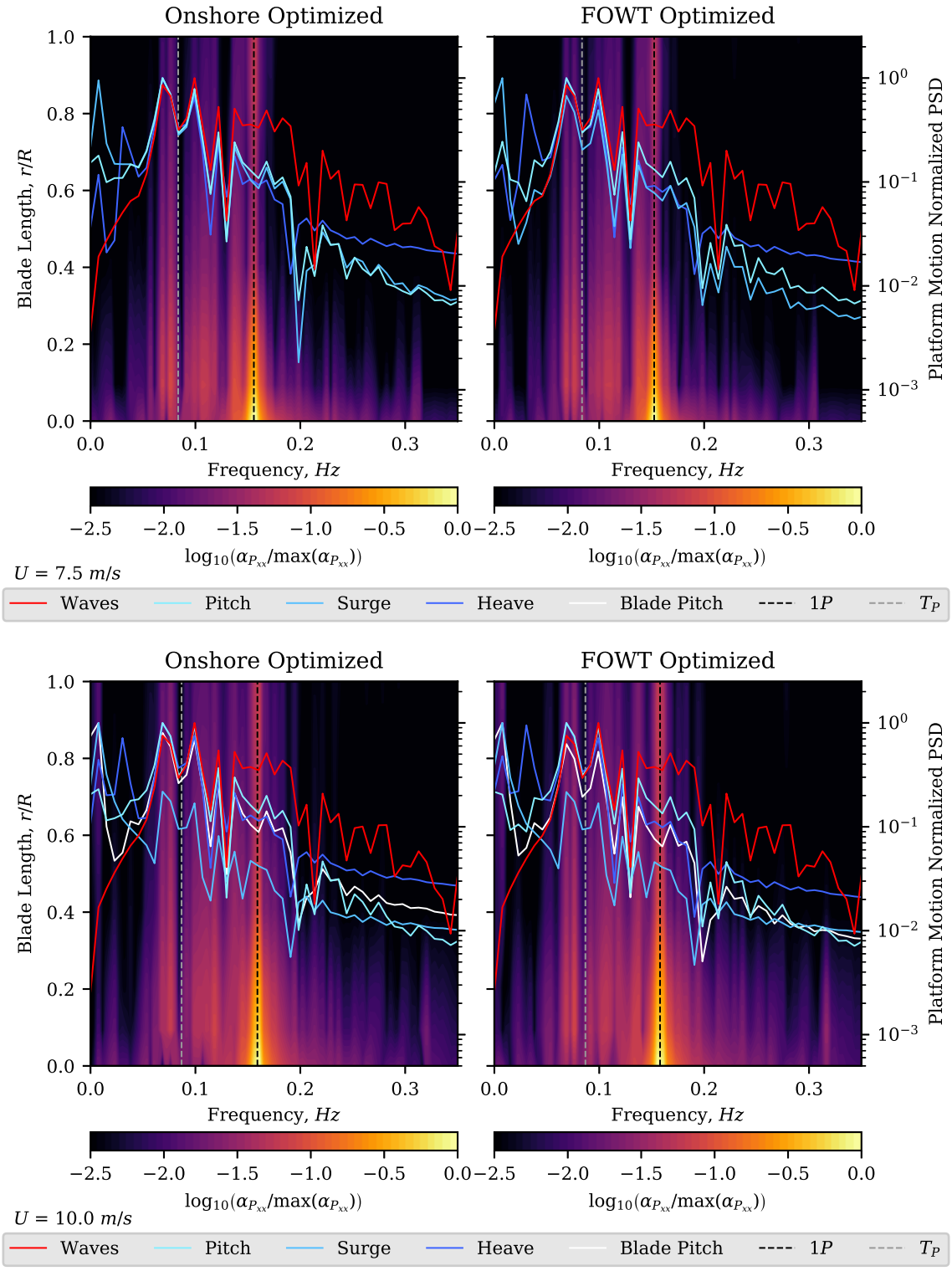

Figure 6.6: Normalized frequency analysis for optimized blades

At both below and near rated wind speeds the PSDs for both blades are nearly identical. The largest frequency response occurs as the rotor frequency, 1P, as a result of the turbine shaft tilt and wind shear, causing cyclical angle of attack variations during the blade azimuthal sweep. More interestingly, an additional response can be seen between frequencies of 0.06 Hz to 0.2 Hz, directly corresponding to the platform motion modes. At above rated conditions, the controller pitch angle closely tracks the platform pitch motion. These plots clearly show that the FOWT platform motion increases the unsteady aerodynamic loading on the blade and demonstrate that there are no platform motion-induced rotor or controller instabilities.

While the frequency content of the angles of attack for the two blades are quite similar, driven by the wave loading, the different twist distributions for the two blades result in different operation angles of attack distributions. The box plots in Figure 6.7 give the mean, standard deviation, maximum, and minimum values for α, C_L, and C_D for both blades at 7.5 m/s and 10 m/s, below rated and near rated respectively.

The less-linear twist distribution of the FOWT-optimized blade is apparent in below rated conditions, angles of attack are lower for most of its span and higher near the tip. From the C_L and C_D plots, the lower spanwise α leads to lighter loading for most of the length of the blade. The higher blade twist reduces angle of attack, reducing the lift and drag, and consequently the power and thrust coefficients. The blade tip mean α near 8° is at the peak lift-to-drag ratio for the NACA 64-618 airfoil. In below rated conditions, the FOWT-optimized blade has higher mean lift-to-drag ratios for the outboard 60% of span, increased by 1 to 5%, helping reduce thrust on the rotor.

It is possible that higher fidelity models would find the concentration of loading near the FOWT-optimized blade tip to be less desirable. The pressure differential between the suction and pressure side of the airfoil leads to three-dimensional flow

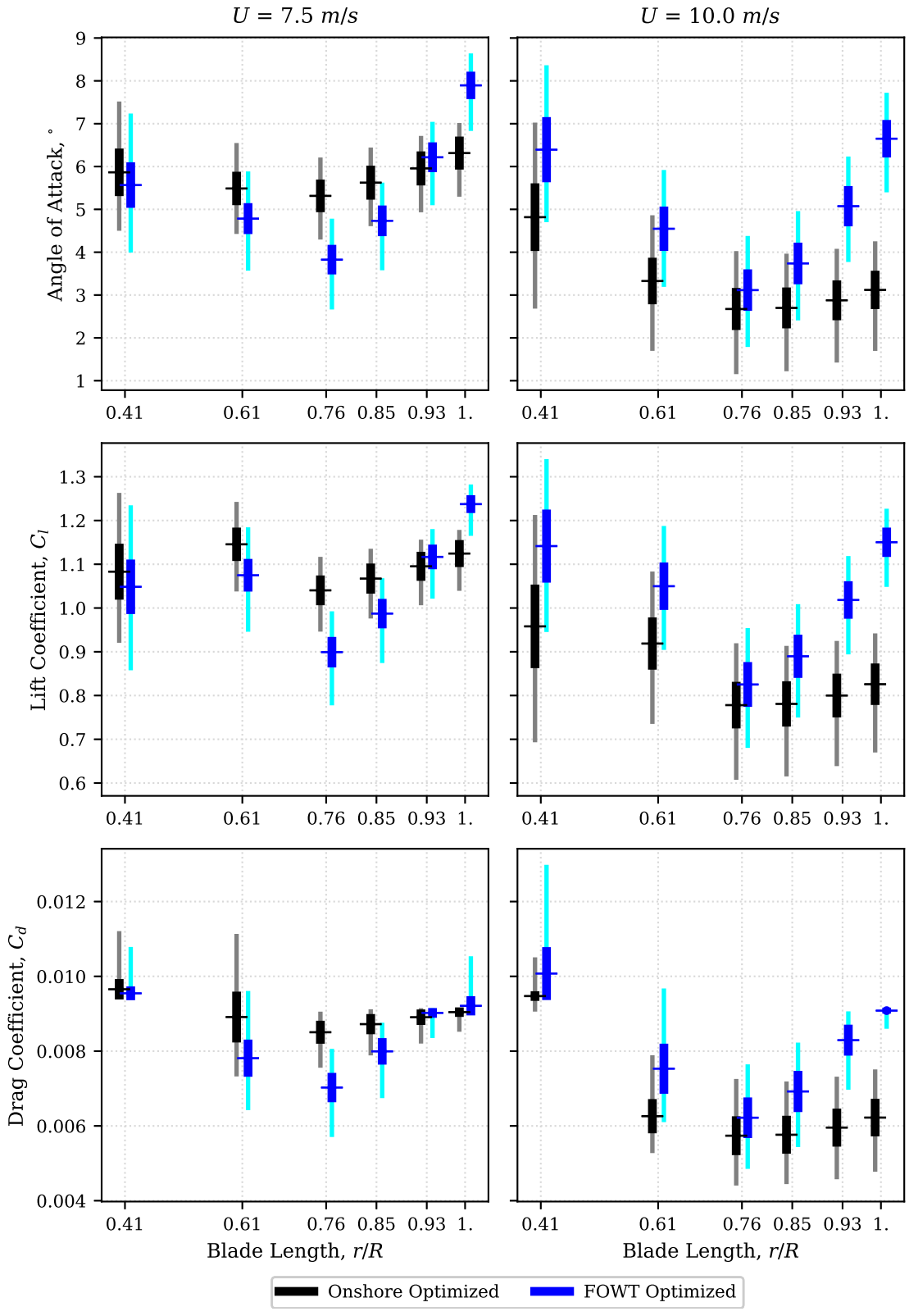

Figure 6.7: Statistics for spanwise angles of attack, lift, and drag, for below and above rated conditions

over the blade tip, leading to losses. OpenFAST uses an empirical Prandtl tip loss model, but this is limited in its physical accuracy.

At 10 m/s, both blades are operating in Region III, actively pitching the blades to maintain rated rotor speed. The onshore-optimized blade requires slightly larger blade pitching actions to affect rotor speed and consequently has higher standard deviations for outboard lift and drag. In above-rated conditions, the twist distribution for the FOWT-optimized blade works against it, with higher outboard drag at rated rotor speed than the onshore-optimized blade. Thrust at operational above-rated conditions will therefore be increased. This was not accounted for in the optimization problem formulation, with thrust and root bending moments constrained at rated rotor speeds where their peak values occur. Fatigue damage during above rated operation will likely be increased for FOWT blade, but this may be offset by lower loads at more frequent lower wind speeds.

6.2.4 Performance as a function of metocean conditions

The power curve and loads as a function of wind speed are shown in Figure 6.8. This figure was created by simulating the blades at a range of operational wind speeds. For the FOWT-optimized blade and the onshore-optimized blade operating on the spar buoy, the expected significant wave height and peak spectral periods for the West Coast offshore reference site were used. Similar trends can be observed as discussed in the previous sections. The FOWT-optimized blade has generally higher below-rated and rated peak loads than the onshore-optimized blade operating onshore, but less so than the onshore-optimized operating on a FOWT platform. Thrust and root bending moment at above rated are higher for the FOWT-optimized blade due to its higher outboard drag when the blades are pitched to maintain rated rotor speed. Operational tip deflections are lower for the floating-optimized blade due to its increased stiffness to survive more severe extreme loading.

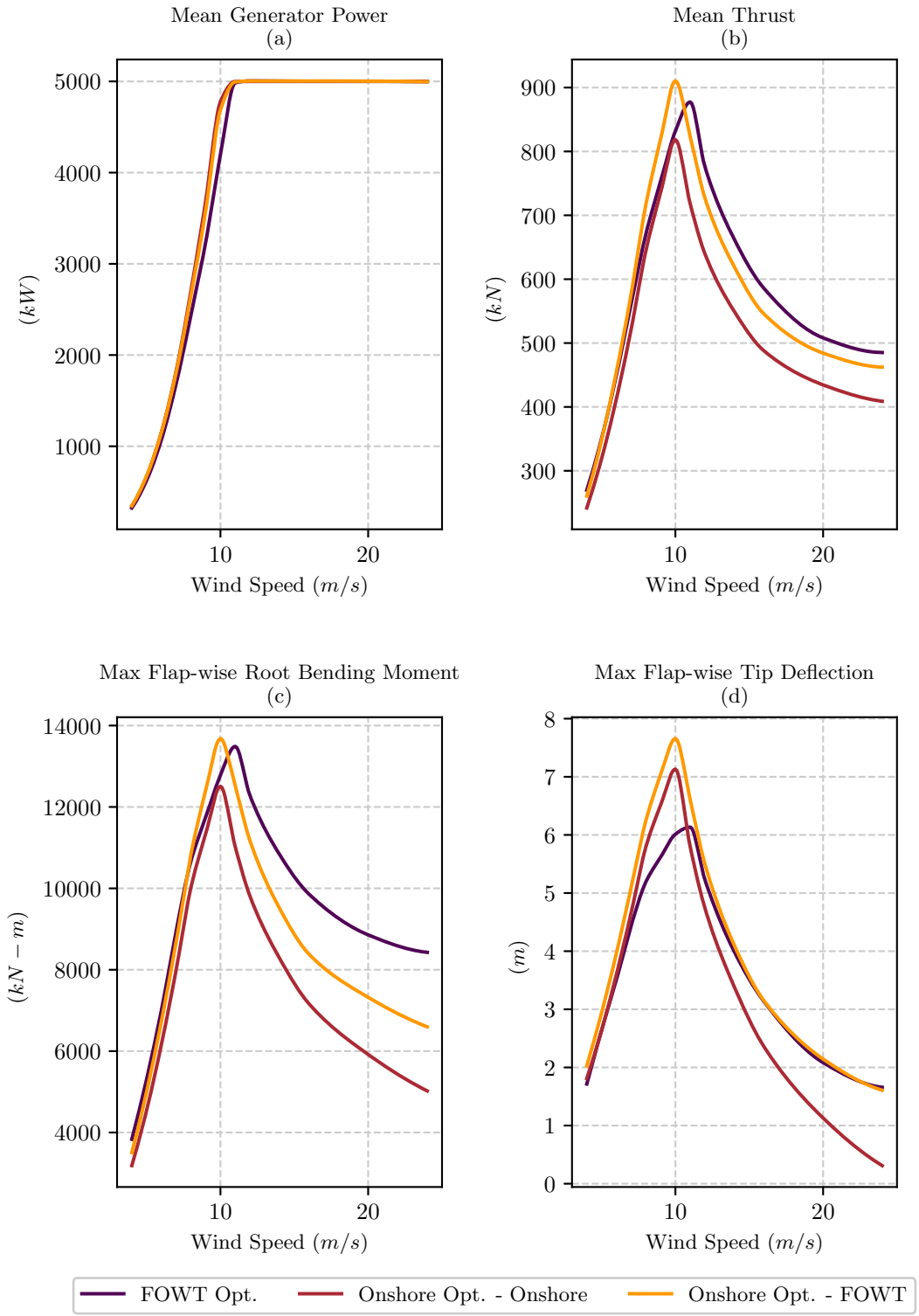

Figure 6.8: Power curve and loads as function wind speed and expected metocean conditions for optimized blades

6.3 Discussion and Conclusions

Onshore and floating wind turbine blades were optimized using dynamic simulations. This addressed many of the oversimplifications in the previous study, but at significant additional computational costs. Aerodynamically, the arrived upon floating offshore wind turbine blade differed in that it was a lower induction turbine. Structurally, the blade is much stiffer, with significantly thicker spar caps. Both of these design changes are in direct response to the more dynamic loading conditions during the optimization process.

In a sense, both blade designs are suboptimal for FOWT operation. The onshore-optimized blade does not satisfy the design constraints when operating on a FOWT, unsurprisingly. While it does not violate any constraints as defined, the FOWT-optimized blade is excessively heavy, which would very likely not be justifiable from a COE perspective. However, as discussed in the previous chapter, there is a fundamental trade-off between increasing AEP and decreasing loads, with the presented designs representing different points along that axis. Using low induction, lower specific power blades can help alleviate this problem, by reducing blade loading and increasing blade length to compensate for the lost aerodynamic efficiency. A lower mass FOWT blade could be achieved by modifying the problem objective and constraints, but as demonstrated, this will come at the cost of further decreased AEP. This requires sophisticated COE analysis tools to strike the right balance. Increased system level design and analysis could help inform some of these trade-off decisions and drive the analysis closer to the global optimum. For example, the tower design would also benefit from reduced platform pitch angles and thrust loading, potentially providing material savings.

Future work in this area should focus on reduction of computational costs. This could potentially be achieved using more sophisticated multidisciplinary design concepts such as surrogate modeling and multi-fidelity modelling that requires less frequent

dynamic simulation of the candidate designs. Surrogate modeling should also have the added benefit of smoothing the design space, enabling gradient search methods, rather than the extreme computationally expensive genetic algorithm used in this study. Reducing computational cost will also allow a wider range of design load cases to be used at each iteration and reduce uncertainty.

This work could also benefit from higher fidelity structural and aerodynamic modeling. For example, finite element modeling of the blade cross sections could be used to calculate the stiffness and mass matrices, enabling more sophisticated design features like bend-twist coupling. Better ultimate strain and buckling failure criteria could do away with the need to limit loads relative to the baseline, which likely over-constrained the problem. Higher fidelity aerodynamics could better capture three dimensional effects and dynamic changes in induction through the rotor caused by the platform induced motion of the rotor

CHAPTER 7

CONCLUSIONS

7.1 Summary of Conclusions

Due to the nascent state of floating offshore wind turbine technology, existing blade designs have been used for floating applications, with the floating platform designed to support a particular turbine model. This work addresses the FOWT design problem in a more holistic manner, based on the understanding that the unique aerodynamic loading conditions brought on by the coupled rotor-platform dynamics makes existing rotor designs suboptimal for FOWT operation. Methodologies were developed for the design optimization of FOWT blades and used to assess how FOWT blade design can be improved for their operating conditions.

The key finding of this work is that low induction wind turbine blades will offer improved performance over fixed bottom designs for FOWT operation. Fore-aft platform motion for catenary moored floating platforms is driven by the thrust loading on the rotor. This has a number of negative consequences. The mean platform pitch pushes the rotor out of alignment decreasing power producing and exacerbates 1P rotational sampling of the wind field. The cyclical platform fore-aft motions creates an additional velocity component, which can allow for increased power production, but at the cost of increased loading on the turbine. A low induction rotor helps address these problems. By increasing blade length and operating at a lower power coefficient, the increased loading from platform kinematics are alleviated. Through carefully formulated optimization problems, these trade-offs can be teased out, resulting in

blades that both increase annual energy production with decreased loads. Two optimization methods where developed, bother supporting this conclusion.

A lower fidelity, state-state optimization methodology was developed that artificially increased the loads on the turbine. By optimizing the turbine over a range of load amplification factors, a range of blades designs were generated. These designs were analyzed with dynamic simulations on a floating platform, representing the Pareto front of trade-off solutions between maximum AEP and load alleviation. Use of low-order computationally efficient models makes this a useful technique that is extendable to explore further FOWT design problems and will be particularly useful for system level optimizations that include additional FOWT subsystems. However, a number of limitations were identified, including difficulties in accurately modeling an extreme load case with steady state models and over- and under-prediction of floating AEP and loads due to the missing dynamic loading. These techniques are therefore best used for first-pass design studies, looking for broader trends, than attempting to generate a detailed, realistic design.

To address these limitations and better explore how FOWT dynamics affect the optimization process, a higher fidelity methodology was developed using time domain simulations in the optimization workflow. This optimization study proved quite challenging due to the complexities of the design space and challenges brought on by numeric simulations. A genetic algorithm was required due to the nonconcave search space, brought on by nonlinear controller actions and numerical noise. An unfortunate consequence of using a gradient-free optimization method was computational costs increased by approximately three orders of magnitude relative to the steady-state method. The relative differences in computational cost and insight into the physics provided by these two optimization methodologies suggest they should be used in conjunction for future studies.

To support this work, significant efforts were made to develop and improve open source design tools in NREL's WISDEM toolbox. RotorSE, the rotor aerodynamics and structural dynamics toolbox, underwent significant modification. As part of work contributing to the International Energy Agency's Wind Task 37 on Systems Engineering, a blade ontology format was developed, that can be used to standardize and simplify the transfer of data between software tools and between collaborative partners. RotorSE was modified to use this as its primary input and output methodology, which significantly increased the variety and scope of blade design problems it can handle. A multifidly switch was also added to RotorSE, allowing OpenFAST simulations of arbitrary rotor designs rather than the base steady state models in RotorSE. This was enabled through AeroelasticSE, the OpenFAST drive in WISDEM, which underwent a large modernization and expansion effort to support this work. AeroelasticSE contributions include: support for the OpenFAST offshore modules, implementation of an IEC load case wind file generator, creation of case generators for automatically change OpenFAST input files over arbitrary batches of simulations, and support for MPI parallelization of design load cases on HPC resources. These tools are publicly available and should prove invaluable to the larger research community.

7.2 Recommendations for Future Work

This work should be viewed as a first step towards the larger goal of parallel multidisciplinary design optimization of the full FOWT system. Just as floating support structures designed for conventional rotors is suboptimal, designing FOWT rotors for conventional floating support structures, while a step in the right direction, has not yet reached a globally optimal system. It is expected that significant cost savings can be realized through the combined optimization of the full floating system. Along these lines, FOWT will likely benefit immensely from codesign, the simultaneous optimization of the controller and FOWT system, using controls to help alleviate

the increased dynamic loading. Codesign has been employed in a number of other industries, such as aerospace, but the available literature related to wind energy is quite sparse.

Optimization of the blades while including the couple platform and aerodynamics proved to be a very difficult problem to solve, due to the nonconvex nature of the design space and the large computational costs. These problems will only be compounded as additional subsystems and more design variable are included in the design problem. Future work should focus on methods to reduce the computational costs. New lower fidelity tools that capture the coupled system dynamics may be needed, for example by using frequency domain models, which are common in the floating platform design and analysis space. If floating wind turbine costs are to continue to decrease, researchers need to address these issues in order to design more globally optimized systems.

BIBLIOGRAPHY

[1] Ashwill, T., Kanaby, G., Jackson, K., and Zuteck, M. Development of the Swept Twist Adaptive Rotor (STAR) Blade. In *48th AIAA Aerospace Sciences Meeting* (2010).

[2] Bak, Christian, Zahle, Frederik, Bitsche, Robert, Kim, Taeseong, Yde, Anders, Henriksen, Lars Christian, Natarajan, Anand, and Hansen, Morten Hartvig. Description of the DTU 10 MW Reference Wind Turbine. Tech. Rep. DTU Wind Energy Report-I-0092, DTU Wind Energy, 2013.

[3] Barltrop, N. Multiple Unit Floating Offshore Wind Farm (MUFOW). *Wind Engineering 17*, 4 (1993), 183–188.

[4] Beiter, P., Musial, W., Kilcher, L., Maness, M., and Smith, A. An Assessment of the Economic Potential of Offshore Wind in the United States from 2015-2030. Tech. Rep. NREL/TP-6A20-67675, National Renewable Energy Laboratory, Golden, CO, 2017.

[5] Benini, Ernesto, Lazzaretto, Andrea, and Toffolo, Andrea. Optimal Design of Horizontal-Axis Wind Turbines Using Blade-Element Theory and Evolutionary Computation. *Journal of Solar Energy Engineering 124*, November 2002 (2002), 357–363.

[6] Berg, Jonathan C., and Resor, Brian R. Numerical Manufacturing And Design Tool (NuMAD v2.0) for Wind Turbine Blades: User's Guide. Tech. Rep. SAND2012-7028, Sandia National Laboratories, Albuquerque, NM, 2012.

[7] Betz, Albert. *Windenergie und Ihre Ausnutzung durch Windmüullen*. Vandenhoeck and Ruprecht, Göttingen, 1926.

[8] Bir, G. User's Guide to BModes. Tech. Rep. NREL/TP-500-39133, National Renewable Energy Laboratory, Golden, Colorado, 2005.

[9] Bir, Gunjit S. Computerized Method for Preliminary Structural Design of Composite Wind Turbine Blades. *Journal of Solar Energy Engineering 123*, 4 (2001), 372.

[10] Bir, Gunjit S. User's Guide to PreComp. Tech. rep., National Renewable Energy Laboratory, Golden, CO, 2005.

[11] Bortolotti, P., Berry, D., Murray, R., Gaertner, E., Dale, J., Damiani, R., and Dykes, K. A detailed wind turbine blade cost model. Tech. rep., NREL, 2019.

[12] Bortolotti, P., Tarrés, H., Dykes, K., Merz, K., Sethuraman, L., Verelst, D., and Zahle, F. IEA Wind Task 37 on Systems Engineering in Wind Energy WP2.1 Reference Wind Turbines. Tech. rep., 2019.

[13] Bottasso, C.L., Campagnolo, F., and Croce, A. Computational Procedures for the Multi-Disciplinary Constrained Optimization of Wind Turbines. Tech. Rep. DIA-SR 10-02, Dipartimento di Ingegneria Aerospaziale, Milano, Italy, 2011.

[14] Brent, R. P. *Algorithms for Minimization Without Derivatives*. Prentice-Hall, Englewood Cliffs, NJ, 1973.

[15] Burton, Tony, Sharpe, David, Jenkind, Nick, and Bossanyi, Ervin. *Wind Energy Handbook*, 2nd ed. John Wiley & Sons, Ltd, 2011.

[16] Butterfield, Sandy, Musial, W., Jonkman, Jason, and Sclavounos, Paul D. Engineering Challenges for Floating Offshore Wind Turbines. *2005 Copenhagen Offshore Wind Conference* (2005), 13.

[17] Campobasso, M. Sergio, Minisci, Edmondo, and Caboni, Marco. Aerodynamic design optimization of wind turbine rotors under geometric uncertainty. *Wind Energy 19*, November 2014 (2014), 51–65.

[18] Chaviaropoulos, P., Beurskens, H.J.M., and Voutsinas, S.G. Moving towards Large(r) Rotors - Is that a good idea? In *European Wind Energy Conference and Exhibition, EWEC 2013* (2013).

[19] Chaviaropoulos, P., and Voutsinas, S. Design of Low Induction Rotors for use in large offshore wind farms. In *EWEA 2014* (2014).

[20] Chehouri, Adam, Younes, Rafic, Ilinca, Adrian, and Perron, Jean. Review of performance optimization techniques applied to wind turbines. *Applied Energy 142* (2015), 361–388.

[21] Chehouri, Adam, Younes, Rafic, Ilinca, Adrian, Perron, Jean, and Lakiss, Hassan. Optimal design for a composite wind turbine blade with fatigue and failure constraints. *Transactions of the Canadian Society for Mechanical Engineering 39*, 2 (2015), 171–186.

[22] CPACS. Common Language for Aircraft Design, 2018.

[23] Crawford, C. The Path from Fuctional to Detailed Design of a Coning Rotor Wind Turbine Concept. In *CDEN/C2E2* (Winnipeg, Manitoba, Canada, 2007).

[24] Dambolena, I. G. *A planning methodology for the analysis and design of wind-power systems*. PhD thesis, University of Massachusetts Amherst, 1974.

[25] de Vries, 0. Fluid Dynamic Aspects of Wind Energy Conversion. Tech. Rep. AGARDograph No. 243, National Aerospace Laboratory NLR, 1979.

[26] Deb, K., Pratap, A., Agarwal, S., and Meyarivan, T. A fast and elitist multiobjective genetic algorithm: NSGA-II. *IEEE Transactions on Evolutionary Computation 6*, 2 (2002).

[27] Det Norske Veritas. Design and Manufacture of Wind Turbine Blades, Offshore and Onshore Wind Turbines. Tech. Rep. DNV-DS-J102, 2010.

[28] Diveux, T., Sebastian, P., Bernard, D., Puiggali, J., and Grandidier, J. Horizontal Axis Wind Turbine Systems: Optimization Using Genetic Algorithms. *Wind Energy 4* (2001), 151–171.

[29] Du, Z., and Selig, M. A 3-D Stall-Delay Model for Horizontal Axis Wind Turbine Performance Prediction. In *1998 ASME Wind Energy Symposium, 36th AIAA Aero. Sci. Mtg.* (1998), no. AIAA 1998-0021.

[30] Dykes, K., Bortolotti, P., Perez-Moreno, S. S., Quaghebeur, E., Zahle, F., McWilliam, M., Bottasso, C., Merz, K., Ning, A., Gaertner, E., Canet, H., and Zaaijer, M. System Modeling Frameworks for Wind Turbines and Plants: Review and Requirements Specifications. Tech. rep., 2019.

[31] Dykes, K., Meadows, R., Felker, F., Graf, P., Hand, M., Lunacek, M., Michalakes, J., Moriarty, P., Musial, W., and Veers, P. Applications of Systems Engineering to the Research, Design and Development of Wind Energy Systems. Tech. Rep. NREL/TP-5000-52616, National Renewable Energy Laboratory, 2011.

[32] Dykes, K, Platt, A, Guo, Y, Ning, A, King, R, Parsons, T, Petch, D, Veers, P, and Resor, B. Effect of Tip-Speed Constraints on the Optimized Design of a Wind Turbine. Tech. Rep. NREL/TP-5000-61726, National Renewable Energy Laboratory, 2014.

[33] Dykes, K., Rethore, P., Zahle, F., and Merz, K. Wind Energy Systems Engineering: Integrated RD&D. Tech. rep., IEA Task 37 Final Proposal, 2015.

[34] Dykes, K., Veers, P., Lantz, E., Holttinen, H., Carlson, O., Tuohy, A., Sempreviva, A. M., Clifton, A., Rodrigo, J. S., Berry, D., Laird, D., Carron, S., Moriarty, P., Marquis, M., Meneveau, M., Peinke, J., Paquette, J., Johnson, N., Pao, L., Fleming, P., Bottasso, C., Lehtomaki, V., Robertson, A., Muskulus, M., Manwell, J., Tande, J. O., Sethuraman, L., Roberts, O., and Fields, J. Results of IEA Wind TCP Workshop on a Grand Vision for Wind Energy Technology. Tech. Rep. NREL/TP-5000-72437, IEA Wind, 2019.

[35] Dykes, Katherine, Graf, Peter, Scott, George, Ning, Andrew, King, Ryan, Guo, Yi, Parsons, Taylor, Damiani, Rick, Felker, Fort, and Veers, Paul. Introducing WISDEM: An Integrated System Model of Wind Turbines and Plants. In *Third Wind Energy Systems Engineering Workshop, January 14, 2015* (Boulder, CO, 2015).

[36] Edenhofer, Ottmar, Pichs-Madruga, Ramón, Sokona, Youba, Seyboth, Kristin, Eickemeier, Patrick, Matschoss, Patrick, Hansen, Gerrit, Kadner, Susanne, Schlömer, Steffen, Zwickel, Timm, and Stechow, Christoph Von. *IPCC Special Report on Renewable Energy Sources and Climate Change Mitigation*. Cambridge University Press, New York, NY, 2011.

[37] Eggers, A., Chaney, K., Holley, W., and Ashley, H. Modeling of Yawing and Furling Behavior of Small Wind Turbines. In *2000 ASME Wind Energy Symposium, 38th AIAA Aero. Sci. Mtg.* (2000), no. AIAA 2000-0020.

[38] Eke, G.B., and Onyewudiala, J.I. Optimization of Wind Turbine Blades Using Genetic Algorithm. *Global Journal of Research in Engineering 10*, 7 (2010).

[39] Endo, M. *Wind Turbine Airfoil Optimization by Particle Swarm Method*. Master of science, Case Western Reserve University, 2011.

[40] Evans, Clarkj. The Official {YAML} Web Site, 2011.

[41] Farrugia, R, Sant, T, and Micallef, D. A study on the aerodynamics of a floating wind turbine rotor. *Renewable Energy 86* (2016), 770–784.

[42] Fleming, P., Peiffer, A., and Schlipf, D. Wind Turbine Controller to Mitigate Structural Loads on a Floating Wind Turbine Platform. *Journal of Mechanics and Arctic Engineering 141*, 6 (2019).

[43] Fleury, Claude, and Braibant, Vincent. Structural optimization: A new dual method using mixed variables. *International Journal for Numerical Methods in Engineering 23*, 3 (1986), 409–428.

[44] Fortin, F-A, De Rainville, F-M, Gardner, M-A, Parizeau, M, and Gagne, C. DEAP: Evolutionary Algorithms Made Easy. *Journal of Machine Learning Research 13* (2012).

[45] Fritsch, F. N., and Carlson, R. E. Monotone Piecewise Cubic Interpolation. *SIAM J. Numer. Anal. 17*, 2 (1980).

[46] Fuglsang, P., Bak, C., Schepers, J., Bulder, B., Cockerill, T., Claiden, P., Olesen, A., and van Rossen, R. Site-Specific Design Optimization of Wind Turbines. *Wind Energy 5*, 4 (2002), 261–279.

[47] Fuglsang, P., and Madsen, H. A. Optimization method for wind turbine rotors. *Journal of Wind Engineering and Industrial Aerodynamics 80* (1999), 191–206.

[48] Fuglsang, P., and Thomsen, K. Site-Specific Design Optimization of 1.5–2.0 MW Wind Turbines. *ASME J. Sol. Energy Eng. 123*, 4 (2001), 296–303.

[49] Gaertner, E.M., and Lackner, M.A. Modeling dynamic stall for a free vortex wake model. *Wind Engineering 39*, 6 (2015), 675–692.

[50] Gaudern, Nicholas, and D. Symons, Digby. Comparison of Theoretical and Numerical Buckling Loads for Wind Turbine Blade Panels. *Wind Engineering 34*, 2 (2010), 193–206.

[51] GE Renewable Energy. World's Largest Offshore Wind Turbine - Haliade X, 2018.

[52] Genesereth, M. R., and Nilsson, N. J. *Logical Foundations of Artificial Intelligence*. Morgan Kaufmann Publishers, San Mateo, CA, 1987.

[53] Glauert, H. A General Theory of the Autogyro. Tech. Rep. ARCR R&M No. 1111, 1926.

[54] Glauert, H. *Aerodynamic Theory*. Springer Verlag, Berlin, 1935.

[55] Goldstein, S. On the Vortex Theory of Screw Propeller. In *Royal Society of London (A)* (1929), pp. 440–465.

[56] Graf, Peter A., Stewart, Gordon, Lackner, Matthew, Dykes, Katherine, and Veers, Paul. High-throughput computation and the applicability of Monte Carlo integration in fatigue load estimation of floating offshore wind turbines. *Wind Energy 19* (2015), 861–872.

[57] Gray, Justin, Moore, Kenneth, and Naylor, Bret. OpenMDAO: An Open Source Framework for Multidisciplinary Analysis and Optimization. In *13th AIAA/ISSMO Multidisciplinary Analysis Optimization Conference* (2010), pp. 1–12.

[58] Griffith, D Todd. The SNL100-02 Blade : Advanced Core Material Design Studies for the Sandia 100- meter Blade. Tech. Rep. SAND2013-10162, Sandia National Laboratories, Albuquerque, NM, 2013.

[59] Griffith, D Todd, and Ashwill, Thomas D. The Sandia 100-meter All-glass Baseline Wind Turbine Blade : SNL100-00. Tech. Rep. SAND2011-3779, Sandia National Laboratories, 2011.

[60] Griffith, D Todd, and Resor, Brian R. Description of Model Data for SNL100-00 : The Sandia 100-meter All-glass Baseline Wind Turbine Blade. Tech. Rep. SAND2011-9309P Description, Sandia National Laboratories, Albuquerque, NM, 2011.

[61] Griffith, D Todd, and Richards, Phillip W. The SNL100-03 Blade : Design Studies with Flatback Airfoils for the Sandia 100-meter Blade. Tech. Rep. SAND2014-18129, Sandia National Laboratories, Albuquerque, NM, 2014.

[62] Gruber, T. A Translation Approach to Portable Ontology Specifications. *Knowledge Acquisition 5*, 2 (1993), 199–220.

[63] Gruber, T. Toward Principles for the Design of Ontologies Used for Knowledge Sharing. *International Journal Human-Computer Studies 43* (1993), 907–928.

[64] Halfpenny, A. *Dynamic Analysis of Both On and Offshore Wind Turbines in the Frequency Domain*. PhD thesis, University College London, 1998.

[65] Halpin, J. *Primer on Composite Materials Analysis*, 2 ed. 1992.

[66] Hansen, A. Yaw Dynamics of Horizontal Axis Wind Turbines. Tech. Rep. NREL/TP-442-4822, National Renewable Energy Laboratory, 1992.

[67] Hansen, M. *Aerodynamics of Wind Turbines*, 2 ed. Earthscan, London, 2008.

[68] Hayman, G J. MLife Theory Manual for Version 1.00. Tech. rep., National Renewable Energy Laboratory, 2012.

[69] Henderson, A. R., and Patel, M. H. On the Modelling of a Floating Offshore Wind Turbine. *Wind Energy 6*, 1 (2003).

[70] Heronemus, W. E. Pollution-Free Energy From Offshore Winds. In *8th Annual Conference and Exposition Marine Technology Society* (Washington D.C., 1972).

[71] Honnef, Hermann. *Windkraftwerke*. Friedrich Vieweg & Sohn Akt-Ges, Braunschweig, Germany, 1932.

[72] Huber, F. The first floating wind turbines. In *2nd International Conference on Ocean Energy* (Brest, France, 2008).

[73] International Electrotechnical Commission. Wind Turbines – Part 1: Design requirements. Tech. Rep. IEC 61400-1 Ed.3, 2005.

[74] International Electrotechnical Commission. Wind Turbines – Part 3: Design requirements for offshore wind turbines. Tech. Rep. IEC 61400-3 Ed.1, 2009.

[75] James, R., and Ros, M. C. Floating Offshore Wind: Market and Technology Review. Tech. rep., Carbon Trust, 2015.

[76] Jason M. Jonkman, and Buhl Jr., Marshall L. FAST User's Guide. Tech. Rep. NREL/EL-500-38230, National Renewable Energy Laboratory, Golden, Colorado, 2005.

[77] Johnson, A. Handbook of Polymer Compsites for Engineers. Woodhead Publishing, 1994, ch. Structural.

[78] Johnson, K. *Adaptive Torque Control of Variable Speed Wind Turbines*. PhD thesis, University of Colorado Boulder, 2004.

[79] Jones, Eric, Oliphant, Travis, Peterson, Pearu, and Others. SciPy: Open source scientific tools for Python.

[80] Jonkman, Bonnie, and Jonkman, Jason. FAST v8.16.00a-bjj. Tech. rep., National Renewable Energy Laboratory, 2016.

[81] Jonkman, J. Definition of the Floating System for Phase IV of OC3. Tech. Rep. NREL/TP-500-47535, National Renewable Energy Laboratory, Golden, CO, 2010.

[82] Jonkman, J M. Dynamics modeling and loads analysis of an offshore floating wind turbine. Tech. Rep. NREL/TP-500-41958, National Renewable Energy Laboratory, Golden, Colorado, 2007.

[83] Jonkman, J. M. Influence of Control on the Pitch Damping of a Floating Wind Turbine. In *2008 ASME Wind Energy Symposium* (Reno, NV, 2008), no. NREL/CP-500-42589.

[84] Jonkman, Jm, Butterfield, S, Musial, W, and Scott, G. Definition of a 5-MW reference wind turbine for offshore system development. Tech. Rep. NREL/TP-500-38060, National Renewable Energy Laboratory, Golden, Colorado, 2009.

[85] Jonkman, J.M., and Matha, D. Dynamics of offshore floating wind turbines - analysis of three concepts. *Wind Energy 14* (2011), 557–569.

[86] JSON Schema. The Home of JSON Schema, 2016.

[87] Jureczko, M., Pawlak, M., Mezyk, A., and Mężyk, A. Optimisation of wind turbine blades. *Journal of Materials Processing Technology 167*, 2-3 (2005), 463–471.

[88] Kelley, C. Optimal Low-Induction Rotor Design. In *Wind Energy Science Conference 2017* (2017).

[89] Kenway, G., and Martins, J. Aerostructural Shape Optimization of Wind Turbine Blades Considering Site-Specific Winds. In *Proceedings of the 12th AIAA/ISSMO Multidisciplinary Analysis and Optimization Conference* (Victoria, Canada, 2008).

[90] Lackner, M. A., and Rotea, M. A. Structural control of floating wind turbines. *Mechatronics 21*, 4 (2011), 704–719.

[91] Laks, J, Pao, L, and Wright, A. Control of Wind Turbines: Past, Present, and Future. In *2009 American Control Confernce* (St. Louis, MO, 2009).

[92] Larsen, T. J., and Hanson, T. D. A Method to Avoid Negative Damped Low Frequent Tower Vibrations for a Floating, Pitch Controlled Wind Turbine. In *Journal of Physics: Conference Series, The 2nd Conference on The Science of Making Torque From Wind* (Copenhagen, Denmark, 2007).

[93] Larwood, S. *Dynamic Analysis Tool Development for Advanced Geometry Wind Turbine Blades*. PhD thesis, University of California Davis, 2009.

[94] Leishman, J. Gordon. Challenges in Modeling the Unsteady Aerodynamics of Wind Turbines. In *40th AIAA Aerospace Sciences Meeting* (Reno, NV, 2002).

[95] Liao, C.C., Zhaoa, X.L., and Xua, J.Z. Blade layers optimization of wind turbines using FAST and improved PSO Algorithm. *Renewable Energy 42* (2012), 227–233.

[96] Lindenburg, C. Aeroelastic Modelling of the LMH64-5 Blade. Tech. Rep. DOWEC-02-KL-083/0, 2002.

[97] Liu, Y, Qing, X, Incecik, A, and Wan, D. Investigation of the effects of platform motion on the aerodynamics of a floating offshore wind turbine. *Journal of Hydrodynamics 28*, 1 (2016), 95–101.

[98] Lobitz, D., Veers, P., and Migliore, P. Enhanced Performance of HAWTs Using Adaptive Blades. In *Wind Energy 1996 ASME Wind Energy Symposium* (1996).

[99] Loth, E., Kaminski, M., Qin, C., Fingersh, L.J., and Griffith, D.T. Gravo-Aeroelastic Scaling for Extreme-Scale Wind Turbines. In *35th AIAA Applied Aerodynamics Conference* (Denver, CO, 2017).

[100] Maalawia, K Y, and Badr, M A. Frequency optimization of a wind turbine blade in pitching motion. *Proceedings of the Institution of Mechanical Engineers, Part A: Journal of Power and Energy 224*, 4 (2010), 545–554.

[101] Maalawia, Karam Y., and Negm, Hani M. Optimal frequency design of wind turbine blades. *Journal of Wind Engineering and Industrial Aerodynamics 90* (2002), 961–986.

[102] Maki, Kevin, Sbragio, Ricardo, and Vlahopoulos, Nickolas. System design of a wind turbine using a multi-level optimization approach. *Renewable Energy 43* (2012), 101–110.

[103] Maniaci, David C. An Investigation of WT_Perf Convergence Issues. In *49th AIAA Aerospace Sciences Meeting including the New Horizons Forum and Aerospace Exposition* (Orlando, Florida, 2011).

[104] Manwell, James F, McGowan, Jon G, and Rogers, Anthony L. *Wind energy explained: theory, design and application*. 2009.

[105] Matha, D. Model Development and Loads Analysis of a Wind Turbine on a Floating Offshore Tension Leg Platform. *European Offshore Wind Conference*, February (2010), 129.

[106] Matha, Denis. *Model Development and Loads Analysis of an Offshore Wind Turbine on a Tension Leg Platform, with a Comparison to Other Floating Turbine Concepts*. PhD thesis, University of Colorado Boulder, Golden, Colorado, 2009.

[107] Matha, Denis, Schlipf, Markus, Cordle, Andrew, Pereira, Ricardo, and Jonkman, J.M. Challenges in Simulation of Aerodynamics, Hydrodynamics, and Mooring-Line Dynamics of Floating Offshore Wind Turbines. In *21st Offshore and Polar Engineering Conference* (Maui, Hawaii, 2011), vol. 8, pp. 421–428.

[108] Mathew, J., Singh, A., Madsen, J., and Arce León, C. Serration Design Methodology for Wind Turbine Noise Reduction. *Journal of Physics: Conference Series 753* (2016).

[109] Miner, A. Cumulative Damage in Fatigue. *Trans. ASME 67* (1945).

[110] Minisci, E, Campobasso, M, and Vasile, M. Robust Aerodynamic Design of Variable Speed Wind Turbine Rotors. In *Proceedings of Gas Turbine Technical Congress and Exposition, ASME Turbo Expo 2012* (Copenhagen, Denmark, 2012).

[111] Moriarty, P., and Hansen, A. AeroDyn Theory Manual. Tech. Rep. NREL/EL-500-36881, National Renewable Energy Laboratory, 2005.

[112] Moriarty, P., and Migliore, P. Semi-Empirical Aeroacoustic Noise Prediction Code for Wind Turbines. Tech. Rep. NREL/TP-500-34478, National Renewable Energy Laboratory, 2003.

[113] Mueller-Vahl, H., Pechlivanoglou, G., Nayeri, C., and Paschereit, C. Vortex Generators for Wind Turbine Blades: A Combined Wind Tunnel and Wind Turbine Parametric Study. In *ASME Turbo Expo 2012: Turbine Technical Conference and Exposition* (Copenhagen, 2012).

[114] Musial, W., Beiter, P., Spitsen, P., Nunemaker, J., and Gevorgian, V. 2018 Offshore Wind Technologies Market Report. Tech. Rep. DOE/GO-102019-5192, U.S. Department of Energy Office of Energy Efficiency and Renewable Energy, 2019.

[115] Musial, W., Butterfield, S., and Boone, A. Feasibility of Floating Platform Systems for Wind Turbines. In *23rd ASME Wind Energy Symposium* (Reno, NV, 2004), no. NREL/CP-500-34874.

[116] Musial, W., and Ram, B. Large-Scale Offshore Wind Power in the United States. Tech. Rep. NREL/TP-500-40745, National Renewable Energy Lab, 2010.

[117] Musial, Walt, Heimiller, Donna, Beiter, Philipp, Scott, George, and Draxl, Caroline. 2016 Offshore Wind Energy Resource Assessment for the United States. Tech. Rep. NREL/TP-5000-66599, National Renewable Energy Laboratory, 2016.

[118] Myhr, Anders, Bjerkseter, Catho, Ågotnes, Anders, and Nygaard, Tor A. Levelised cost of energy for offshore floating wind turbines in a life cycle perspective. *Renewable Energy 66* (2014), 714–728.

[119] Ning, A. A simple solution method for the blade element momentum equations with guaranteed convergence. *Wind Energy 17*, 9 (2014), 1327–1345.

[120] Ning, A., Damiani, Rick, Moriarty, Patrick J, Andrew Ning, S., Damiani, Rick, and Moriarty, Patrick J. Objectives and Constraints for Wind Turbine Optimization. *Journal of Solar Energy Engineering 136*, 4 (2014), 041010.

[121] Ning, A., and Dykes, K. Understanding the Benefits and Limitations of Increasing Maximum Rotor Tip Speed for Utility-Scale Wind Turbines. *Journal of Physics: Conference Series 524* (2014).

[122] Ning, A., Hayman, G., Damiani, R., and Jonkman, J. Development and Validation of a New Blade Element Momentum Skewed Wake Model within AeroDyn. In *AIAA Science and Technology Forum and Exposition* (Kissimmee, FL, 2015), no. NREL/CP-5000-63217.

[123] Park, S., and Lackner, M. A. An investigation on the impacts of passive and semiactive structural control on a fixed bottom and a floating offshore wind turbine. *Wind Energy 22*, 11 (2019), 1451–1471.

[124] Perez, R.E., and Behdinan, K. Particle swarm approach for structural design optimization. *Computers & Structures 85*, 19-20 (2007), 1579–1588.

[125] Perez, Ruben E, Jansen, Peter W, Martins, Joaquim R R A, Jones, Eric, Oliphant, Travis, Peterson, Pearu, and Others. pyOpt: A Python-Based Object-Oriented Framework for Nonlinear Constrained Optimization. *Structures and Multidisciplinary Optimization 45*, 1 (2012), 101–118.

[126] Petrone, Giovanni, de Nicola, Carlo, Quagliarella, Domenico, Witteveen, Jeroen, Axerio-Cilies, John, and Iaccarino, Gianluca. Wind turbine optimization under uncertainty with high performance computing. *41st AIAA Fluid Dynamics Conference, Honolulu, Hawaii*, June (2011), 1–16.

[127] Pitt, D., and Peters, D. Theoretical Prediction of Dynamic-Inflow Derivatives. *Vertica 5*, 1 (1981).

[128] Rao, S. *Engineering Optimization: Theory and Practice*, 4 ed. John Wiley & Sons, Inc., Hoboken, NJ, 2009.

[129] Resor, B. Definition of a 5MW/61.5m Wind Turbine Blade Reference Model. Tech. Rep. SAND2013 - 2569, Sandia National Laboratories, Albuquerque, NM, 2013.

[130] Resor, Brian R., Maniaci, David C., Berg, Jonathon C., and Richards, Phillip. Effects of increasing tip velocity on wind turbine rotor design. Tech. Rep. SAND2014-3136, Sandia National Laboratories, 2014.

[131] Robertson, A., Jonkman, J., and Masciola, M. Definition of the Semisubmersible Floating System for Phase II of OC4. Tech. Rep. NREL/TP-500-47535, National Renewable Energy Laboratory, Golden, CO, 2014.

[132] Robertson, A.N., and Jonkman, J.M. Loads Analysis of Several Offshore Floating Wind Turbine Concepts. In *International Society of Offshore and Polar Engineers 2011 Conference* (Maui, Hawaii, 2011).

[133] Sale, D. User's Guide to Co-Blade: Software for Structural Analysis of Composite Blades. Tech. rep., Northwest National Marine Renewable Energy Center, 2012.

[134] Sant, T, Bonnici, D, Farrugia, R, and Micallef, D. Measurements and modelling of the power performance of a model floating wind turbine under controlled conditions. *Wind Energy 18* (2015), 811–834.

[135] Schubel, Peter J., and Crossley, Richard J. Wind Turbine Blade Design. *Energies 5* (2012), 3425–3449.

[136] Sebastian, Thomas, and Lackner, Matthew. Analysis of the induction and wake evolution of an offshore floating wind turbine. *Energies 5*, 4 (2012), 968–1000.

[137] Sebastian, Thomas, and Lackner, Matthew. Characterization of the unsteady aerodynamics of offshore floating wind turbines. *Wind Energy 16* (2012), 339–352.

[138] Sekar, Kidambi. *Investigation of Root Spoilers on Horizontal Axis Wind Turbines*. Masters of science, Technical University of Delft, 2016.

[139] Selig, M.S. Michael S, and Coverstone-Carroll, Victoria L V.L. Application of a genetic algorithm to wind turbine design. *Journal of Energy Resources Technology 118*, 1 (1996), 22–28.

[140] Simms, D., Schreck, S., Hand, M., and Fingersh, L.J. NREL Unsteady Aerodynamics Experiment in the NASA-Ames Wind Tunnel: A Comparison of Predictions to Measurements. Tech. Rep. NREL/TP-500-29494, National Renewable Energy Lab, 2001.

[141] Snel, H., and Schepers, J. Joint Investigation of Dynamic Inflow Effects and Implementation of an Engineering Method. Tech. Rep. ECN-C-94-107, Energy Research Centre of the Netherlands, 1995.

[142] Stehly, T, Heimiller, D, and Scott, G. 2016 Cost of Wind Energy Review. Tech. Rep. NREL/TP-6A20-70363, National Renewable Energy Laboratory, Golden, CO, 2017.

[143] Stewart, Gordon. *Design Load Analysis of Two Floating Offshore Wind Turbine Concepts*. PhD thesis, University of Massachusetts Amherst, 2016.

[144] Stewart, Gordon, Robertson, Amy, Jonkman, Jason, and Lackner, Matthew. The creation of a comprehensive metocean data set for offshore wind turbine simulations. *Wind Energy 19* (2015), 1151–1159.

[145] Stoddard, W. The Life and Work of Bill Heronemus, wind engineering pioneer. *Wind Engineering 26*, 5 (2002), 335–341.

[146] Sutherland, H.J. On the Fatigue Analysis of Wind Turbines. Tech. Rep. SAND99-0089, Sandia National Laboratories, Albuquerque, NM, 1999.

[147] Tobin, N., Hamed, A., and Chamorro, L. An Experimental Study on the Effects of Winglets on the Wake and Performance of a Model Wind Turbine. *Energies 8* (2015).

[148] Tong, K. C. Technical and economic aspects of a floating offshore wind farm. *Journal of Wind Engineering and Industrial Aerodynamics 74-76* (1998), 399–410.

[149] Tran, Thanh-Toan, and Kim, Dong-Hyun. The platform pitching motion of floating offshore wind turbine: A preliminary unsteady aerodynamic analysis. *Journal of Wind Engineering and Industrial Aerodynamics 142* (2015), 65–81.

[150] U.S. Department of Energy (DOE). Wind Vision: A new era for wind power in the United States. Tech. rep., 2015.

[151] van der Veen, G. J., Couchman, I. J., and Bowyer, R. O. Control of floating wind turbines. In *2012 American Control Conference* (Montreal, Canada, 2012).

[152] Vanderplaats, Garret. CONMIN - A Fortran Program for Constrained Function Minimization. Tech. Rep. NASA TM X-62,282, NASA Ames Research Center and U.S. Army Air Mobility Research and Development Laboratory, 1973.

[153] Wang, Long, Wang, Tong-guang, and Luo, Yuan. Improved non-dominated sorting genetic algorithm (NSGA)-II in multi-objective optimization studies of wind turbine blades. *Applied Mathematics and Mechanics (English Ed) 32*, 6 (2011), 739–748.

[154] Wayman, Elizabeth. *Coupled Dynamics and Economic Analysis of Floating Wind Turbine Systems*. PhD thesis, Massachusetts Institute of Technology, 2006.

[155] Wilson, R., and Lissaman, P. Applied Aerodynamics of Wind Power Machine. Tech. rep., Oregon State University, 1974.

[156] Wilson, R., Lissaman, P., and Walker, S. Aerodynamic Performance of Wind Turbines. Tech. Rep. ERDA/NSF/04014-76/1, Energy Research and Development Administration, 1976.

[157] WindEurope. Offshore Wind in Europe: Key trends and statistics 2018. Tech. rep., 2019.

[158] Wiser, R., and Bolinger, M. 2018 Wind Technologies Market Report. Tech. rep., U.S. Department of Energy Office of Energy Efficiency and Renewable Energy, 2019.

[159] Yang, Hezhen, and Zhu, Yun. Robust design optimization of supporting structure of offshore wind turbine. *Journal of Marine Science and Technology 20*, 4 (2015), 689–702.

[160] Young, A.C. *Investigations into the use of a composite tower on floating offshore wind turbine platforms*. PhD thesis, University of Maine, 2013.

[161] Yu, Q., and Chen, X. Floating Wind Turbines. Tech. rep., BSEE TA&R 669, 2012.

[162] Zhu, Jie, Cai, Xin, Pan, Pan, and Gu, Rongrong. Optimization design of spar cap layup for wind turbine blade. *Frontiers of Structural and Civil Engineering 6*, 1 (2012), 53–56.